Idealized test cases for the dynamical cores of Atmospheric General Circulation Models: A proposal for the NCAR ASP 2008 summer colloquium

Christiane Jablonowski (University of Michgan)
Peter Lauritzen (NCAR)
Ram Nair (NCAR)
Mark Taylor (Sandia National Laboratory)

1   Idealized test cases for 3D dynamical cores

This document describes the idealized dynamical core test cases that are proposed for the NCAR ASP Summer Colloquium in June 2008. All test cases are dry and adiabatic. No physical parameterizations or vertical diffusion are applied. All dynamical cores should be run in their operational configurations which includes the typical diffusion mechanisms and coefficients, filters, time steps and other tunable parameters. In addition, the runs should utilizes their standard *a posteriori* fixers like mass or energy fixers if applicable. These standard runs serve as control simulations. All parameters and fixers need to be documented to foster model comparisons. In addition, the documentation needs to list the prognostic variables, the equation set (e.g. shallow-atmosphere hydrostatic, or shallow-atmosphere nonhydrostatic), the horizontal grid staggering, time stepping approach, vertical coordinate, and horizontal and vertical resolutions.

The modeling groups are also invited to test their models in non-operational configurations that, for example, use less explicit diffusion. In particular, Rayleigh friction at the model top should be avoided if applied. These non-standard configurations are often viable for idealized test cases as considered here, but note that they might not be applicable in real weather or climate simulations. Therefore, any conclusions need to be carefully drawn and are not necessarily valid for models with physics parameterizations. More details are provided in section 2. The parameter p_0 in models with hybrid η coordinates in the vertical direction needs be set to $p_0 = 1000$ hPa which might not be the standard choice.

Table 1 lists all test case that are proposed for the NCAR ASP summer program. We suggest using the unique multiple-digit test case number $F - x - y$ from column 3 to distinguish the model runs. The first digit identifies the test case family F. The second digit x indicates a variation of the initial conditions such as a different rotation angle or background velocity. The x choices for selected rotation angles are listed in Table 2. The optional third digit y denotes a specific tracer distribution if applicable. An overview of the tracer distributions y is given in table 3. It is encouraged to transport all tracers during a single model run. Then the tracer numbers y can be concatenated to form a longer identifier, such as 2-0-1234 which denotes

Family F	Test case	Test case F-x-y	Test case variant	Parameter choices
1	Steady-state	1-0-y	no rotation	$\alpha = 0$
		1-3-y	midlatitudinal flow	$\alpha = \pi/4$
		1-6-y	flow over the poles	$\alpha = \pi/2$
2	Baroclinic wave	2-0-y	no rotation	$\alpha = 0$
		2-3-y	midlatitudinal flow	$\alpha = \pi/4$
		2-6-y	flow over the poles	$\alpha = \pi/2$
3	Advection test solid body rotation	3-0-y	no rotation	$\alpha = 0$
		3-3-y	midlatitudinal flow	$\alpha = \pi/4$
		3-6-y	flow over the poles	$\alpha = \pi/2$
4	3D Rossby-Haurwitz wave	4-0-0		
5	Mountain-induced Rossby wave	5-0-0	wind amplitude	$u_0 = 20$ m/s
6	Pure gravity wave (non-rotating)	6-0-0	$\Omega = 0$ s^{-1} $\lambda_c, \varphi_c = (\pi, 0)$	$N = 0.01$ s^{-1}, $u_0 = 0$ m/s
		6-1-0		isotherm, $u_0 = 0$ m/s
		6-2-0		isotherm, $u_0 = 40$ m/s
6	Inertio-gravity wave	6-3-0	Earth's rotation	isotherm, $u_0 = 0$ m/s

Table 1: Overview of the test case families F with their specifications F-x-y. The symbol x identifies the test case variant. Selected choices for the rotation angles are listed in table 2. The symbol y is a placeholder for different tracer distributions as listed in table 3. The parameter α denotes the flow orientation angle, u_0 a maximum background wind speed, N symbolizes the Brunt-Väisälä frequency and (λ_c, φ_c) points to a grid point position in spherical coordinates. More details are provided in the section for each test case.

a baroclinic wave run without rotation and advected tracers $q1$, $q2$, $q3$ and $q4$. The y numbers might also be used to the distinguish the tracer distributions in graphical depictions of the model runs. Note that multiple resolutions can be selected for each test case. We recommend noting the $lat \times lon$ resolutions as part of the output file names, such as *181x360L26* for 181 latitudes including the poles, 360 longitudes (starting at the zero meridian) and 26 vertical levels.

1.1 Steady-state initial conditions

The idealized steady-state and baroclinic instability (section 1.2) test cases were suggested by Jablonowski (2004) and recently applied to four very different dynamical cores by Jablonowski and Williamson (2006a,b). Among them were the three dynamical cores that are part of the NCAR CAM3.1 modeling framework. These are the spectral transform Eulerian (EUL) and semi-Lagrangian (SLD) models (Collins et al. 2004, 2006) as well as the Finite Volume (FV) dynamical core developed by Lin (2004). In addition, the icosahedral finite-difference model GME of the German Weather Service (DWD) was tested (Majewski et al. 2002). These hydrostatic dynamical cores represent a broad range of numerical approaches and, at very high resolutions, provide independent reference solutions. These are used to assess whether new model runs fall within the uncertainty range of the reference solutions. In addition, the steady-

x	Rotation angle	Flow orientation
0	$\alpha = 0$	0°: no rotation, flow parallel to the equator
1	$\alpha = \pi/12$	15°: flow confined to the tropics
2	$\alpha = \pi/6$	30°: subtropical flow
3	$\alpha = \pi/4$	45°: midlatitudinal flow
4	$\alpha = \pi/3$	60°: flow in the mid- to high latitudes
5	$\alpha = 5\pi/12$	75°: flow reaches high latitudes
6	$\alpha = \pi/2$	90°: flow straight over the poles

Table 2: List of the placeholder x that symbolizes selected rotation angles for test case families 1-3.

y	Tracer field	Test case family (F)
0	no tracer	(1), (4), (5), (6)
1	$q1$	
2	$q2$	steady-state (1), optional
3	$q3$	baroclinic wave (2)
4	$q4$	
5	$q5$	solid body rotation (3)
6	$q6$	

Table 3: List of the placeholder y that denotes the tracer distributions. The definitions of the tracer variables $q1 - q6$ are described in the corresponding sections of the test case families.

state model runs can be compared against the initial state which is an analytic solution to the primitive equations.

The steady-state and baroclinic wave test cases have been developed for dry dynamical cores with pressure-based vertical coordinates like the pure pressure coordinate p, the pure $\sigma = p/p_s$ coordinate (Phillips 1957) or the η (hybrid $\sigma - p$) coordinate (Simmons and Burridge 1981) with p_s symbolizing the surface pressure. The latter two coordinate systems are typically used in GCMs today. The definition of the η-system with

$$p(\lambda, \varphi, \eta) = A(\eta)p_0 + B(\eta)p_s(\lambda, \varphi) \qquad (1)$$

together with the specification of all interface coefficients A and B (half indices) for the integrations in Jablonowski and Williamson (2006a) are provided in Appendix C. λ and φ denote the longitudinal and latitudinal directions, respectively. Note that the reference pressure p_0 is set to 10^5 Pa. This reference value might not be standard in all GCMs that utilize the hybrid system. As an example, the model GME sets the standard value to $p_0 = 1013.25$ hPa which has been changed for the tests described here.

The surface pressure p_s is constant and chosen to be $p_s(\lambda, \varphi) = p_0 = 10^5$ Pa. This guarantees that constant η-surfaces coincide with constant σ or pressure surfaces if there are no variations in the surface pressure, which is the case here. If other σ-systems like

$$\sigma = (p - p_{top})/(p_s - p_{top}) \qquad (2)$$

with non-zero p_{top} are selected (Kasahara 1974), the conversion

$$\eta = \sigma + \frac{p_{top}(1 - \sigma)}{p_0} \qquad (3)$$

3

can be used in the equations below. This expression recovers $\eta = \sigma$ for $p_{top} = 0$ hPa. In general, the choice of the vertical coordinate system is left to the modeling group despite the fact that each vertical coordinate system implies a different boundary condition for the vertical velocity. In practice, this has been found to be insignificant for the steady state test or the evolution of the baroclinic wave over a 10-day time period. If other generalized vertical coordinate systems are used, like height-based or hybrid isentropic-σ levels, either an iterative method or vertical interpolations of the initial conditions become necessary. Details of the iterative method, which is the preferred choice, are provided in Appendix D

The initial state is defined by analytic expressions in spherical (λ, φ, η) coordinates where $\lambda \in [0, 2\pi]$ stands for the longitude, $\varphi \in [-\pi/2, \pi/2]$ represents the latitude and $\eta \in [0, 1]$ denotes the position in the vertical direction which is unity at the surface and approaches zero at the model top. The subsequent expressions can also be straightforwardly transformed into different, e.g. Cartesian, coordinate systems. All physical constants used in the test specification are listed below and in Appendix G. Users of the test case are encouraged to select the same parameter set in their models to foster model intercomparisons.

Assuming that a model utilizes η-levels an auxiliary variable η_v is defined by

$$\eta_v = (\eta - \eta_0) \frac{\pi}{2} \tag{4}$$

with $\eta_0 = 0.252$. Eq. (4) can also be directly applied to models with pure pressure coordinates if $\eta = p/p_s$ is adopted at each pressure level p (for models with $p_{top} = 0$ hPa)..

The flow field is comprised of two symmetric zonal jets in midlatitudes. The zonal wind u and meridional wind v are defined as

$$u(\lambda, \varphi, \eta) = u_0 \cos^{\frac{3}{2}} \eta_v \ \sin^2 (2\varphi) \tag{5}$$
$$v(\lambda, \varphi, \eta) = 0 \text{ m s}^{-1}. \tag{6}$$

Here the maximum amplitude u_0 is set to 35 m s^{-1} which is close to the wind speed of the zonal-mean time-mean jet streams in the troposphere. In addition, the vertical velocity is set to zero for non-hydrostatic setups. This flow field in nondivergent and allows the derivation of the analytic initial data even for models in vorticity-divergence (ζ, δ) form. In particular, the radial outward component of the relative vorticity ζ is given by

$$\zeta(\lambda, \varphi, \eta) = \frac{-4 u_0}{a} \ \cos^{\frac{3}{2}} \eta_v \ \sin \varphi \ \cos \varphi \ (2 - 5\sin^2 \varphi) \tag{7}$$

and $\delta = 0$ s^{-1} is automatically fulfilled. $a = 6.371229 \times 10^6$ m indicates the mean radius of the Earth.

The horizontally averaged temperature $\bar{T}(\eta)$ is split into two representations for the lower (Eq. (8)) and middle (Eq. (9)) atmosphere. This introduces the characteristic atmospheric temperature profiles especially at upper levels. They are given by

$$\bar{T}(\eta) = T_0 \ \eta^{\frac{R_d \Gamma}{g}} \qquad \qquad (\text{for } \eta_s \geq \eta \geq \eta_t) \tag{8}$$
$$\bar{T}(\eta) = T_0 \ \eta^{\frac{R_d \Gamma}{g}} + \Delta T \ (\eta_t - \eta)^5 \qquad \qquad (\text{for } \eta_{top} > \eta) \tag{9}$$

with the surface level $\eta_s = 1$, the tropopause level $\eta_t = 0.2$ and the horizontal-mean temperature at the surface $T_0 = 288$ K. The temperature lapse rate Γ is set to 0.005 K m^{-1} which is similar

to the observed diabatic lapse rate. Additionally, the empirical temperature difference $\Delta T = 4.8 \times 10^5$ K is chosen. $R_d = 287.04$ J (kg K)$^{-1}$ represents the ideal gas constant for dry air and $g = 9.80616$ m s^{-2} is the gravitational acceleration. The total temperature distribution comprises the horizontal-mean temperature and a horizontal variation at each level. It is given by

$$
T(\lambda, \varphi, \eta) = \bar{T}(\eta) + \frac{3}{4} \frac{\eta \, \pi \, u_0}{R_d} \, \sin \eta_v \, \cos^{\frac{1}{2}} \eta_v \, \times
$$
$$
\left\{ \left(-2 \sin^6 \varphi \, (\cos^2 \varphi + \frac{1}{3}) + \frac{10}{63} \right) 2 \, u_0 \, \cos^{\frac{3}{2}} \eta_v + \right.
$$
$$
\left. \left(\frac{8}{5} \cos^3 \varphi \, (\sin^2 \varphi + \frac{2}{3}) - \frac{\pi}{4} \right) a \, \Omega \right\} \tag{10}
$$

where $\Omega = 7.29212 \times 10^{-5}$ s^{-1} denotes the Earth's angular velocity.

The geopotential $\Phi = gz$ completes the description of the steady-state initial conditions where z symbolizes the elevation of a model level η. The total geopotential distribution $\Phi = \bar{\Phi} + \Phi'$ comprises the horizontal-mean geopotential $\bar{\Phi}$ and a horizontal variation Φ' at each level. This is analogous to the description of the temperature field. The geopotential is determined by

$$
\Phi(\lambda, \varphi, \eta) = \bar{\Phi}(\eta) + u_0 \, cos^{\frac{3}{2}} \eta_v \, \times
$$
$$
\left\{ \left(-2 \sin^6 \varphi \, (\cos^2 \varphi + \frac{1}{3}) + \frac{10}{63} \right) u_0 \, \cos^{\frac{3}{2}} \eta_v + \right.
$$
$$
\left. \left(\frac{8}{5} \cos^3 \varphi \, (\sin^2 \varphi + \frac{2}{3}) - \frac{\pi}{4} \right) a \, \Omega \right\}. \tag{11}
$$

with

$$
\bar{\Phi}(\eta) = \frac{T_0 \, g}{\Gamma} \left(1 - \eta^{\frac{R_d \Gamma}{g}} \right) \qquad \text{(for } \eta_s \geq \eta \geq \eta_t) \tag{12}
$$

$$
\bar{\Phi}(\eta) = \frac{T_0 \, g}{\Gamma} \left(1 - \eta^{\frac{R_d \Gamma}{g}} \right) - R_d \, \Delta T \, \times \qquad \text{(for } \eta_t > \eta) \tag{13}
$$
$$
\left\{ \left(\ln \left(\frac{\eta}{\eta_t} \right) + \frac{137}{60} \right) \eta_t^5 - 5 \, \eta_t^4 \, \eta + 5 \, \eta_t^3 \, \eta^2 - \frac{10}{3} \, \eta_t^2 \, \eta^3 + \frac{5}{4} \, \eta_t \, \eta^4 - \frac{1}{5} \, \eta^5 \right\}.
$$

This formulation enforces the hydrostatic balance analytically and ensures the continuity of the geopotential at the tropopause level η_t. In hydrostatic models with pressure-based vertical coordinates, it is only necessary to initialize the surface geopotential $\Phi_s = gz_s$. It balances the non-zero zonal wind at the surface with surface elevation z_s and is determined by setting $\eta = \eta_s$ in Eq. (11). This leads to the following equation for the surface geopotential

$$
\Phi_s(\lambda, \varphi) = u_0 \, \cos^{\frac{3}{2}} \left((\eta_s - \eta_0) \frac{\pi}{2} \right) \times
$$
$$
\left\{ \left(-2 \sin^6 \varphi \, (\cos^2 \varphi + \frac{1}{3}) + \frac{10}{63} \right) u_0 \, \cos^{\frac{3}{2}} \left((\eta_s - \eta_0) \frac{\pi}{2} \right) + \right.
$$
$$
\left. \left(\frac{8}{5} \cos^3 \varphi \, (\sin^2 \varphi + \frac{2}{3}) - \frac{\pi}{4} \right) a \, \Omega \right\} \tag{14}
$$

with $\eta_0 = 0.252$ and $\eta_s = 1$. Note that Φ_s is actually a function of latitude only. As mentioned before the surface pressure is constant and given by

$$
p_s = p_0 = 1000 \text{ hPa.} \tag{15}
$$

5

The geopotential equation (11) can fully be utilized for dynamical cores with height-based vertical coordinates. Then, a root-finding algorithm is recommended to determine the corresponding η-level for any given height z. This iterative method, which is also applicable to isentropic vertical coordinates, is outlined in Appendix D. The resulting η-level is accurate to machine precision and can consequently be used to compute the initial data set.

The balanced initial flow field comprises a zonally symmetric basic state with a jet in the midlatitudes of each hemisphere and a quasi-realistic temperature distribution, which are displayed in Figs. 1(a) and (b). In addition, the figure shows the profile of the surface geopotential (Fig. 1(c)), three selected vertical temperature distributions on a logarithmic scale (Fig. 1(d)), the initial geopotential height field (Fig. 1(e)) and the unperturbed relative vorticity distribution (Fig. 1(f)). Overall, the atmospheric conditions resemble the climatic state of a winter hemisphere reasonably well. The centers of the midlatitudinal jets at $45°$N/S are placed at the pressure level $p = \eta_0 p_s = 252$ hPa, which lies just below the tropopause level at $p = 200$ hPa. Furthermore, the globally averaged temperature of this distribution is approximately 256.4 K, which closely matches the observed global temperature of the atmosphere. The horizontally averaged temperature at the surface is $\bar{T}(\eta = 1) = T_0 = 288$ K which corresponds exactly to the surface temperature of the so-called U.S. standard atmosphere (U.S. Standard Atmosphere 1976). In addition, the temperature distribution captures an idealized stratospheric and mesospheric temperature profile and prescribes a low-level temperature inversion in polar regions. The test design guarantees static, inertial and symmetric stability properties, but is unstable with respect to baroclinic or barotropic instability mechanisms.

The following test strategy is suggested. The dynamical core is initialized with the balanced initial conditions and run for 30 model days at varying horizontal resolutions. This is a stringent test of the dynamics that not only serves as a debugging tool but also as an assessment tool for the algorithmic design of the numerical scheme and its horizontal grid. For these model runs error norms can be directly assessed since the initial state is the true solution. If possible, the unperturbed model simulations should be run without horizontal or vertical diffusion. Most often, the latter is a component of the physics package and therefore already inactive in a dynamical core simulation. In addition, no Rayleigh friction near the model top (if included in the model) should be applied. All three aforementioned diffusion mechanisms would damp the initial data over time which is consequently reflected in the error statistics.

1.1.1   Rotated steady-state initial data set

The steady-state initial data are zonally uniform which favors models with orthogonal latitude-longitude or Gaussian grids. Therefore, a rotated version of the initial conditions is suggested for both the steady-state and baroclinic wave (see section 1.2) test cases. It rotates the computational grid by a flow orientation angle $\alpha \in [0, \pi/2]$. This rotation is also depicted in Fig. 28 in Appendix E. For $\alpha = 0$ the original zonal flow parallel to the equator is recovered, whereas the flow orientation angle of $\alpha = \pi/2$ directs the flow field straight over the poles. The latter setup has the potential to expose filter effects that are associated with polar filters in latitude-longitude grids. These are frequently used to alleviate the effects of the converging meridians in spherical geometry. A flow orientation angle greater zero therefore diminishes the advantages of the traditional orthogonal grids for zonal flows. In addition, a flow orientation angle like $\alpha = \pi/4$ challenge the design of cubed-sphere grids that place the corners of the cubed-sphere in midlatitudes at $\varphi \pm 45°$.
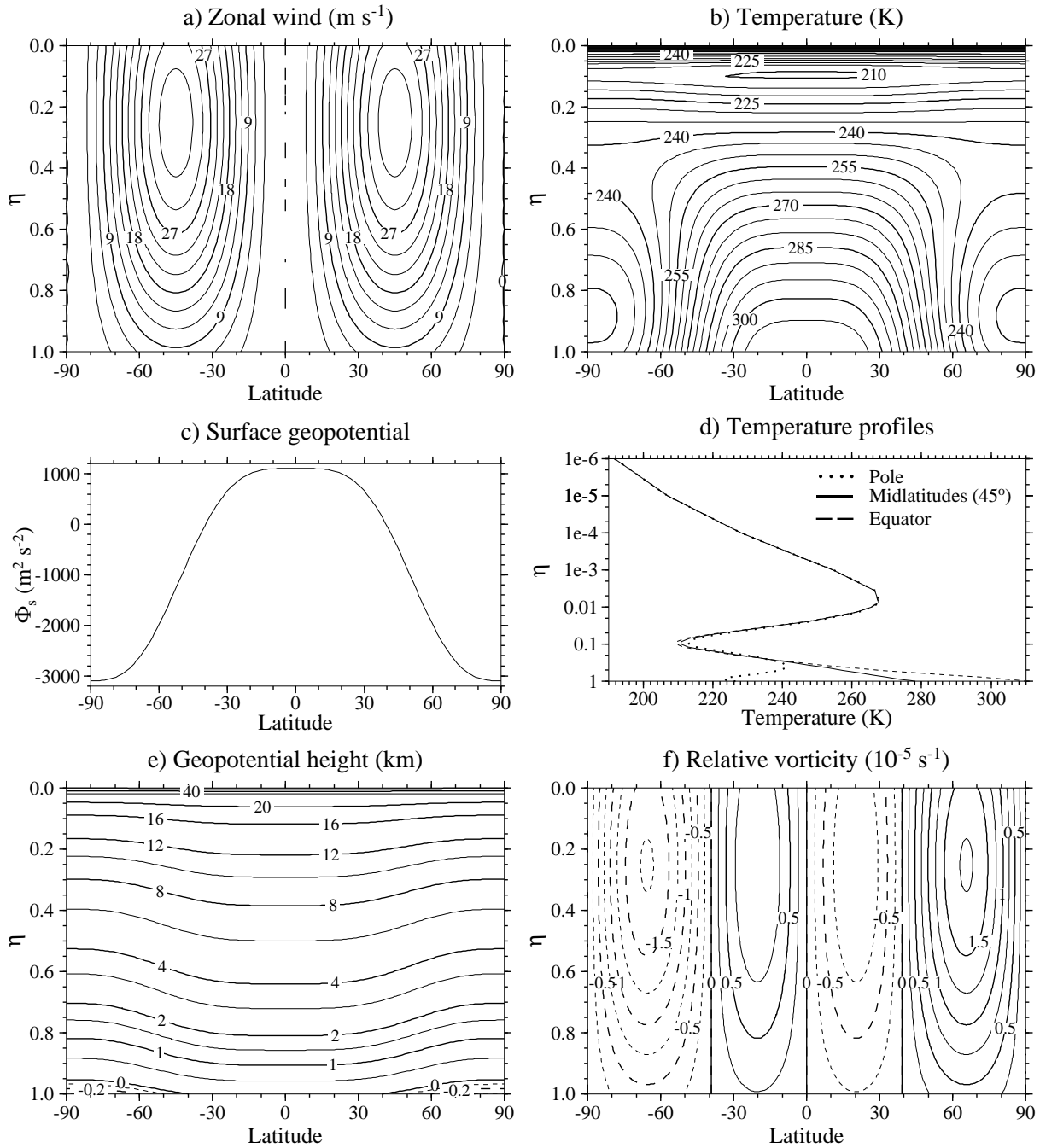
a) Zonal wind (m s⁻¹)

b) Temperature (K)

c) Surface geopotential

d) Temperature profiles

Pole
Midlatitudes (45°)
Equator

e) Geopotential height (km)

f) Relative vorticity (10⁻⁵ s⁻¹)

Figure 1: Initial conditions for the (a) unperturbed zonal wind u, (b) temperature T, (c) surface geopotential Φ_s, (d) vertical temperature profiles at the equator, $45°$N/S and the poles, (e) geopotential height field z (in km) and (f) the unperturbed relative vorticity ζ (in 10^{-5} s^{-1}). The contour levels in (e) are non-uniformally spaced, negative contours are dashed. Note that the η coordinate coincides with $\sigma = p/p_s$ for $p_{top} = 0$ hPa.
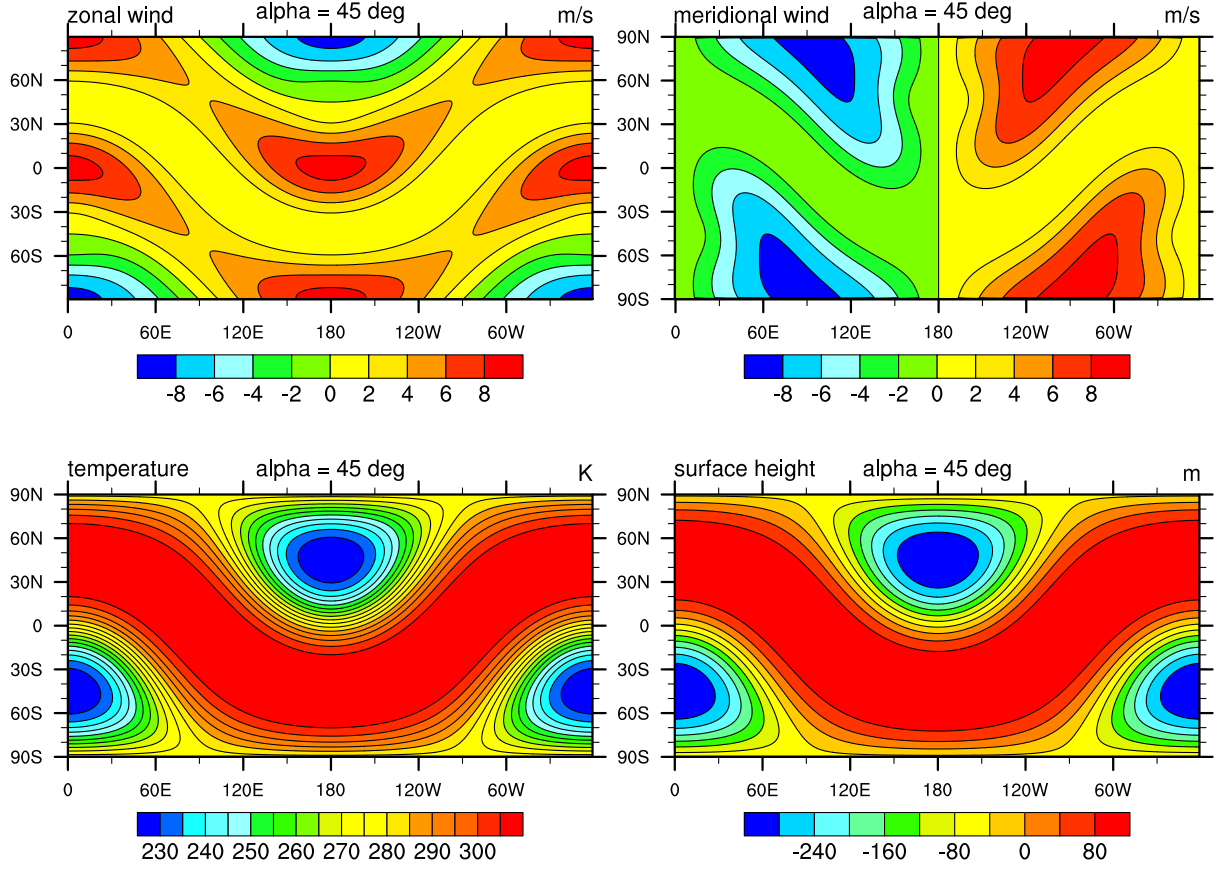
Figure 2: Initial conditions for the unperturbed zonal wind u (top left), meridional wind v (top right), temperature T (bottom left) and surface geopotential height z_s (bottom right) at the lowestmost model level ($p = 992.6$ hPa) with the flow orientation angle $\alpha = 45°$.

Very minor modifications of the model code and initial conditions are necessary for the rotated test case. In particular, the change in the model configuration is a rotated Coriolis parameter $f(\lambda, \varphi)$ that now becomes a 2D field. This is in contrast to the regular 1D setting $f(\varphi) = 2\Omega \sin(\varphi)$. The rotated Coriolis parameter is

$$f(\lambda, \varphi) = 2\,\Omega\,[-\cos\lambda\cos\varphi\sin\alpha + \sin\varphi\cos\alpha]. \tag{16}$$

The same representation of f is also used in Williamson et al. (1992) for rotated shallow water test cases.

In addition, the initial conditions for u, v, T and Φ_s need to be rotated. Following Staniforth and White (2007) the necessary steps are documented in Appendix E and also implemented in the Fortran test case routines for the initial conditions. Two examples of the rotated initial conditions are shown in Figs. 2 and 3. They depict the steady-state initial data at the lowest most model level ($p = 992.6$ hPa) with the flow orientation angle $\alpha = 45°$ and $\alpha = 90°$.
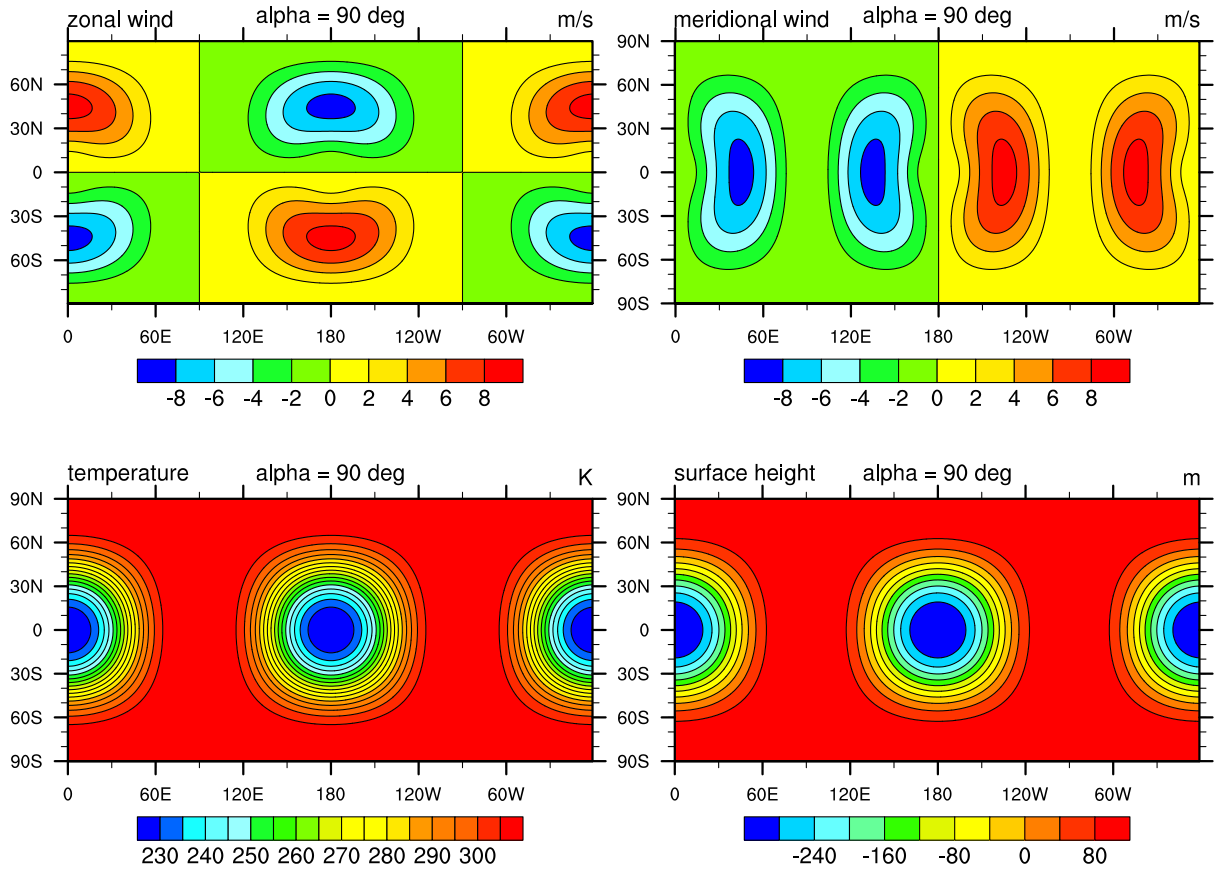
Figure 3: Initial conditions for the unperturbed zonal wind u (top left), meridional wind v (top right), temperature T (bottom left) and surface geopotential height z_s (bottom right) at the lowestmost model level ($p = 992.6$ hPa) with the flow orientation angle $\alpha = 90°$.

1.1.2 Resolution, output data and analysis

We suggest running the steady-state test case with flow orientation angle $\alpha = 0°$ at the spectral resolutions T21, T42, T85 and T170 with 26 vertical levels. These resolutions correspond approximately to the grid point resolutions $4° \times 4°$, $2° \times 2°$, $1° \times 1°$ and $0.5° \times 0.5°$. Similar information on the resolutions and time steps are provided in Appendix 2 that lists the choices for the three NCAR CAM3.5 dynamical cores and the icosahedral model GME.

We recommend repeating two rotated 30-day model run at the T85 spectral resolution or the $1° \times 1°$ grid point resolution with 26 vertical levels. The flow orientation angles are $\alpha = 45°$ and $\alpha = 90°$.

For each model run the following instantaneous model variables to the NetCDF should be written to the output file: PS, U, V, T, PHIS, Z3 (geopotential height at all model levels, if available) and T850 (temperature at 850 hPa, if available). The output frequency is daily (every 24 hours starting with the initial state). Plot the snapshots of the surface pressure field at days 5, 10, 20 and 30. Assess whether the total mass and total energy is conserved during the 30-day model run (see also Appendix F). Ideally, both quantities should be computed on the native grid during the model run. Quantify the total loss or gain of mass and total energy in percent at the end of the run (day 30). In addition, we recommend analyzing the zonal wind symmetry deviations from the zonal mean and the degradation of the zonal wind average with respect to the analytic solution. Both can be assessed via l_2 error norms which are displayed in Eqs. 17 and 18 for pressure-based hybrid vertical coordinates. If other vertical coordinate systems are used, the vertical integration weights (here the η_k thicknesses) need to be modified. The first l_2 error norm evaluates the symmetry-deviations from the zonal average. It is defined as

$$
\begin{aligned}
l_2\big(u(t) - \overline{u}(t)\big) &= \left(\frac{1}{4\pi} \int_0^1 \int_{-\frac{\pi}{2}}^{\frac{\pi}{2}} \int_0^{2\pi} [u(\lambda, \varphi, \eta, t) - \overline{u}(\varphi, \eta, t)]^2 \, \cos\varphi \, d\lambda \, d\varphi \, d\eta \right)^{1/2} \\
&\approx \left(\frac{\sum_k \sum_j \sum_i [u(\lambda_i, \varphi_j, \eta_k, t) - \overline{u}(\varphi_j, \eta_k, t)]^2 \, w_j \, \Delta\eta_k}{\sum_k \sum_j \sum_i w_j \, \Delta\eta_k} \right)^{1/2}
\end{aligned} \tag{17}
$$

where the overbar $\overline{(\ )}$ denotes the zonal average and the sums with indices (i, j, k) are taken over all longitude points λ_i, latitude points φ_j and vertical levels η_k of the global grid. The summation weights w_j are the Gaussian weights for the calculations on the spectral transform grids. On uniform grids $w_j = |\sin(\varphi_{j+1/2}) - \sin(\varphi_{j-1/2})|$ is used where the half indices denote the location of the cell interfaces in the meridional direction. The weights $\Delta\eta_k = (\eta_{k+1/2} - \eta_{k-1/2})$ indicate the thickness of a model layer. Here the half indices $k \pm 1/2$ point to the locations of the level interfaces. Eq. (17) assumes that the longitudinal grid points are equally spaced. The second l_2 norm assesses the degradation of the zonal average with respect to the analytic solution. It is defined by

$$
\begin{aligned}
l_2\big(\overline{u}(t) - \overline{u}(t=0)\big) &= \left(\frac{1}{2} \int_0^1 \int_{-\frac{\pi}{2}}^{\frac{\pi}{2}} [\overline{u}(\varphi, \eta, t) - \overline{u}(\varphi, \eta, t=0)]^2 \, \cos\varphi \, d\varphi \, d\eta \right)^{1/2} \\
&\approx \left(\frac{\sum_k \sum_j [\overline{u}(\varphi_j, \eta_k, t) - \overline{u}(\varphi_j, \eta_k, t=0)]^2 \, w_j \, \Delta\eta_k}{\sum_k \sum_j w_j \, \Delta\eta_k} \right)^{1/2} .
\end{aligned} \tag{18}
$$

Example figures of the two error norms are shown in Jablonowski and Williamson (2006a).

1.2 Baroclinic wave test with tracers

A baroclinic wave can be triggered if the initial conditions for the steady-state test (section 1.1) are overlaid with a perturbation. Here a perturbation with a Gaussian profile is selected and centered at $(\lambda_c, \varphi_c) = (\pi/9, 2\pi/9)$ which points to the location (20°E,40°N). The perturbation overlays the zonal wind field. The zonal wind perturbation u_{pert} is given by

$$u_{pert}(\lambda, \varphi, \eta) = u_p \, \exp\left(-\left(\frac{r}{R}\right)^2\right) \tag{19}$$

with radius $R = a/10$ and maximum amplitude $u_p = 1 \text{ m s}^{-1}$. It superimposes on the balanced zonal wind field (Eq. (5)) by adding u_{pert} to the wind field at each grid point at all model levels. It yields

$$u(\lambda, \varphi, \eta) = u_0 \, \cos^{\frac{3}{2}} \eta_v \, \sin^2(2\,\varphi) + u_p \, \exp\left(-\left(\frac{r}{R}\right)^2\right) \tag{20}$$

where the great circle distance r is given by

$$r = a \, \arccos\left(\sin\varphi_c \, \sin\varphi + \cos\varphi_c \, \cos\varphi \, \cos(\lambda - \lambda_c)\right) \quad . \tag{21}$$

The corresponding overlaying (ζ', δ') perturbations at each level for models in vorticity-divergence form are

$$\zeta'(\lambda, \varphi, \eta) = \frac{u_p}{a} \, \exp\left(-\left(\frac{r}{R}\right)^2\right) \times \left\{ \tan\varphi - \right.$$
$$\left. 2\left(\frac{a}{R}\right)^2 \arccos(X) \, \frac{\sin\varphi_c \, \cos\varphi - \cos\varphi_c \, \sin\varphi \, \cos(\lambda - \lambda_c)}{\sqrt{1 - X^2}} \right\} \tag{22}$$

$$\delta'(\lambda, \varphi, \eta) = \frac{-2\,u_p\,a}{R^2} \, \exp\left(-\left(\frac{r}{R}\right)^2\right) \arccos(X) \, \frac{\cos\varphi_c \, \sin(\lambda - \lambda_c)}{\sqrt{1 - X^2}} \tag{23}$$

with $X = \left(\sin\varphi_c \, \sin\varphi + \cos\varphi_c \, \cos\varphi \, \cos(\lambda - \lambda_c)\right)$. For both singular points (λ_c, φ_c) and $(\lambda_c + \pi, -\varphi_c)$ with $X^2 = 1$, δ' is identical zero. In addition, $\zeta'(\lambda_c, \varphi_c) = u_p \tan\varphi/a$ is well-defined and $\lim_{\lambda \to \lambda_c + \pi, \varphi \to -\varphi_c} \zeta'$ is zero. Similarly, $\lim_{\varphi \to \pm\frac{\pi}{2}} \zeta'$ is zero at the poles. The perturbation fields u', ζ' and δ' are shown in Fig. 4.

The evolution of a baroclinic wave in the Northern Hemisphere is triggered when using the steady-state initial conditions with the overlaid zonal wind perturbation. As before, different horizontal resolutions should be assessed to estimate the convergence characteristics. In general, the baroclinic wave starts growing observably around day 4 and evolves rapidly thereafter with explosive cyclogenesis at model day 8. The wave train breaks after day 9 and generates a full circulation in both hemispheres between day 20-30 depending on the model formulation. Therefore, the simulation should cover at least a 10-day time period that captures the initial and rapid development stages of the baroclinic disturbance. If longer time integrations are performed (e.g. up to 30 days as in the subsequent examples) the spread of the numerical solutions increases noticeably from model day 12 onwards. This indicates the predictability limit of the test case. Nevertheless, the initial development stages of new systems at the leading edge of the baroclinic wave train (compare also to Simmons and Hoskins (1979)) are still predicted reliably until day 16.

The baroclinic wave, although idealized, represents very realistic flow features. Strong temperature fronts develop that are associated with the evolving low and high pressure systems.
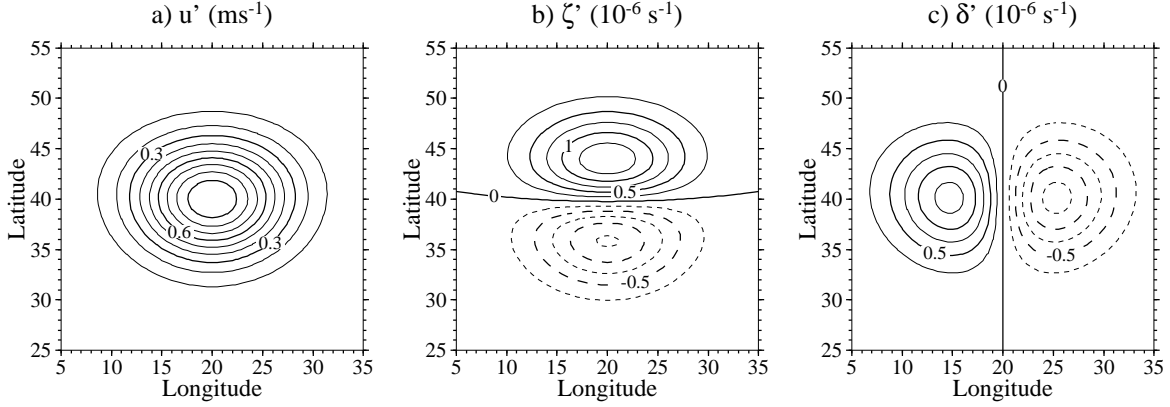
Figure 4: Perturbation patterns for the (a) zonal wind, (b) relative vorticity and (c) divergence. The zero contour in (a) is omitted.

In addition, the wavenumber with maximum growth rate lies between 5 and 9 which agrees well with observations and assessments in the literature (for example Simmons and Hoskins (1977)). It is important to note that the baroclinic wave test case does not have an analytic solution. Therefore, high resolution reference solutions and their uncertainties can be assessed.

We suggest adding a variety of passive tracers to the baroclinic wave test case. The scientific questions are

- whether the advection scheme is monotonic and/or positive definite.

- how thin filaments are represented and diffused.

- whether a constant tracer distribution is preserved in nondivergent flow fields. In particular, the steady state flow is expected to preserve a constant tracer.

- how accurate and diffusive the vertical transport is.

- whether the model traps tracer mass at the top or bottom of the domain.

The tracer distributions are denoted by the variables names $q1$, $q2$, $q3$ and $q4$. Their initial distributions are given by

$$q1(\lambda, \varphi, \eta) = \begin{cases} x & \text{if } |x| \geq 10^{-8} \\ 0 & \text{if } |x| < 10^{-8} \end{cases} \tag{24}$$

with

$$x = \exp\left\{ -\left[\left(\frac{r}{R}\right)^2 + \left(\frac{\eta - \eta_c}{\eta_{hw}}\right)^2 \right] \right\} \tag{25}$$

where $R = a/10$ and $\eta_{hw} = 0.1$ determine the horizontal and vertical half widths of the tracer distribution. The maximum amplitude in the vertical direction is placed at mid-levels with $\eta_c = 0.6$. r is the great circle distance between the grid point position (λ, φ) and the center, initially set to $(\lambda_c, \varphi_c) = (\pi/9, 11\pi/18) = (20°\text{E}, 55°\text{N})$. The great circle distance r is defined as

$$r = a \ \arccos\left[\sin\varphi_c \sin\varphi + \cos\varphi_c \cos\varphi \cos(\lambda - \lambda_c)\right]. \tag{26}$$

12

A variant of $q1$ is created when $\eta_c = 0.6$ is replaced with $\eta_c = 1$. This places the vertical peak of the tracer distribution at the surface where strong gradients occur during the evolution of the baroclinic wave. This choice of η_c is defined as tracer field $q2$.

The other tracer distributions are

$$q3(\lambda, \varphi, \eta) = \frac{1}{2} \Big[\tanh \big(3|\varphi| - \pi \big) + 1 \Big], \tag{27}$$

$$q4(\lambda, \varphi, \eta) = 1. \tag{28}$$

Note that $q3$ only depends on the latitudinal position φ and $q4$ is constant everywhere.

1.2.1 Rotated baroclinic wave initial data set

The steady-state initial data without the perturbation are zonally uniform which favors models with orthogonal latitude-longitude or Gaussian grids. Therefore, a rotated version of the initial conditions is suggested. It rotates the computational grid by a flow orientation angle $\alpha \in [0, \pi/2]$. This rotation is also depicted in Fig. E in Appendix 28. For $\alpha = 0$, the original zonal flow parallel to the equator is recovered, whereas $\alpha = \pi/2$ directs the flow field straight over the poles. The latter setup has the potential to expose filter effects that are associated with polar filters in latitude-longitude grids. These are frequently used to alleviate the effects of the converging meridians in spherical geometry. A rotation angle greater zero therefore diminishes the advantages of the traditional orthogonal grids for zonal flows. In addition, an angle like $\alpha = \pi/4$ challenge the design of cubed-sphere grids that place the corners of the cubed-sphere in midlatitudes at $\varphi \pm 45°$.

Very minor modifications of the model code and initial conditions are necessary for the rotated test case. In particular, the change in the model configuration is a rotated Coriolis parameter $f(\lambda, \varphi)$ that now becomes a 2D field. This is in contrast to the regular 1D setting $f(\varphi) = 2\Omega \sin(\varphi)$. The rotated Coriolis parameter is

$$f(\lambda, \varphi) = 2\,\Omega \left[- \cos \lambda \cos \varphi \sin \alpha + \sin \varphi \cos \alpha \right]. \tag{29}$$

The same representation of f is also used in Williamson et al. (1992) for rotated shallow water test cases.

In addition, the initial conditions for u, v, T and Φ_s need to be rotated. Following Staniforth and White (2007) the necessary steps are documented in Appendix E and also implemented in the Fortran test case routines for the initial conditions.

1.2.2 Resolution, output data and analysis

We suggest running the baroclinic wave test case with the flow orientation angle $\alpha = 0°$ at the spectral resolutions T21, T42, T85, T170 and T340 with 26 vertical levels. These resolutions correspond approximately to the grid point resolutions $4° \times 4°$, $2° \times 2°$, $1° \times 1°$, $0.5° \times 0.5°$ and $0.25° \times 0.25°$. Similar information on the resolutions and time steps are provided in Appendix 2 that lists the choices for the three NCAR CAM3.5 dynamical cores and the icosahedral model GME. The integration time is 30 days for T21, T42, T85, T170 and 15 days for T340 to reduce the compute time.

We suggest repeating two rotated 30-day model runs at the T170 spectral resolution or the $0.5° \times 0.5°$ grid point resolution with 26 vertical levels. If the compute time becomes

prohibitive the lower resolution T106 or the $1° \times 1°$ grid point resolution with 26 vertical levels are recommended. The flow orientation angles are $\alpha = 45°$ and $\alpha = 90°$.

For each model run the following instantaneous model variables to the NetCDF should be written to the output file: PS, U, V, T, OMEGA, PHIS, Z3 (geopotential height at all model levels, if available), T850 (temperature at 850 hPa, if available) and all tracers. T850 is a valuable output quantity for at least the first 20 days. At later days the minimum surface pressure might locally drop below 850 hPa which requires an extrapolation of the temperature to the 850 hPa level. The output frequency is daily (every 24 hours starting with the initial state). Plot the surface pressure, 850 hPa temperature and 850 hPa relative vorticity field at days 7 and 9 in an equidistant cylindrical map projection. An example is provided in Fig. 5 that was computed with the NCAR CAM3.5.41 Eul model at the resolution T106 with 26 levels. In addition, compute the time sequence at day 15, 20, 25 and 30 of the kinetic energy spectra at 700 hPa. Assess whether the total energy and mass are conserved during the 30-day model run (see also Appendix F). Ideally, both quantities should be computed on the native grid during the model run. The total energy time series should show the energy difference between the daily (or more frequent) output and the initial state. In addition, quantify the final energy loss or gain in percent (normalized energy difference).

Interpolate the tracer field $q1$ at day 9 and 15 to the 700, 600 and 500 hPa levels and plot the three pressure levels as equidistant cylindrical maps. The tracer field $q2$ is best evaluated on model levels near the surface. We again suggest visualizing at least day 9 and 15. Interpolate the tracer field $q3$ at day 9 and 15 to the pressure levels 850, 500 and 300 hPa. Plot the three pressure levels as equidistant cylindrical maps. In addition, evaluate whether the initially constant tracer distribution $q4$ shows variations. Assess whether the global tracer masses of $q1$-$q4$ are conserved during the whole forecast period. We will provide NCL (NCAR Command Language) scripts to help interpolate and evaluate all diagnostic quantities.

The following plots show examples of unrotated and rotated baroclinic wave runs with selected tracer distributions. The results were computed with EULT106L26 (see figure captions for the details). The noisy contours are due to the Gibb's ringing effect. The standard diffusion coefficients were used (see section 2).

1.3   Pure tracer advection tests with prescribed wind

This 3D advection test case tests the transport scheme of the dynamical core in isolation. The following model code changes are required

- prescribe the time-invariant horizontal wind speeds u and v

- prescribe the time-variant vertical velocity $\dot{\eta}$, $\dot{\sigma}$, ω or w depending on the choice of the vertical coordinate

- suppress the forecast of all prognostic variables. This is often most easily attained by commenting out the update of the forecast variables or setting the time tendencies of the dynamical core to zero.

- introduce a counter variable that counts the seconds since the start of the advection test. The latter is needed for the prescribed update of the vertical velocity.
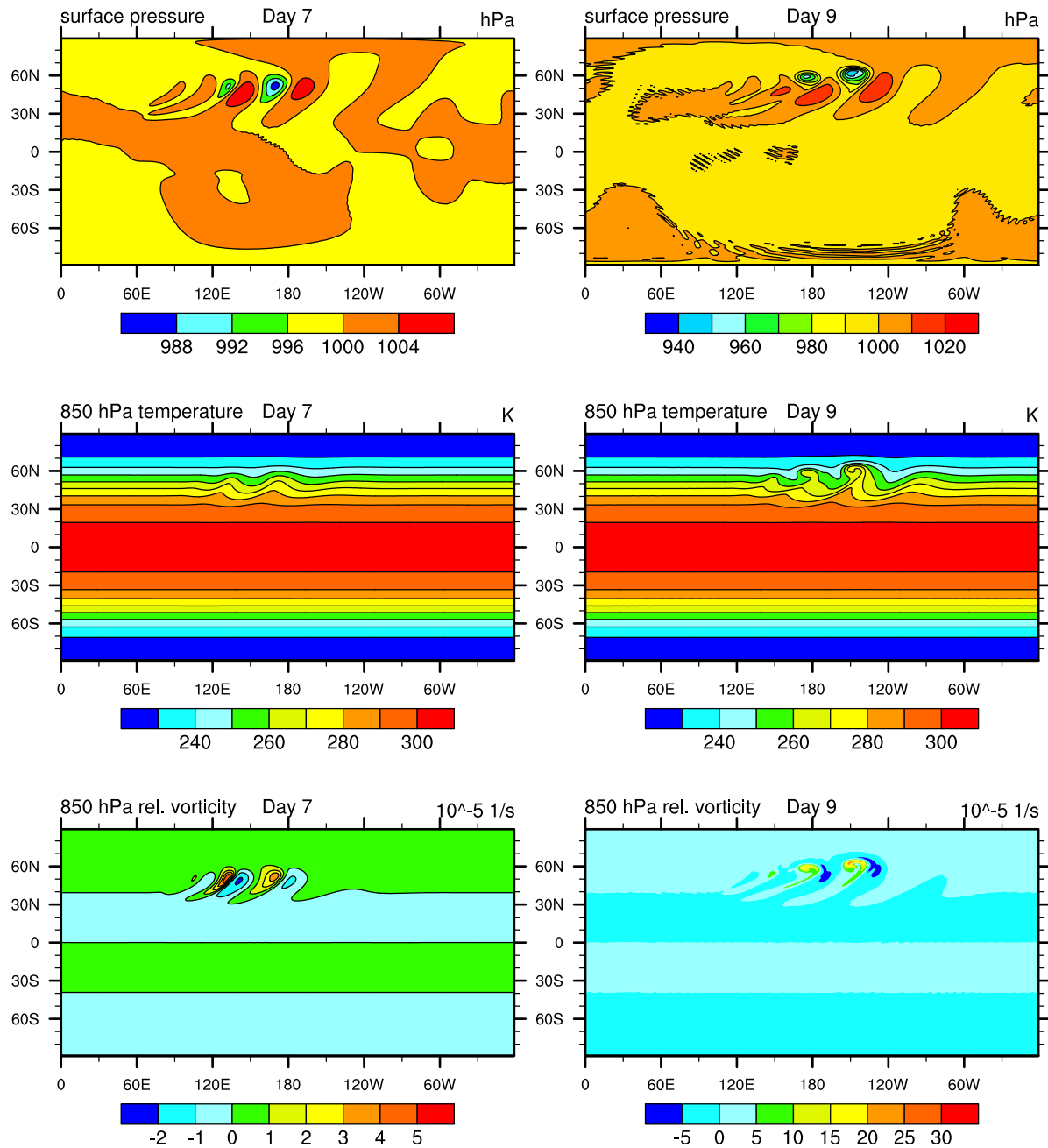
eulT106L26 2-0-1234 bw, $\alpha = 0$

Figure 5: [2-0-y]: Baroclinic wave without rotation simulated with EULT106L26: surface pressure (upper row), 850 hPa temperature (middle row) and 850 hPa relative vorticity at days 7 and 9.
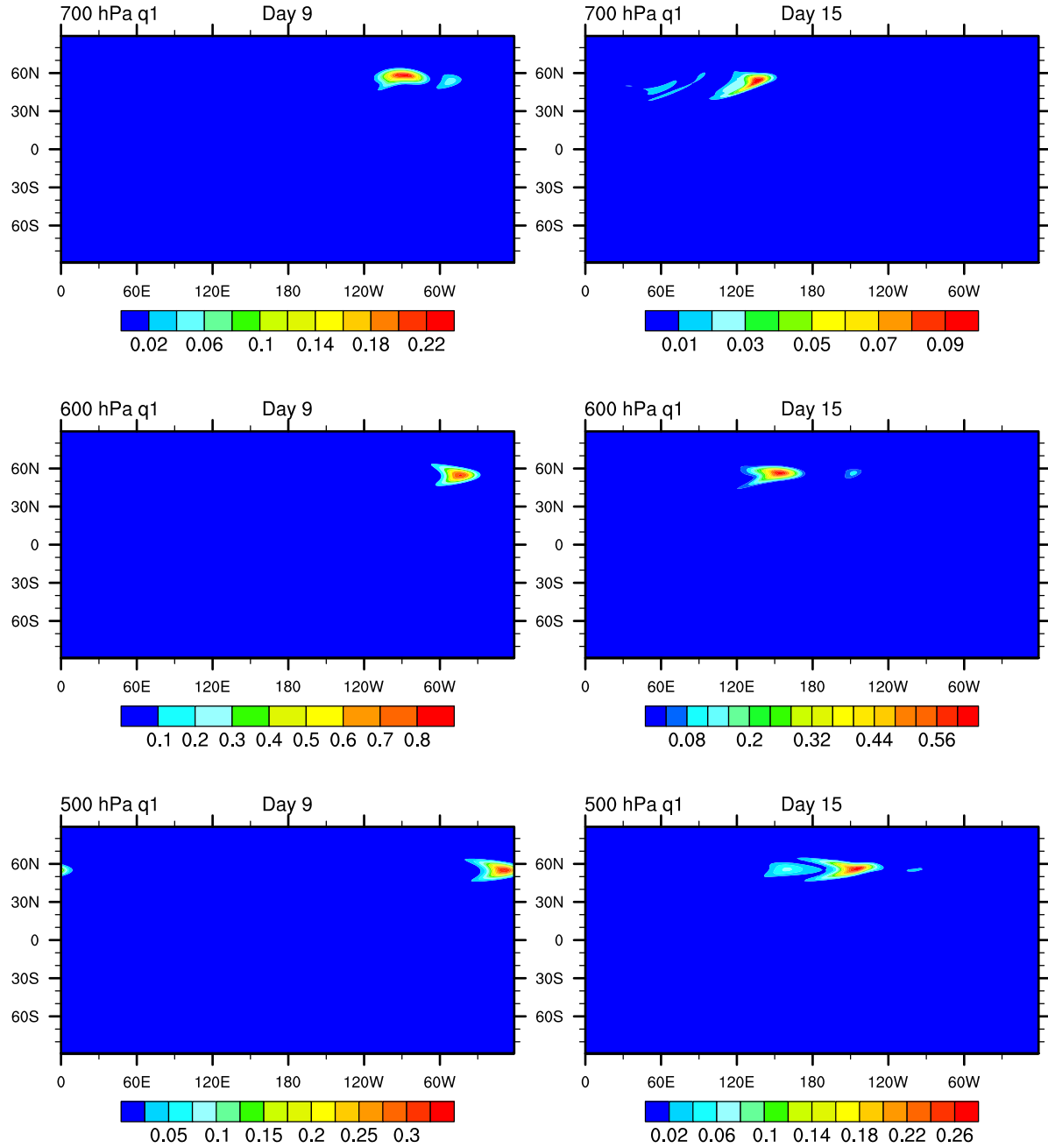
euiT106L26 2-0-1 bw, $\alpha = 0$

Figure 6: [2-0-1] simulated with EULT106L26: Tracer distribution $q1$ at day 9 and day 15 at the pressure levels 700, 600 and 500 hPa. The flow orientation angle is $\alpha = 0$.
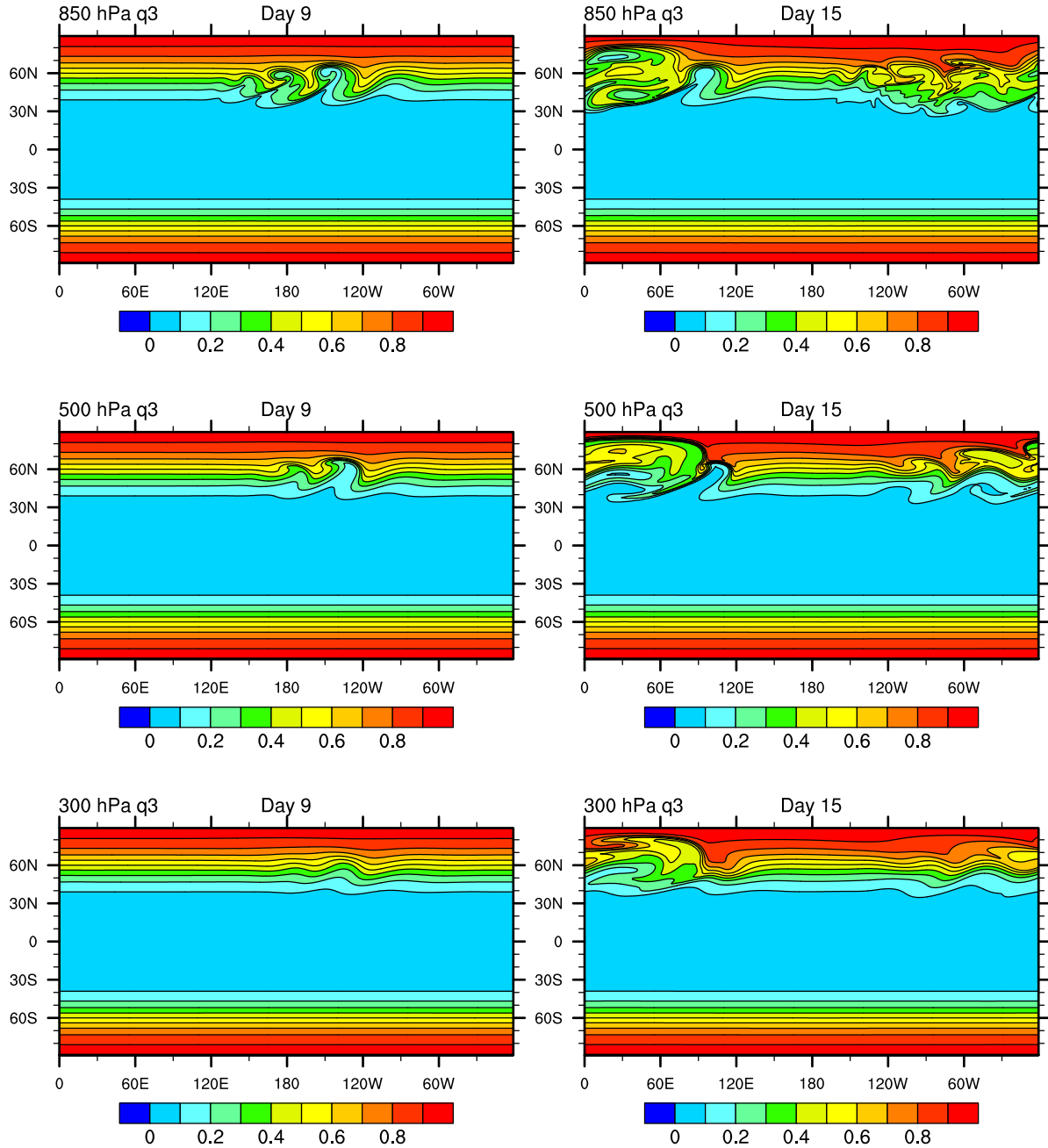
Figure 7: [2-0-3] simulated with EULT106L26: Tracer distribution $q3$ at day 9 and day 15 at the pressure levels 850, 500 and 300 hPa. The flow orientation angle is $\alpha = 0$.
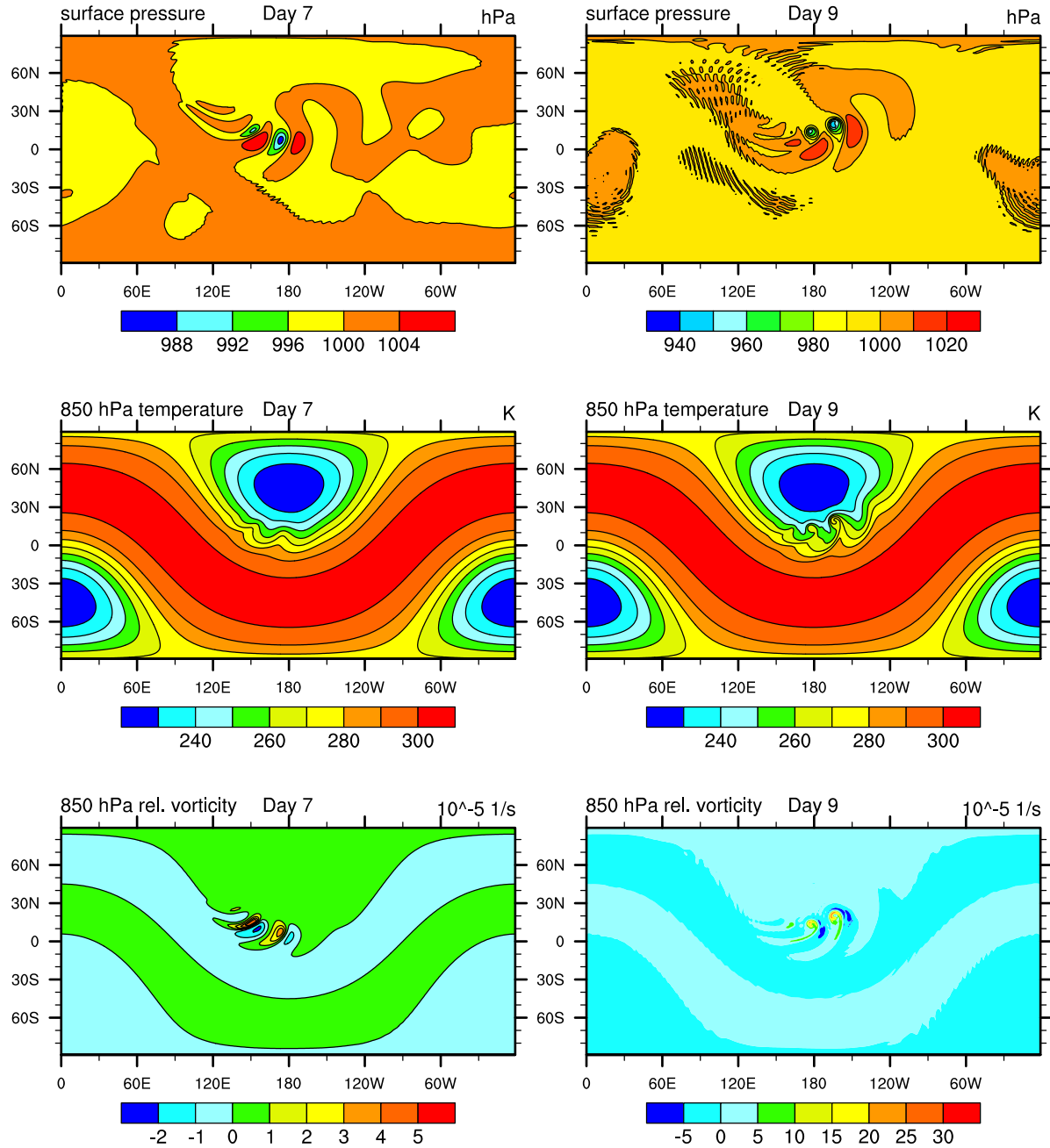
eulT106L26 2-3-1234 bw, $\alpha = 45$

Figure 8: [2-3-y]: Baroclinic wave with flow orientation angle $\alpha = 45°$ simulated with EULT106L26: surface pressure (upper row), 850 hPa temperature (middle row) and 850 hPa relative vorticity at days 7 and 9.
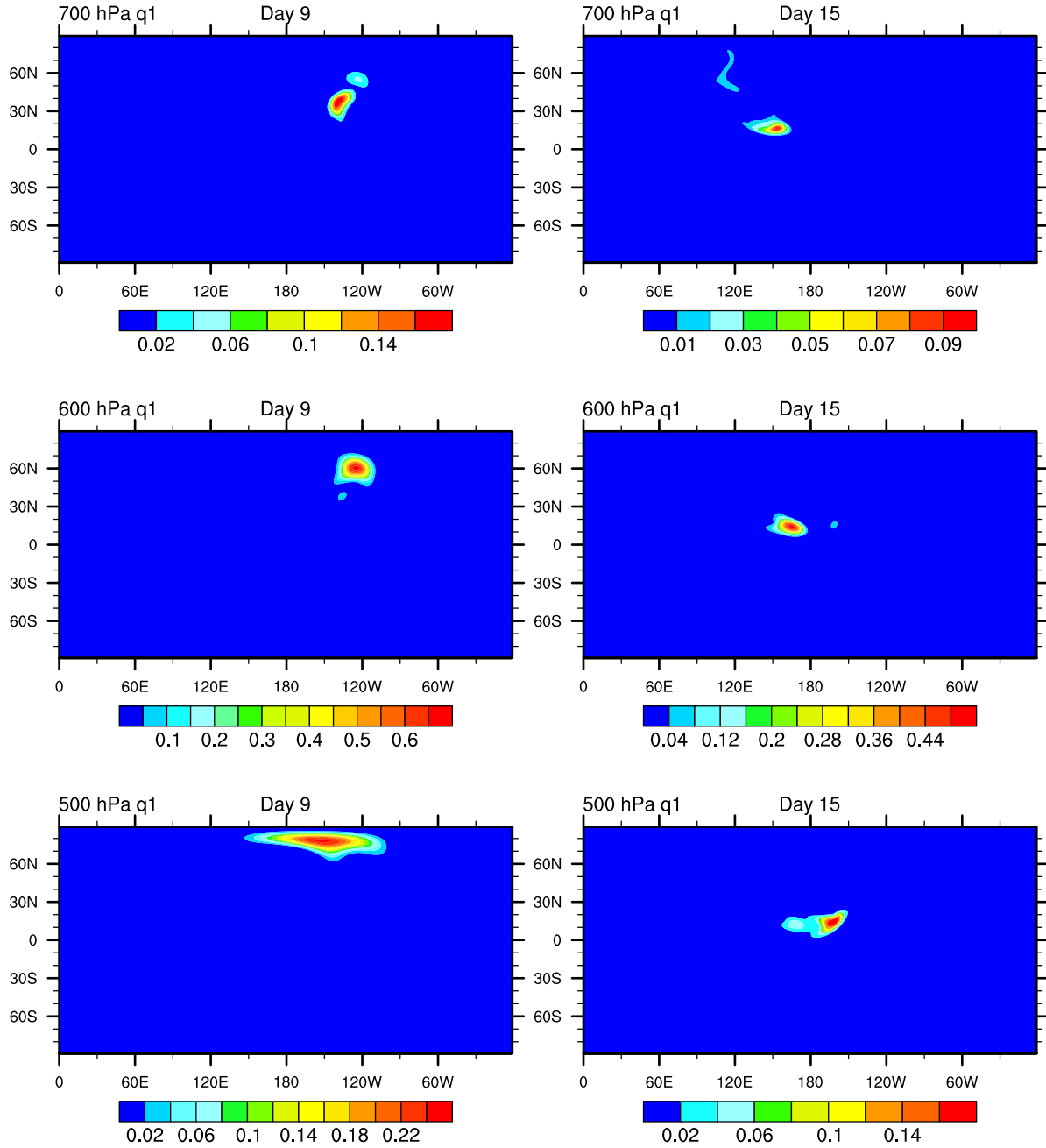
Figure 9: [2-3-1] simulated with EULT106L26: Tracer distribution $q1$ at day 9 and day 15 at the pressure levels 700, 600 and 500 hPa. The flow orientation angle is $\alpha = 45°$.

19

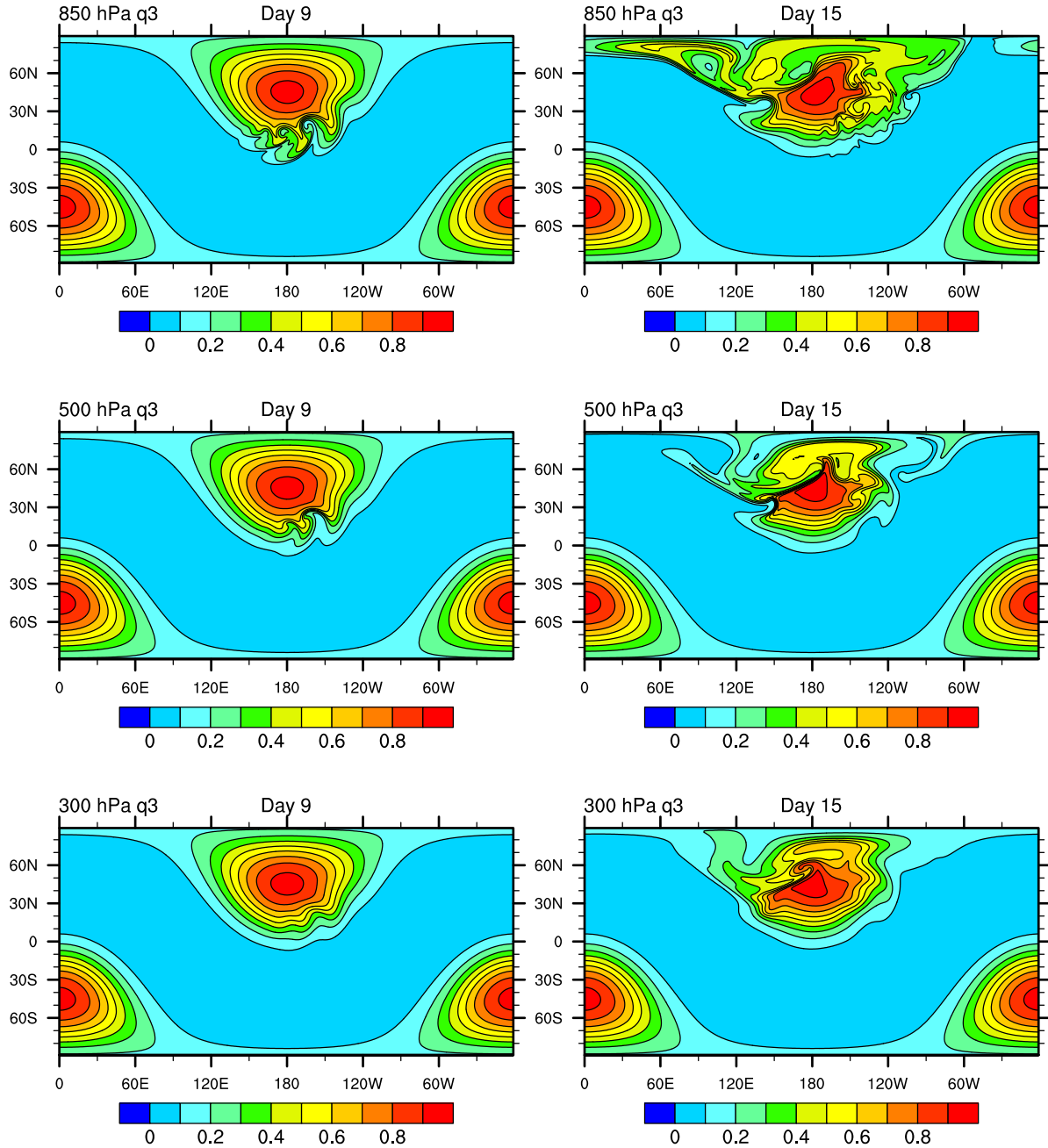# euIT106L26 2-3-3 bw, $\alpha = 45$

Figure 10: [2-3-3] simulated with EULT106L26: Tracer distribution $q3$ at day 9 and day 15 at the pressure levels 850, 500 and 300 hPa. The flow orientation angle is $\alpha = 45°$.
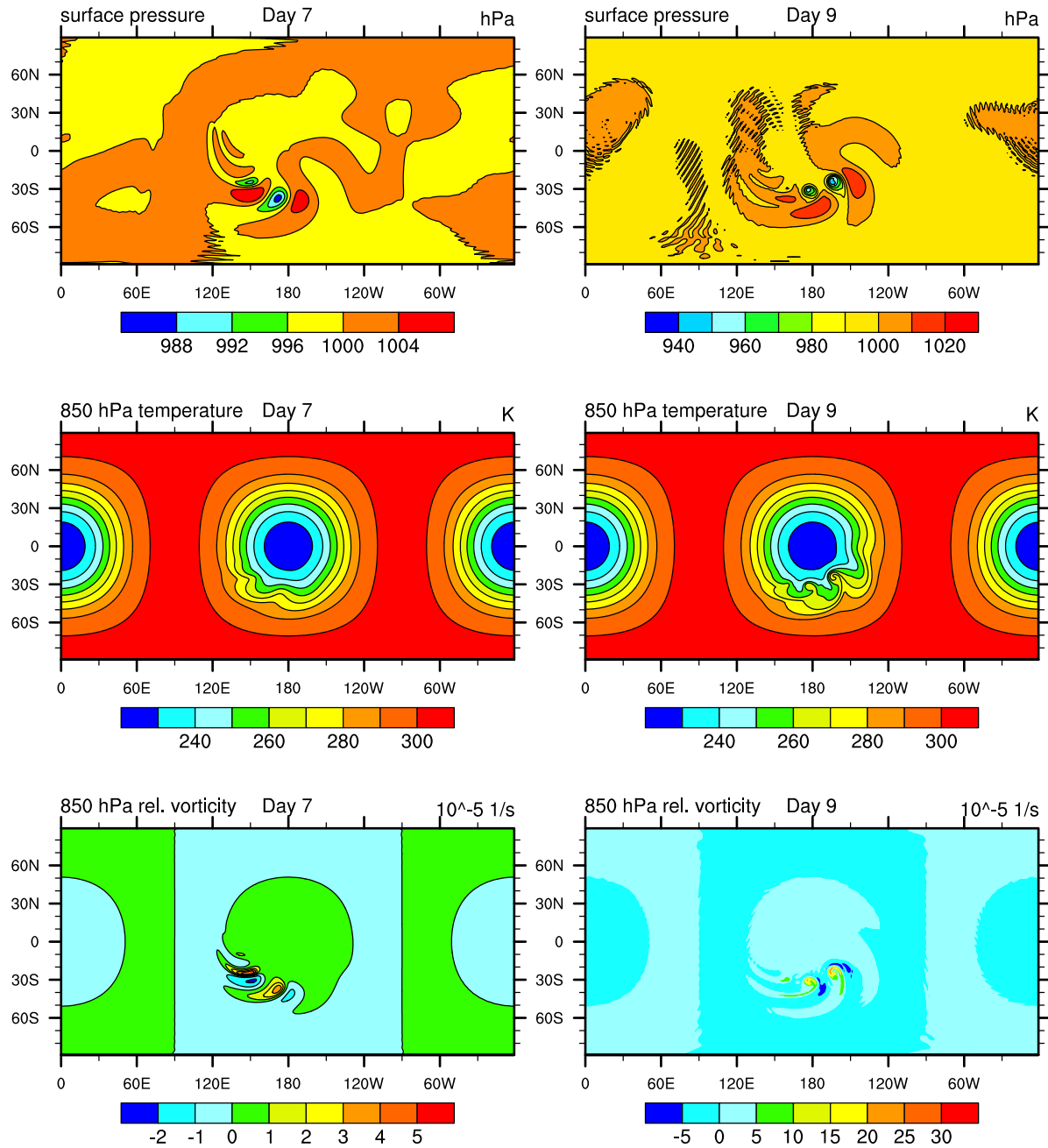
Figure 11: [2-6-y]: Baroclinic wave with flow orientation angle $\alpha = 90°$ simulated with EULT106L26: surface pressure (upper row), 850 hPa temperature (middle row) and 850 hPa relative vorticity at days 7 and 9.
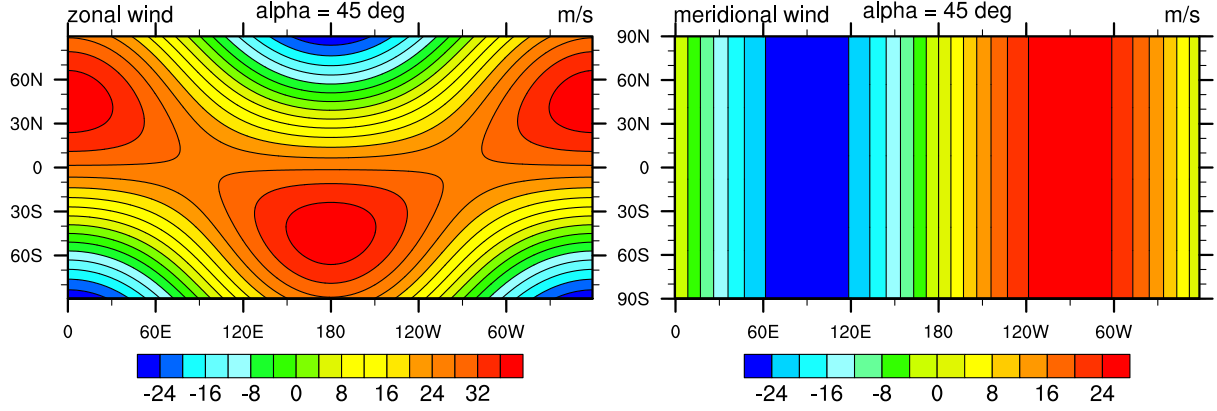
Figure 12: [3-3-y]: Prescribed zonal wind u (left) and meridional wind v (right) with the flow orientation angle $\alpha = 45°$.

The prescribed wind fields in hybrid vertical coordinates are

$$u(\lambda, \varphi, \eta) = u_0 \left(\cos \varphi \, \cos \alpha + \sin \varphi \, \cos \lambda \, \sin \alpha \right) \tag{30}$$

$$v(\lambda, \varphi, \eta) = -u_0 \, \sin \lambda \, \sin \alpha \tag{31}$$

$$\dot{\eta}(\lambda, \varphi, \eta, t) = \frac{\omega_0}{p_0} \, \cos \left(\frac{2\pi}{\tau} \, t \right) \sin \left(s(\eta) \frac{\pi}{2} \right) \tag{32}$$

with $u_0 = 2\pi a / (12 \text{ days})$ which is equivalent to $u_0 \approx 38.61$ m s^{-1}. The oscillation period is $\tau = 345600$ s which corresponds to 4 days. The maximum vertical pressure velocity ω_0 is set to $\omega_0 = \pi \, 4 \times 10^4 \text{Pa}/\tau$ which yields $\omega_0 \approx 0.3636$ Pa/s. This value corresponds to a few cm/s. The shape function is

$$s(\eta) = \min \left[1, 2 \sqrt{\sin \left(\frac{\eta - \eta_{top}}{1 - \eta_{top}} \, \pi \right)} \right]. \tag{33}$$

The horizontal velocities are time-invariant and were also prescribed for shallow water advection tests in Williamson et al. (1992). As before, $\alpha \in [0, \pi/2]$ is the flow orientation angle. Two examples of the horizontal velocities are shown in Figs. 12 and 13. They depict the zonal and meridional wind fields with the flow orientation angle $\alpha = 45°$ and $\alpha = 90°$.

The vertical velocity is time-dependent and kept uniform throughout the majority of the vertical domain. However, the vertical velocity profile is forced to approach zero at the upper and lower boundary which guarantees mass conservation. The surface pressure is uniform and set to $p_0 = 1000$ hPa. The atmosphere is isothermal with $T_0 = 300$ K. The latter determines the scale height $H = R_d T_0 / g \approx 8.78$ km which is used to transform the vertical velocity to height-based coordinate systems. The vertical velocity describes a wave-like trajectory in the vertical direction with a period of four days. For models with σ-, pressure or height coordinates
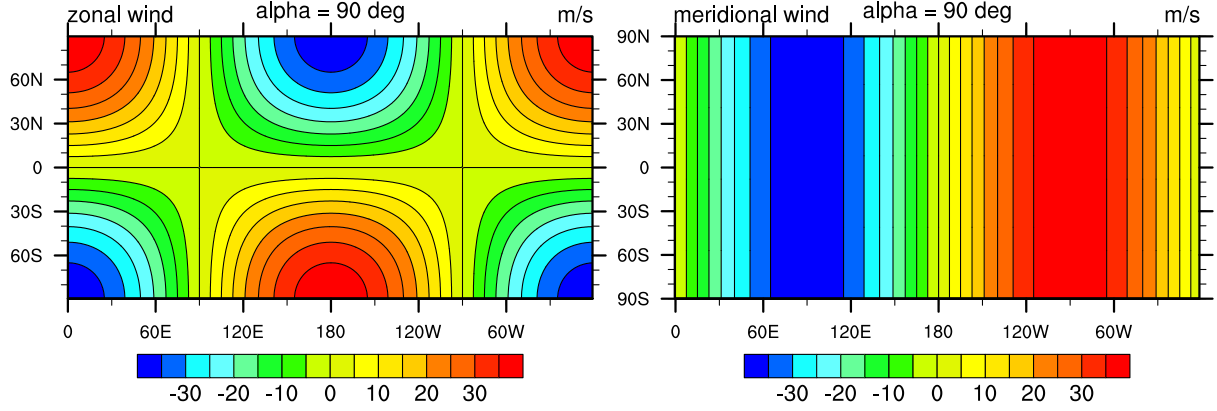
Figure 13: [3-6-y]: Prescribed zonal wind u (left) and meridional wind v (right) with the flow orientation angle $\alpha = 90°$.

the vertical velocity becomes

$$\dot\sigma(\lambda, \varphi, \sigma, t) = \frac{d\sigma}{dt} = \dot\eta(\lambda, \varphi, \eta, t) \tag{34}$$

$$\omega(\lambda, \varphi, p, t) = \frac{dp}{dt} = \omega_0 \, \cos\left(\frac{2\,\pi}{\tau} \, t\right) \sin\left(s(p) \, \frac{\pi}{2}\right) \tag{35}$$

$$w(\lambda, \varphi, z, t) = \frac{dz}{dt} = -\frac{H}{p(z)} \, \omega(\lambda, \varphi, p(z), t) \tag{36}$$

with

$$p(z) = p_0 \, \exp\left(-\frac{z}{H}\right) \tag{37}$$

This pressure profile is equivalent to the height levels

$$z = H \ln\left(\frac{p_0}{p}\right) \tag{38}$$

The shape function s in pressure coordinates becomes

$$s(p) = \min\left[1, 2\,\sqrt{\sin\left(\frac{p - p_{top}}{p_0 - p_{top}} \, \pi\right)}\,\right]. \tag{39}$$

This shape function is mostly identical to unity and drops to zero at the model top above $p = 315$ hPa (≈ 10.14 km) and model bottom below $p = 940$ hPa (≈ 540 m). The tracers approximately cover the area between $897 - 357$ hPa during the transport unless diffusion and numerical effects broaden the edges in the vertical direction. The initial setup renders the velocity field non-divergent in the vicinity of the tracer for pressure-based vertical coordinates. However, the velocity field is divergent for models in height coordinates. If an advection scheme for the tracer q utilize the conservation form

$$\frac{\partial}{\partial t}\big(\rho\,q\big) + \nabla \cdot \big(\vec v \, \rho \, q\big) = 0 \tag{40}$$

23

the following discrete algorithm is recommended to prescribe the pressure p and thereby the density ρ. First, we recommend calculating the pressure values $p(t_2)$ at the future time $t_2 = t_1 + \Delta t$ where Δt symbolizes the time step length and t_1 is the current time counted in seconds since the start of the advection test. The new pressure values are given by

$$p(t_2) = p(t_1) + \Delta t \, \omega_0 \, \cos\left[\frac{2\pi}{\tau}\left(t_1 + \frac{\Delta t}{2}\right)\right] \sin\left(s(p(t_1))\frac{\pi}{2}\right) \tag{41}$$

where a time-centered evaluation of the cos-expression is selected. The time dependent density can then be computed via the ideal gas law

$$\rho(t) = \frac{p(t)}{R_d \, T_0} \tag{42}$$

with constant temperature T_0.

This wind field transports the tracer once around the sphere and reaches its initial position after 12 days. During the revolution the tracer undergoes three wave cycles in the vertical direction. The initital distribution serves as the analytic solution after 12 days. This allows the computation of error norms and thereby an assessment of the numerical diffusion of the transport scheme.

Two tracer distributions are suggested. The first is a smooth distribution given by

$$q5(\lambda, \varphi, z) = \frac{1}{2}\left(1 + \cos(\pi \, d_1)\right) \tag{43}$$

with the ellipse-like function

$$d_1 = \min\left[1, \left\{\left(\frac{r}{R}\right)^2 + \left(\frac{z - z_0}{Z}\right)^2\right\}\right]. \tag{44}$$

As before, r denotes the great circle distance

$$r = a \, \arccos\left(\sin\varphi_c \, \sin\varphi + \cos\varphi_c \, \cos\varphi \, \cos(\lambda - \lambda_c)\right) \tag{45}$$

with center position $(\lambda_c, \varphi_c) = (3\pi/2, 0)$. The vertical center is set to $z_0 = 4.5$ km and the horizontal and vertical half widths are chosen to be $R = a/3$ and $Z = 1$ km. a symbolizes the Earth's radius.

The second tracer field resembles a slotted ellipse with sharp edges. Such a profile challenges the numerical design of the transport schemes since over- and undershoots are likely to occur in non-monotonic advection algorithms. The slotted ellipse is given by

$$q6(\lambda, \varphi, \eta) = \begin{cases} 1 & \text{if } d_2 \leq 1 \\ 0 & \text{if } d_2 > 1 \end{cases} \tag{46}$$

with

$$d_2 = \left(\frac{r}{R}\right)^2 + \left(\frac{z - z_0}{Z}\right)^2 \tag{47}$$

with the same parameters as above. The slot is cut out of the ellipse by the additional condition

$$q6 = 0 \quad \text{if} \quad z > z_0 \quad \text{and} \quad \varphi_c - \frac{1}{8} < \varphi < \varphi_c + \frac{1}{8} \tag{48}$$
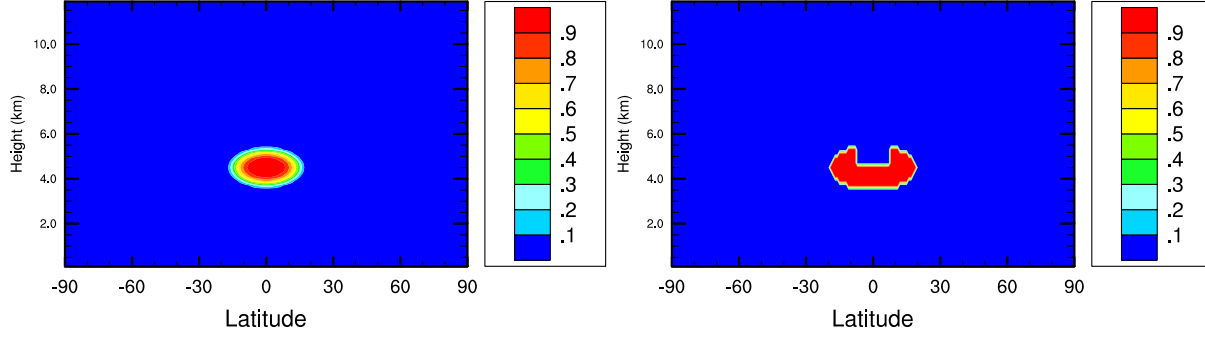
Figure 14: Latitude-height cross sections of the tracer fields $q5$ (left) and $q6$ (right) at the longitudinal position $\lambda = 3\pi/2$.

The two initial tracer distributions are shown in Fig. 14. It depicts a latitude-height cross section at $\lambda = 3\pi/2$ of the tracer fields $q5$ and $q6$. Figure 15(a) shows the trajectory of the center position of the tracer fields in the vertical direction. The tracer distributions follow the wave motion and undergo three oscillations in the vertical direction until day 12. The figure also depicts the time variation of the vertical velocities (b) ω and (c) $\dot{\eta}$. Recall that a positive ω velocity corresponds to a downward motion in height coordinates.

1.3.1 Resolution, output data and analysis

We recommend using an equidistant $\Delta z = 200$ m spacing of the vertical levels with the lower and upper boundary (interface) positions $z_0 = 0$ m and $z_{top} = 12$ km. This choice leads to 60 model levels with 61 model interfaces. They can be translated into a pressure-based system via $p(z) = p_0 \exp\left(-z/H\right)$ with scale height H. The σ-levels are

$$\sigma(z) = \frac{p(z) - p(z_{top})}{p_s - p(z_{top})}. \tag{49}$$

For hybrid vertical coordinate systems like

$$p(\eta) = A(\eta)\, p_0 + B(\eta)\, p_s \tag{50}$$

we suggest using the hybrid coefficients A and B

$$A(\eta) = \eta - B(\eta) \tag{51}$$

$$B(\eta) = \left(\frac{\eta - \eta_{top}}{1 - \eta_{top}}\right) \tag{52}$$

for the level interfaces as defined by Laprise and Girard (1990). For $p_s = p_0$, the definitions are $\eta = p(z)/p_0$ and $\eta_{top} = p(z_{top})/p_0 \approx 0.254992$. This hybrid coordinate system is a variant of the one used by Simmons and Burridge (1981). It guarantees the conditions $p(\eta = \eta_{top}) = p_{top}$ and $p(\eta = 1) = p_s$ at the upper and lower interface boundaries. The hybrid coefficients at the full model levels can then be computed via the linear average

$$A_k = \frac{1}{2}\big(A_{k+1/2} + A_{k-1/2}\big), \tag{53}$$

$$B_k = \frac{1}{2}\big(B_{k+1/2} + B_{k-1/2}\big) \tag{54}$$

a) Trajectory of the tracer (center position)

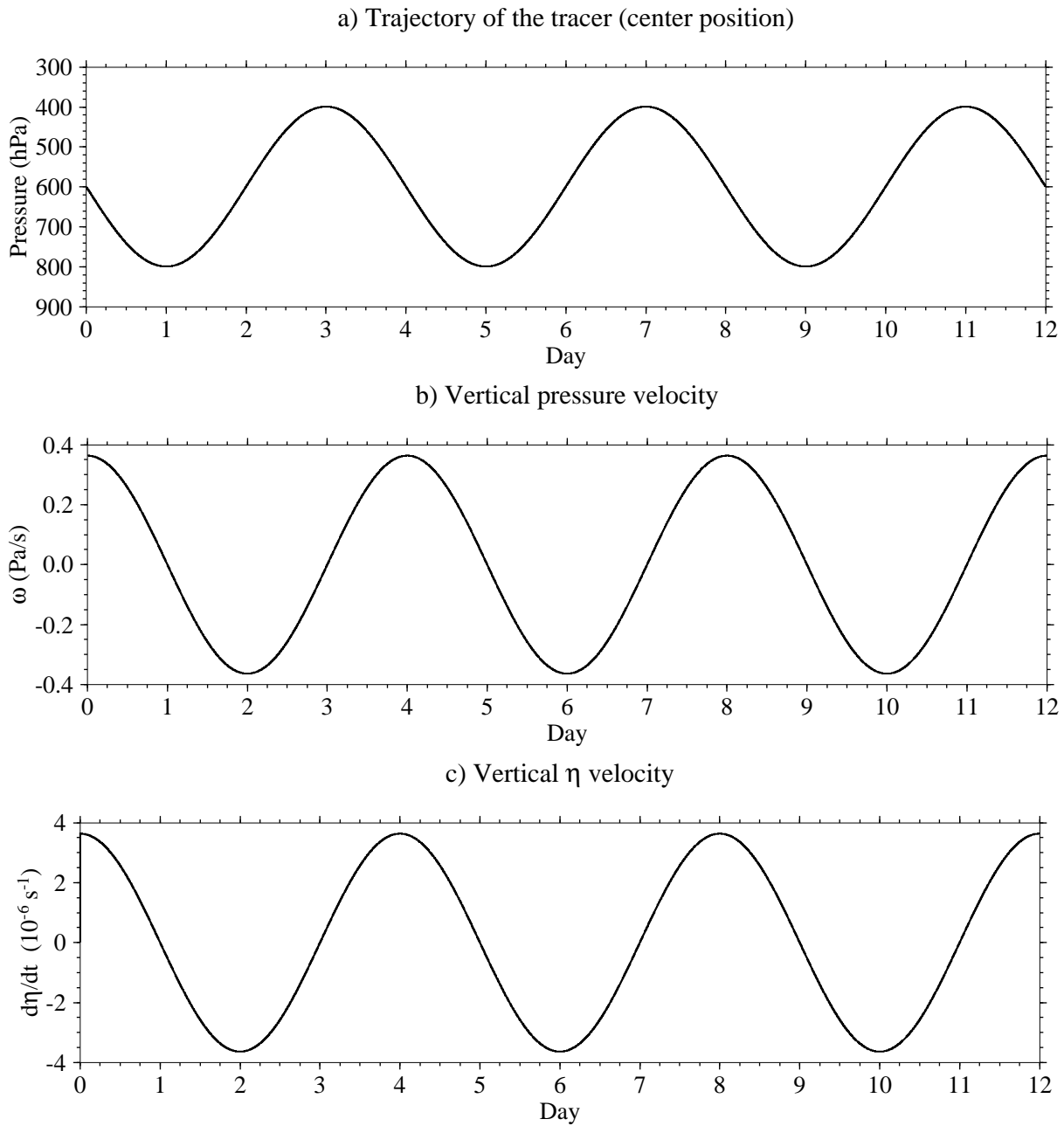## b) Vertical pressure velocity

c) Vertical η velocity

Figure 15: Time series of the (a) tracer trajectory, (b) vertical pressure velocity ω and (c) vertical velocity in the hybrid coordinate system $\dot{\eta}$.

where the index k denotes the discrete full model level which is surrounded by the two interface levels shown with half indices. The linear average guarantees that vertical differencing operations conserve energy. Note that some models (Majewski et al. 2002) use the alternative definition of Eq. (50)

$$p(\eta) = A(\eta) + B(\eta)\,p_s. \tag{55}$$

Then Eq. (51) is represented by $A(\eta) = p_0[\eta - B(\eta)]$.

We suggest running the pure advection test case for one revolution (12 days) at an approximately $1° \times 1°$ horizontal resolution with 60 model levels. The horizontal resolution corresponds to 180×361 grid points in the latitudinal and longitudinal directions if including the pole points. The longitudes should start at position $\lambda = 0$. Additional higher or lower horizontal and vertical resolutions might also be used to test the sensitivity of the results to the resolutions. In particular, a model run with only 30 model levels ($\Delta z = 400$ m) might be valuable since GCMs typically have very low vertical resolutions.

The flow orientation angles are $\alpha = 0$, $\alpha = \pi/4$ and $\alpha = \pi/2$. The output data are 6-hourly snapshots of the tracer fields $q5$ and $q6$ on model levels which results in a total of 49 time stamps (including the initial state) for the 12-day forecast period.

For the flow orientation angle $\alpha = 0$ the analysis of the model run concentrates on

1. longitude-height cross sections of the $q5$ and $q6$ contours at the equator ($\varphi = 0$) at days 0, 3, 6, 9 and 12.

2. latitude-height cross sections of the $q5$ and $q6$ contours at day 0 ($\lambda = 270°$), day 3 ($\lambda = 0°$), day 5 ($\lambda = 60°$), day 6 ($\lambda = 90°$), day 9 ($\lambda = 180°$) and day 12 ($\lambda = 270°$).

For the flow orientation angle $\alpha = \pi/4$ the analysis of the model run concentrates on

1. longitude-height cross sections of the $q5$ and $q6$ contours at day 0 ($\varphi = 0$), day 3 ($\varphi = \pi/4$), day 6 ($\varphi = 0$), day 9 ($\varphi = -\pi/4$) and day 12 ($\varphi = 0$).

2. latitude-height cross sections of the $q5$ and $q6$ contours at day 0 ($\lambda = 270°$), day 3 ($\lambda = 0°$), day 6 ($\lambda = 90°$), day 9 ($\lambda = 180°$) and day 12 ($\lambda = 270°$).

For the flow orientation angle $\alpha = \pi/2$ the analysis of the model run concentrates on

1. longitude-height cross sections of the $q5$ and $q6$ contours at day 0 ($\varphi = 0$), day 3 ($\varphi = \pi/2$), day 6 ($\varphi = 0$), day 9 ($\varphi = -\pi/2$) and day 12 ($\varphi = 0$).

2. latitude-height cross sections of the $q5$ and $q6$ contours at days 0 and 3 ($\lambda = 270°$), days 5, 6 and 7 ($\lambda = 90°$), and day 12 ($\lambda = 270°$).

In addition, we recommend plotting the following fields for all three rotation angles:

1. latitude-longitude cross section of $q5$ and $q6$ at position $z_0 = 4.5$ km at days 0 and 12.

2. normalized l_1, l_2 and l_∞ error norms after 12 days.

3. optional: time sequence of the $q5$ and $q6$ fields in 3D at days 0, 1, 3, 5, 6, 7, 9 and 12.

Define I to be the discrete approximation to the global integral

$$I(q) = \frac{1}{4\,\pi\,(\eta_s - \eta_{top})} \int_{\eta_{top}}^{\eta_s} \int_0^{2\pi} \int_{-\pi/2}^{\pi/2} q(\lambda, \varphi, \eta)\ \cos\varphi\, d\varphi\, d\lambda\, d\eta \qquad (56)$$

that is consistent with the numerical scheme implemented in the dynamical core. Then the normalized error norms of the tracer field q are

$$l_1(q) = \frac{I[\,|q(\lambda, \varphi, \eta) - q_T(\lambda, \varphi, \eta)|\,]}{I[\,|q_T(\lambda, \varphi, \eta)|\,]} \qquad (57)$$

$$l_2(q) = \frac{\left\{ I\big[\, \big(q(\lambda, \varphi, \eta) - q_T(\lambda, \varphi, \eta)\big)^2\big]\right\}^{1/2}}{\left\{ I\big[\, q_T(\lambda, \varphi, \eta)^2\big]\right\}^{1/2}} \qquad (58)$$

$$l_\infty(q) = \frac{\max_{all\ \lambda, \varphi, \eta} |q(\lambda, \varphi, \eta) - q_T(\lambda, \varphi, \eta)|}{\max_{all\ \lambda, \varphi, \eta} |q_T(\lambda, \varphi, \eta)|} \qquad (59)$$

where q_T indicates the analytic solution. After 12 days the tracers return to their initial position and the initial state serves as the analytic solution.

1.4 3D Rossby-Haurwitz wave

The Rossby-Haurwitz (RH) wave test case is a 3D extension of the 2D shallow water RH wave discussed in Williamson et al. (1992). The 2D test was originally proposed by Phillips (1959) and later extended to three dimensions by Monaco and Williams (1975). The 3D extensions are also described in Wan (2008) and Giraldo and Rosmond (2004). Note that the latter reference contains a few inaccuracies. The main differences between the 2D shallow water formulation and the 3D extension are the introduction of a temperature field and the derivation of the surface pressure. All other equations are identical to Williamson et al. (1992). The Rossby-Haurwitz wave is an analytical solution of the barotropic vorticity equation and approximately preserves its shape even in nonlinear shallow water and primitive equation models. Therefore, it has become a de facto standard for shallow water tests. In 3D hydrostatic dynamical cores the model response mainly remains barotropic. It reveals the diffusion and conservation characteristics over the forecast period.

The initial velocity field is nondivergent and defined via the streamfunction

$$\psi(\lambda, \varphi) = -a^2\, M\, \sin\varphi + a^2\, K\, \cos^n\varphi\ \sin\varphi\ \cos(n\,\lambda) \qquad (60)$$

where a symbolizes the Earth's radius and n denotes the wave number, here set to $n = 4$. In addition, the parameters $M = K = u_0/(n\,a)$ with $u_0 = 50$ m s^{-1} are chosen which yields $M = K \approx 1.962 \times 10^{-6}$ s^{-1}. For nondivergent barotropic models Haurwitz (1940) showed that this streamfunction moves in the zonal direction without change of shape with an angular velocity of

$$\nu = \frac{n(3+n)M - 2\,\Omega}{(1+n)\,(2+n)}. \qquad (61)$$

The parameter choices for n and M determine whether the Rossby-Haurwitz wave moves eastward (+) or westward (-). Using the parameters above and the Earth's angular velocity Ω

Eq. (61) yields a westward propagation. The time period $\tau = 2\pi/\nu$ for a full revolution around the sphere is approximately 24 days which corresponds to a propagation speed of about $-15.2°$ day^{-1}. This value is approximate for 3D hydrostatic flows as shown by Wan (2008).

The horizontal velocity components are vertically uniform and given by

$$u(\lambda, \varphi, \eta) = a\, M\, \cos\varphi + a\, K\, \cos^{n-1}\varphi\, \cos(n\,\lambda)\,(n\,\sin^2\varphi - \cos^2\varphi) \tag{62}$$
$$v(\lambda, \varphi, \eta) = -a\, K\, n\, \cos^{n-1}\varphi\, \sin\varphi\, \sin(n\,\lambda)\,. \tag{63}$$

This results in the vorticity distribution

$$\zeta(\lambda, \varphi, \eta) = 2\, M\, \sin\varphi - K\, \sin\varphi\, \cos^n\varphi\, \cos(n\,\lambda)\,(n^2 + 3n + 2) \tag{64}$$

The vertical velocity vanishes. The temperature profile $T = T_0 - \Gamma\, z$ is characterized by a linear decrease with height. The lapse rate is set to $\Gamma = 0.0065$ K m^{-1} which mimics the moist-adiabatic lapse rate in the atmosphere. The temperature T_0 is set to 288 K. Substituting the temperature profile into the hydrostatic approximation $\partial p/\partial z = -\rho g$ yields the expression

$$z = \frac{T_0}{\Gamma}\left(1 - \left(\frac{p}{p_{ref}}\right)^{\frac{\Gamma R_d}{g}}\right) \tag{65}$$

for the *equivalent* height z. Note that z does not represent the geopotential height. The reference pressure is set to $p_{ref} = 955$ hPa which also determines the surface pressure at both pole points. The pole points are anchored at the equivalent height $z = 0$ m. The height (65) transforms the temperature profile into a pressure-based vertical coordinate system. In particular, it becomes

$$T(p) = T_0 \left(\frac{p}{p_{ref}}\right)^{\frac{\Gamma R_d}{g}} \tag{66}$$

where the pressure p is given by

$$p(\lambda, \varphi, \sigma) = \sigma\,[p_s(\lambda, \varphi) - p_{top}] + p_{top} \tag{67}$$
$$p(\lambda, \varphi, \eta) = A(\eta)\, p_0 + B(\eta)\, p_s(\lambda, \varphi) \tag{68}$$

for models with σ- and η-coordinates. Both expressions utilize the surface pressure p_s that can be derived via a second integration of the hydrostatic relationship with the temperature profile (66). The integration yields

$$p_s(\lambda, \varphi) = p_{ref}\left(1 + \frac{\Gamma}{g\, T_0}\Phi(\lambda, \varphi, \eta = 1)\right)^{\frac{g}{\Gamma R_d}}. \tag{69}$$

where the geopotential $\Phi = gz = \bar{\Phi}(\eta) + \Phi'(\lambda, \varphi)$ is comprised of a mean horizontal state $\bar{\Phi}(\eta)$ and a perturbation $\Phi'(\lambda, \varphi)$. It is obtained from Eq. (60) by solving a balance equation that forces the initial time tendency of the divergence to be zero. A flat surface elevation with $\bar{z}(\eta = 1) = z_s = 0$ m is selected. It yields the constant surface geopotential $\Phi_s = 0$ m^2 s^{-2} which eliminates the influence of $\bar{\Phi}(\eta = 1)$ at the surface. The surface pressure equation (69) becomes

$$p_s(\lambda, \varphi) = p_{ref}\left(1 + \frac{\Gamma}{g\, T_0}\Phi'(\lambda, \varphi)\right)^{\frac{g}{\Gamma R_d}} \tag{70}$$
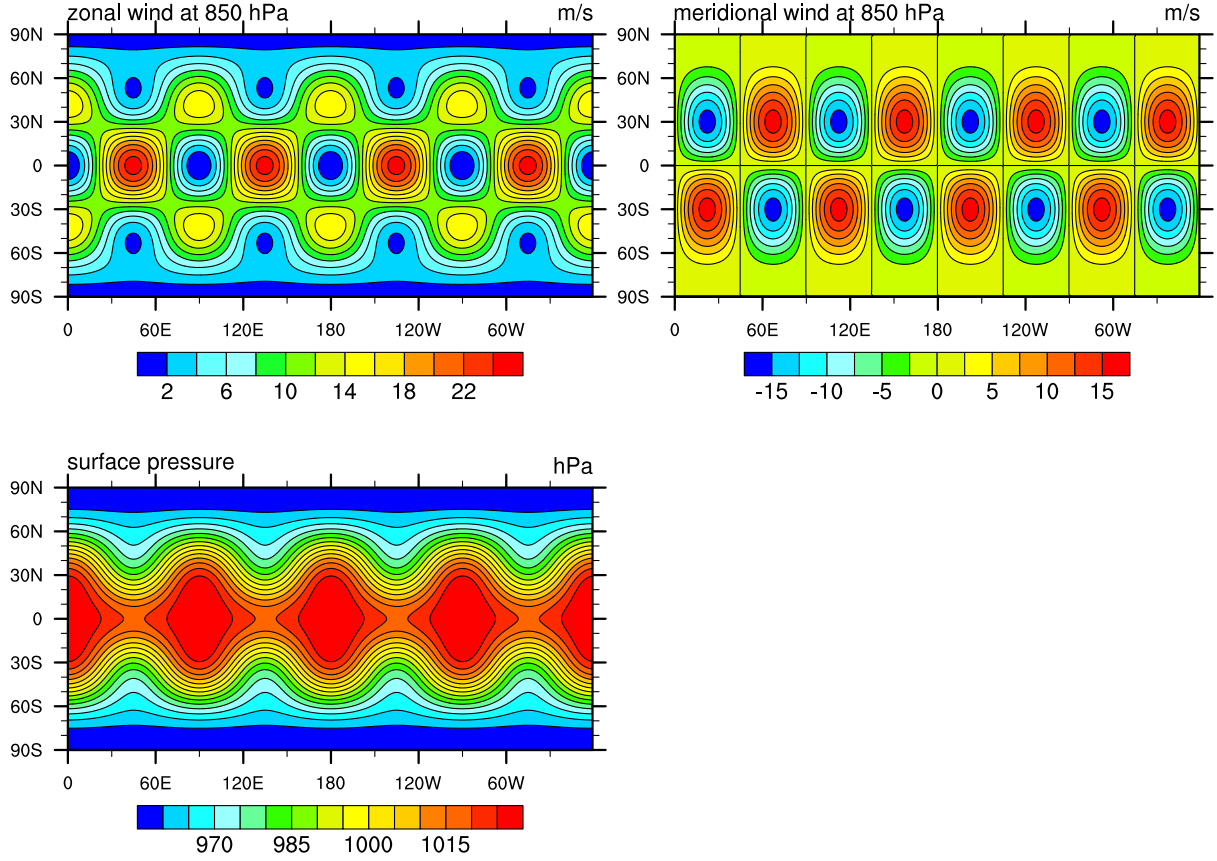
Figure 16: Initial conditions for the Rossby-Haurwitz wave: 850 hPa zonal wind u (top left), 850 hPa meridional wind v (top right) and surface pressure p_s (bottom right).

with

$$\Phi'(\lambda, \varphi) = a^2\, A(\varphi) + a^2\, B(\varphi)\, \cos(n\lambda) + a^2\, C(\varphi)\, \cos(2n\lambda). \tag{71}$$

The coefficients are defined by

$$A(\varphi) = \frac{M\,(2\,\Omega + M)}{2}\, \cos^2\varphi + \frac{K^2}{4}\, \cos^{2n}\varphi\, \left[(n+1)\, \cos^2\varphi + (2\,n^2 - n - 2)\right]$$

$$- \frac{n^2\, K^2}{2}\, \cos^{2(n-1)}\varphi \tag{72}$$

$$B(\varphi) = \frac{2(\Omega + M)\, K}{(n+1)(n+2)}\, \cos^n\varphi\, \left[(n^2 + 2n + 2) - (n+1)^2\, \cos^2\varphi\right] \tag{73}$$

$$C(\varphi) = \frac{K^2}{4}\, \cos^{2n}\varphi\, \left[(n+1)\, \cos^2\varphi - (n+2)\right] \tag{74}$$

The choice of $p_{ref} = 955$ hPa yields a horizontal mean surface pressure of about $\bar{p}_s \approx 1000.377$ hPa for the parameters M, K, n and u_0 given above. The mean value of the surface pressure might be important for models with mass fixers. The initial data are shown in Fig. 16. The figure depicts the 850 hPa zonal and meridional wind and the surface pressure p_s.

1.4.1   Resolution, output data and analysis

We recommend running the Rossby-Haurwitz test case for 30 days at an approximately $1° \times 1°$ horizontal resolution with 26 vertical levels as outlined in Appendix C. This horizontal resolution corresponds to 181×360 grid points in the latitudinal and longitudinal directions if including the pole points. If height-based vertical coordinates are used the model top must lie below $z_{top} = T_0/\Gamma = 44.307$ km.

The output data are daily snapshots of the fields U, V, OMEGA, T, PS, PHIS and Z3 (if available) on model levels. In addition, the output variables T850, T300, U850, U200, V850, V200, OMEGA850, OMEGA500 and Z500 should be selected (if available). The analysis of the model run concentrates on

1. 500 hPa geopotential height Z500 contours at days 5, 10, 15 and 30 on an equidistant cylindrical latitude-longitude map.

2. U, V, T and the OMEGA fields at $p = 850$ hPa at days 5, 10, 15 and 30 on equidistant cylindrical latitude-longitude maps. The contour spacings are 4 m s $^{-1}$ for U and V, and 0.1 K for T.

3. equidistant cylindrical latitude-longitude map of PS at day 5, 10, 15 and 30. The contour spacing is 10 hPa.

4. time series of the domain integrated total energy (see Appendix F). Plot the energy difference between the daily (or more frequent) output and the initial state. In addition, quantify the final energy loss or gain in percent (normalized energy difference).

5. evaluation of the Rossby-Haurwitz wave without explicit horizontal diffusion (if applicable). Are the simulations computationally stable?

6. effects of enhanced explicit diffusion near the model top (if applicable). Plot U, V, T at the second model level ($p \approx 7.3$ hPa) on equidistant cylindrical latitude-longitude maps.

7. the symmetry of the wave in the Northern and Southern hemisphere.

8. whether the wave breaks down over the 30-day forecast period and if yes when?

The geopotential height is given by

$$\int_{z_s}^{z} dz' = -\frac{R_d}{g} \int_{p_s}^{p} T d(\ln p') \tag{75}$$

which can be approximated in the discrete system as

$$z_m = z_s + \frac{R_d}{g} \sum_{k=K_{max}}^{m} T_k \Delta(\ln p_k)$$

$$= z_s + \frac{R_d}{g} \sum_{k=K_{max}}^{m} T_k (\ln p_{k+1/2} - \ln p_{k-1/2}) \tag{76}$$

This expression results in the geopotential height z_m at level index $m < K_{max}$. The summation starts near the surface with maximum level number K_{max} with decreasing level index k in the

upward direction. The half-indices describe the interface levels. $z_s = \Phi_s/g$ is the surface elevation which is zero in this test case. For the computation of the geopotential height at a fixed pressure surface $p_{500} = 500$ hPa the summation over the full model levels stops at the interface level that lies just below p_{500}. This interface level is denoted by index $m + 1/2$. The remaining fractional contribution upward of interface level $m + 1/2$ is added via the last term in

$$z_p = z_s + \frac{R_d}{g} \sum_{k=K_{max}}^{m+1} \left[T_k (\ln p_{k+1/2} - \ln p_{k-1/2}) \right] + T_m (\ln p_{m+1/2} - \ln p_{500}). \qquad (77)$$

The 850 hPa wind velocities and temperature can be derived via a linear interpolation in $\ln p$ coordinates that takes the two surrounding model levels into account.

Snapshots of the output data at day 15 are presented in Fig. 17. The figure shows the 850 hPa zonal wind, meridional wind, temperature and vertical velocity fields as well as the 500 hPa geopotential height and surface pressure. These model results were computed with the CAM3.5.41 verison of the NCAR Finite Volume (FV) dynamical core at the resolution $1° \times 1°$ with 26 hybrid levels.

1.5   Mountain-induced Rossby wave train

The definition of the mountain-induced Rossby wave train closely resembles the description of the initial conditions by Tomita and Sato (2004). The main difference is the derivation of the surface pressure for hydrostatic conditions as considered here. The simulation starts from smooth isothermal initial conditions that are a balanced analytic solution to the primitive equations. They are also a solution to the non-hydrostatic shallow atmosphere equation set. An idealized mountain then triggers the evolution of a Rossby wave train over the course of 15 days. We recommend integrating the models until day 30 to investigate the further evolution of the circulation.

The horizontal wind components are prescribed as

$$u(\lambda, \varphi, \eta) = u_0 \cos \varphi \qquad (78)$$
$$v(\lambda, \varphi, \eta) = 0 \text{ m s}^{-1}. \qquad (79)$$

The amplitude of the zonal wind u_0 is set to 20 m s^{-1}, the vertical velocity vanishes. The temperature is isothermal and given by $T(\lambda, \varphi, \eta) = T_0 = 288$ K. This yields the constant Brunt-Väisälä frequency

$$N = \sqrt{\frac{g^2}{c_p T_0}} \approx 0.0182 \text{ s}^{-1}. \qquad (80)$$

The gravitational acceleration g and specific heat at constant pressure c_p are listed in Appendix G. An idealized bell-shape mountain is introduced via the surface geopotential

$$\Phi_s(\lambda, \varphi) = g z_s = g h_0 \exp \left[- \left(\frac{r}{d} \right)^2 \right] \qquad (81)$$

where $h_0 = 2000$ m determines the peak height of the mountain and $d = 1500$ km is the half width of the Gaussian mountain profile. As before, r is defined as the great circle distance

$$r = a \, \arccos \left[\sin \varphi_c \sin \varphi + \cos \varphi_c \cos \varphi \cos(\lambda - \lambda_c) \right] \qquad (82)$$
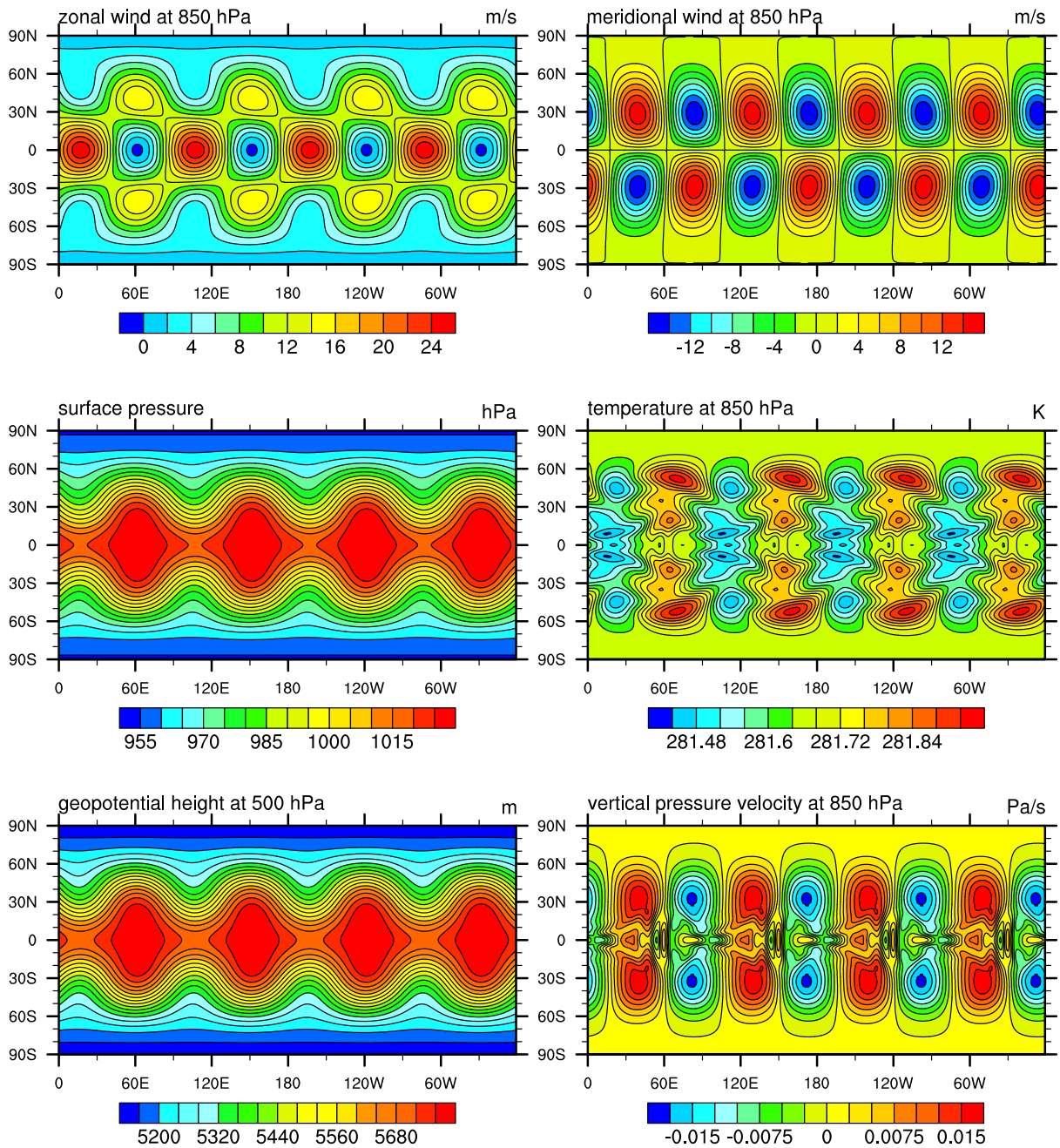
Figure 17: Snapshots of the Rossby-Haurwitz wave at day 15 simulated with FV181x360L26. Top row: 850 hPa zonal wind u and meridional wind v, middle row: surface pressure p_s and 850 hPa temperature T, bottom row: 500 hPa geopotential height and 850 hPa vertical pressure velocity ω.
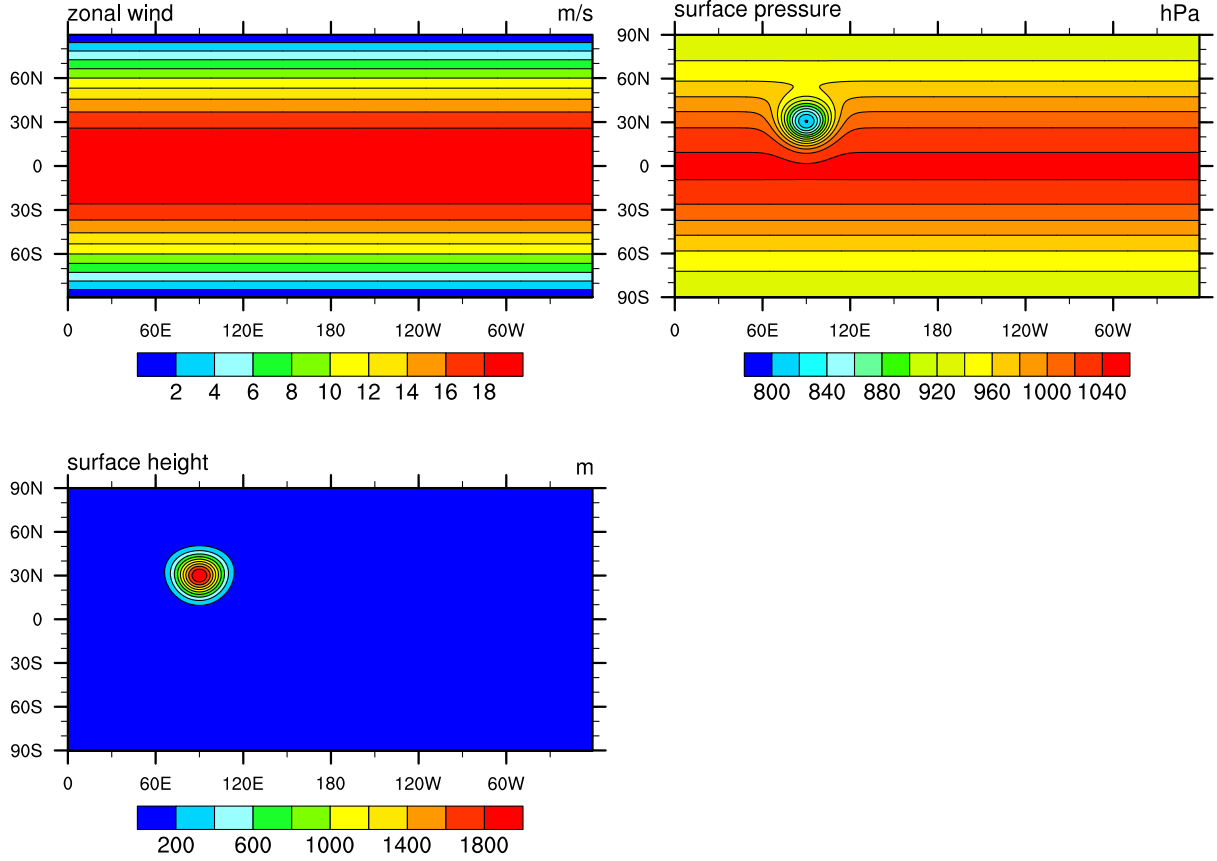
Figure 18: Initial conditions for the mountain induced Rossby wave: zonal wind u, surface pressure p_s and surface elevation z_s. The meridional wind v is zero, the temperature is isothermal with $T = 288$ K.

to the center point here selected to be in the midlatitudes with $(\lambda_c, \varphi_c) = (\pi/2, \pi/6)$. The surface pressure field balances the initial conditions. For hydrostatic primitive equation models it is defined as

$$p_s(\lambda, \varphi) = p_{sp} \exp\left[-\frac{a\,N^2\,u_0}{2\,g^2\,\kappa} \left(\frac{u_0}{a} + 2\,\Omega \right) (\sin^2 \varphi - 1) - \frac{N^2}{g^2\,\kappa} \Phi_s(\lambda, \varphi) \right] \qquad (83)$$

with $\kappa = 2/7$ and the Earth's radius a. p_{sp} denotes the surface pressure at the South Pole which is set to $p_{sp} = 930$ hPa. This choice of p_{sp} yields a horizontal mean surface pressure of about $\bar{p}_s \approx 1001.456$ hPa. The mean value of the surface pressure might be important for models with mass fixers. The initial conditions are depicted in Fig. 18 which shows the zonal wind, surface pressure and surface elevation.

The parameters N, d, h_0 and u_0 determine the physical characteristics of the mountain wave response. Non-hydrostatic effects can be measured by the ratio of the horizontal to the vertical wave lengths. The ratio is

$$\frac{N\,d}{u_0} = 1139.45 \gg 1 \qquad (84)$$

where the half width d represents a quarter wave length. The ratio greatly exceeds unity which separates the hydrostatic from the non-hydrostatic flow regimes. Therefore, the mountain wave

34

response is hydrostatic. In addition, the non-linear effects are measured by the gravity wave strength $N h$ normalized by the base state wind

$$\frac{N h}{u_0} = 1.82. \tag{85}$$

This is the inverse Froude number that is a more than twice the critical value of 0.85 for which a flow transition is expected. The mountain therefore triggers a nonlinear finite-amplitude wave response. At mid-levels it resembles the barotropic mountain wave train described in Williamson et al. (1992).

1.5.1 Resolution, output data and analysis

We recommend running the Rossby wave train test for 30 days at an approximately $1° \times 1°$ horizontal resolution with 26 vertical levels as outlined in Appendix C. This horizontal resolution corresponds to 181×360 grid points in the latitudinal and longitudinal directions if including the pole points.

The output data are daily snapshots of the fields U, V, OMEGA, T, PS, PHIS and Z3 on model levels. In addition, the output variables T300, U200, V200, OMEGA500, Z700, Z500 and Z300 should be selected (if available). The analysis of the model run concentrates on

1. U, V, T, OMEGA and geopotential height at 700 hPa km at days 5, 10, 15, 20 and 25 on equidistant cylindrical latitude-longitude maps. Contour intervals are 5 m/s for U and V, 3 K for T, and 100 m for the geopotential height. We also recommend plotting the temperature at 300 hPa with a 1K contour interval.

2. OMEGA longitude-pressure cross section at 45°N at day 15.

3. time series of the domain integrated total energy. Plot the energy difference between the daily (or more frequent) output and the initial state. In addition, quantify the final energy loss or gain in percent (normalized energy difference).

The computation of the geopotential height and the vertical interpolations of U, V, T and OMEGA to the 700 hPa level are outlined in section 1.4. The computation of the geopotential and interpolations can also be a post-processing step which is e.g. supported by the NCAR Command Language NCL.

Snapshots of the 700 hPa geopotential height and 700 hPa temperature fields at days 5, 15 and 25 are presented in Fig. 19. In addition, Fig. 20 shows snapshots of the zonal and meridional wind field at 700 hPa. The results were computed with the CAM3.5.41 version of the NCAR Finite Volume (FV) dynamical core at the resolution $1° \times 1°$ with 26 hybrid levels.

1.6 Gravity waves with and without the Earth's rotation

This test case explores with propagation of gravity waves in the spherical domain. Two variants of the test case are considered. First, the Earth's rotation Ω and thereby the Coriolis parameter $f = 2\Omega \sin \varphi$ are set to zero which assesses the propagation of pure gravity waves. Second, the Earth's rotation and Coriolis parameter are retained that allows the analysis of inertia-gravity
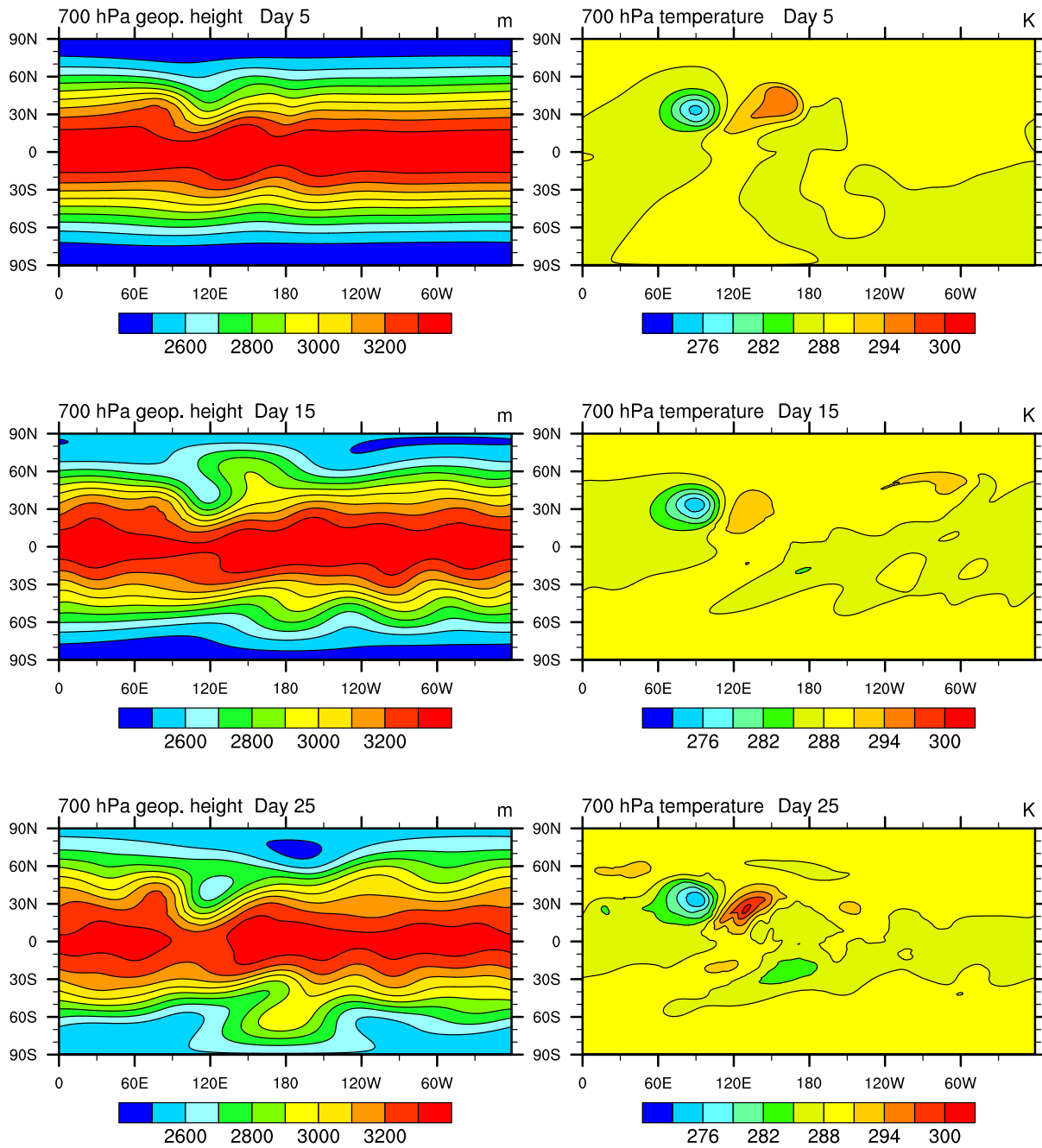
Figure 19: Snapshots of the mountain induced Rossby wave at days 5, 15 and 25 simulated with FV181x360L26. Left column: 700 hPa geopotential height, right column: 700 hPa temperature T.
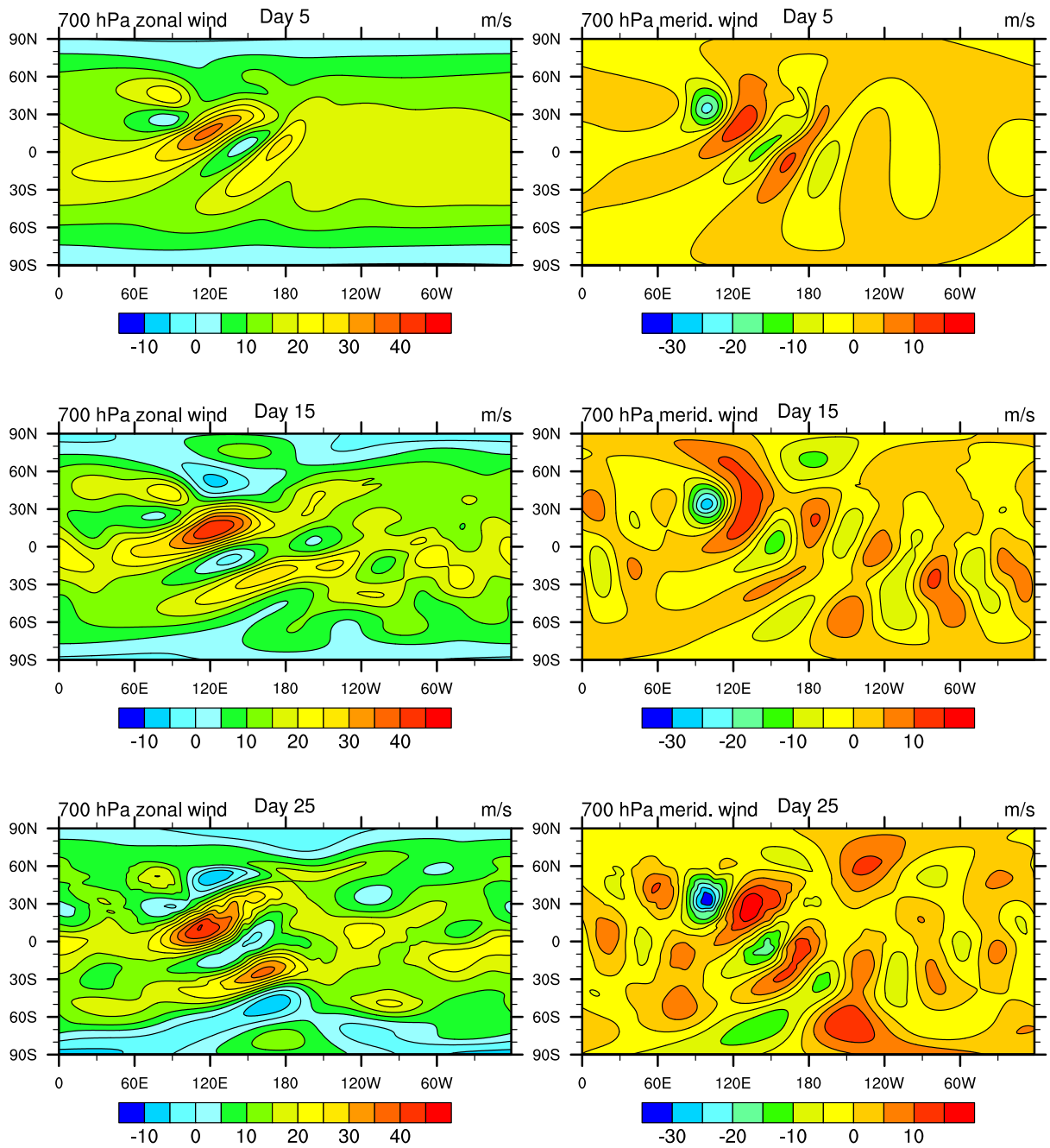
Figure 20: Snapshots of the mountain induced Rossby wave at days 5, 15 and 25 simulated with FV181x360L26. Left column: 700 hPa zonal wind u, right column: 700 hPa meridional wind v.

waves. The initial data trigger large-scale and thereby hydrostatic waves that propagate outward in concentric circles. The wind speeds are given by

$$u = u_0 \cos \varphi$$
$$v = 0 \text{ m s}^{-1}$$

which results in

$$\zeta = \frac{2 \, u_0}{a} \sin \varphi \tag{86}$$
$$\delta = 0 \text{ s}^{-1}$$

for models in vorticity-divergence form. a denotes the Earth's radius and u_0 is the maximum wind amplitude which is set to either 0 or 40 m s-1 depending on the chosen test case variant. In addition, the vertical velocity and and surface geopotential Φ_s are set to zero. The surface pressure field is balanced for the zonally symmetric (unperturbed) state and given by

$$p_s(\lambda, \varphi) = p_{eq} \exp \left[- \frac{a \, N^2 \, u_0}{2 \, g^2 \, \kappa} \left(\frac{u_0}{a} + 2\Omega \right) \sin^2 \varphi \right] \tag{87}$$

with $\kappa = R_d/c_p = 2/7$. The values for the gas constant R_d, specific heat at constant pressure c_p and the gravitational acceleration g are listed in Appendix G. N^2 symbolizes the squared Brunt-Väisälä frequency. p_{eq} denotes the surface pressure at the equator which is set to $p_{eq} = p_0 = 1000$ hPa. Note that the surface pressure is constant with $p_s = p_{eq} = p_0$ for initial states at rest with $u_0 = 0$ m s^{-1}.

The initial temperature field is given by analytic expressions for models with pressure-based or height-based vertical coordinates. In case of $p_s = p_0$ the pressure p and height z positions are interchangeable and represented by

$$p(z) = p_0 \left[\left(1 - \frac{S}{T_0} \right) + \frac{S}{T_0} \exp \left(- \frac{N^2 z}{g} \right) \right]^{\frac{c_p}{R_d}} \tag{88}$$

$$z(p) = -\frac{g}{N^2} \ln \left[\frac{T_0}{S} \left\{ \left(\frac{p}{p_0} \right)^{\kappa} - 1 \right\} + 1 \right] \tag{89}$$

with the parameter $S = g^2/(c_p \, N^2)$. S has temperature units. T_0 represents a reference temperature at the surface which is set to $T_0 = 300$ K. N denotes the Brunt-Väisälä frequency that is either chosen to be

$$N = 0.01 \text{ s}^{-1} \text{ or}$$

$$N = \sqrt{\left(\frac{g^2}{c_p T_0} \right)} \approx 0.01786 \text{ s}^{-1} \tag{90}$$

depending on the test case variant. The latter corresponds to isothermal background conditions with temperature T_0. The pressure-height relationship shown in Eqs. (88) and (89) is not exact for the test case variant [6-2-0] with $p_s \neq p_0$. In the isothermal $T = T_0$ case with Brunt-Väisälä frequency (90) the pressure-height relationship for $p_s \neq p_0$ becomes

$$p(\lambda, \varphi, z) = p_s(\lambda, \varphi) \exp \left(- \frac{g \, z}{R_d \, T_0} \right) \tag{91}$$

$$z(\lambda, \varphi, p) = \frac{R_d \, T_0}{g} \ln \left(\frac{p_s(\lambda, \varphi)}{p} \right) \tag{92}$$

38

However, to simplify the test setup we suggest utilizing Eqs. (88) and (89) for all gravity wave variants. We note that this implies an approximation for the temperature initialization in [6-2-0].

The initial temperature data are composed of a horizontally uniform background field that is overlaid by a large scale temperature perturbation. This approach has also been used by Tomita and Sato (2004). In particular, the temperature perturbation is defined in terms of the potential temperature. The definitions of the initial temperature fields are

$$T(\lambda, \varphi, z) = \Theta(\lambda, \varphi, z)\left(\frac{p(z)}{p_0}\right)^{\kappa} \tag{93}$$

$$T(\lambda, \varphi, p) = \Theta(\lambda, \varphi, p)\left(\frac{p}{p_0}\right)^{\kappa} \tag{94}$$

where $\Theta(\lambda, \varphi, z)$ and $\Theta(\lambda, \varphi, p)$ are composed of the mean state $\bar{\Theta}$ in the vertical direction and a 3D perturbation Θ'. The analytic expression for the height-based potential temperature are

$$\Theta(\lambda, \varphi, z) = \bar{\Theta}(z) + \Theta'(\lambda, \varphi, z)$$
$$= T_0 \exp\left(\frac{N^2 z}{g}\right) + \Delta\Theta \, s(\lambda, \varphi) \, \sin\left(\frac{2\pi z}{L_z}\right) \tag{95}$$

For pressure-based vertical coordinates, the potential temperature field is given as

$$\Theta(\lambda, \varphi, p) = \bar{\Theta}(p) + \Theta'(\lambda, \varphi, p)$$
$$= \frac{T_0}{\frac{T_0}{S}\left(\left(\frac{p}{p_0}\right)^{\kappa} - 1\right) + 1} + \Delta\Theta \, s(\lambda, \varphi) \, \sin\left(\frac{2\pi z(p)}{L_z}\right). \tag{96}$$

The horizontal shape function $s(\lambda, \varphi)$ resembles the cosine hill definition documented in Williamson et al. (1992) (shallow water test case 1). It is defined as

$$s(\lambda, \varphi) = \begin{cases} 0.5\left(1 + \cos(\pi r/R)\right) & \text{if} \quad r < R \\ 0 & \text{if} \quad r \geq R \end{cases} \tag{97}$$

with $R = a/3$. r is the great circle distance between a position (λ, φ) and the center of the cosine bell, initially set to $(\lambda_c, \varphi_c) = (\pi, 0)$. The great circle distance r is defined as

$$r = a \, \arccos\left[\sin\varphi_c \sin\varphi + \cos\varphi_c \cos\varphi \cos(\lambda - \lambda_c)\right] \tag{98}$$

The maximum potential temperature amplitude is $\Delta\Theta = 10$ K and the vertical wave length of the perturbation is set to $L_z = 20$ km. We recommend setting the height of the model top to $z_{top} = 10$ km which corresponds to half a wave length $z_{top} = L_z/2$. Using $N = 0.01$ s^{-1} the top level (interface) pressure then yields $p_{top} = p(z_{top}) \approx 273.819$ hPa according to Eq. (88). When using isothermal conditions with $N = 0.01786$ s^{-1} the position of the top level interface pressure is $p_{top} = p(z_{top}) \approx 320.213$ hPa. Here, both positions of the model tops are computed for $p_s = p_0$. We also recommend using these model tops for test variant [6-2-0] with varying surface pressure.

For completeness, the representation of the mean temperature profiles $\bar{T}$ are

$$\bar{T}(z) = \exp\left(\frac{N^2 z}{g}\right)\left(T_0 - S\right) + S \tag{99}$$

$$\bar{T}(p) = \frac{T_0\left(\frac{p}{p_0}\right)^{\kappa}}{\frac{T_0}{S}\left(\left(\frac{p}{p_0}\right)^{\kappa} - 1\right) + 1} \tag{100}$$

which are incorporated above in Eqs. 93 and 94. Note that

$$\bar{\Theta}(z) = T_0 \exp\left(\frac{N^2 z}{g}\right)$$
$$= \bar{T}(z)\left(\frac{p_0}{p(z)}\right)^{\kappa} \tag{101}$$

despite the apparent differences in the analytic expressions. The equivalency can easily be confirmed analytically for isothermal conditions.

We suggest using an approximately equidistant $\Delta z = 500$ m spacing of the vertical levels. Strictly speaking (for pressure-based vertical coordinates), the levels are only truly equidistant in height without the temperature perturbation and constant $p_s = p_0$. Placing the model top at $z_{top} = 10$ km leads to 20 full model levels and 21 interface levels. The interface levels include the lower and upper boundaries $z_0 = 0$ m and z_{top}. The level spacing can be translated into a pressure-based system via Eq. (88) or Eq. (92). The σ-levels are

$$\sigma(z) = \frac{p(z) - p(z_{top})}{p_s - p(z_{top})} \tag{102}$$

with constant $p(z_{top})$ as determined above.

For hybrid vertical coordinate systems like

$$p(\eta) = A(\eta)\, p_0 + B(\eta)\, p_s \tag{103}$$

we recommend using the hybrid coefficients A and B

$$A(\eta) = \eta - B(\eta) \tag{104}$$
$$B(\eta) = \left(\frac{\eta - \eta_{top}}{1 - \eta_{top}}\right)^c \tag{105}$$

for the interface levels as suggested by Laprise and Girard (1990). For $p_s = p_0$ and $N = 0.01$ s^{-1}, the definitions are $\eta = p(z)/p_s$ and $\eta_{top} = p(z_{top})/p_s \approx 0.273819$. For $N = 0.0178$ s^{-1} the model top interface level lies at $\eta_{top} = p(z_{top})/p_s \approx 0.320213$. We recommend also using these model top positions for test variant [6-2-0] with $p_s \neq p_0$ which will lead to slight deviations from the equidistant spacing in hybrid coordinates. The exponent c determines the smoothness of the transition between the σ-coordinate at low levels to the pressure coordinate near the upper boundary. We recommend choosing $c = 1$ which closely resembles the σ-system. This hybrid coordinate system is a variant of the one used by Simmons and Burridge (1981). It guarantees the conditions $p(\eta = \eta_{top}) = p_{top}$ and $p(\eta = 1) = p_s$ at the upper and lower boundaries. The hybrid coefficients at the full model levels can then be computed via the linear average

$$A_k = \frac{1}{2}\left(A_{k+1/2} + A_{k-1/2}\right), \tag{106}$$
$$B_k = \frac{1}{2}\left(B_{k+1/2} + B_{k-1/2}\right) \tag{107}$$

where the index k denotes the discrete full model level which is surrounded by the two interface levels shown with half indices. The linear interpolation guarantees that vertical differencing

operations conserve energy. Note that some models (Majewski et al. 2002) use the alternative definition of Eq. (103)

$$p(\eta) = A(\eta) + B(\eta)\, p_s. \tag{108}$$

Then Eq. (104) is represented by $A(\eta) = p_0[\eta - B(\eta)]$.

The gravity wave response is nearly linear and hydrostatic and therefore determined by the dispersion relation

$$\nu^2 = f^2 + N^2 \frac{k^2 + l^2}{m^2} \tag{109}$$

where ν indicates the frequency. The zonal, meridional and vertical wave numbers are defined as $k = 2\pi L_x^{-1}$, $l = 2\pi L_y^{-1}$ and $m = 2\pi L_z^{-1}$ where L_x, L_y and L_z represent the zonal and meridional wave lengths. Here we mainly concentrate on pure gravity waves that travel zonally along the equator with $f = 0$ s^{-1} and $l \approx 0$. Then the phase speed in the zonal direction becomes

$$c_x = \pm \frac{\nu}{k} = \pm \frac{N}{m} = \pm \frac{NL_z}{2\pi}. \tag{110}$$

The hydrostatic estimate of the zonal phase speed along the equator with $N = 0.01$ s^{-1} and $L_z = 20$ km $= 2z_{top}$ is ± 31.8 m s^{-1}. The zonal phase speed is $c_x = \pm 56.9$ m s^{-1} for $N = 0.01786$ s^{-1}. The waves travel both in the westward ($-$) and eastward ($+$) direction. The gravity wave test can also be run with the background flow $u = u_0 \cos \varphi$. This leads to the dispersion relation

$$(\nu - ku)^2 = f^2 + N^2 \frac{k^2 + l^2}{m^2} \tag{111}$$

and therefore

$$c_x = u \pm \frac{NL_z}{2\pi}. \tag{112}$$

The unequal phase speeds lead to asymmetries in the westward and eastward traveling wave packets. Perfect symmetry in the shape of the wave packets is expected for $u_0 = 0$ m s^{-1}. The following sequence of tests is suggested. The parameters are

[6-0-0] $\Omega = 0$ s^{-1}, $N^2 = 1 \times 10^{-4}$ s^{-2}, $u_0 = 0$ m s^{-1}, $(\lambda_c, \varphi_c) = (\pi, 0)$

[6-1-0] $\Omega = 0$ s^{-1}, isothermal, $N^2 = g^2/(c_p T_0)$, $u_0 = 0$ m s^{-1}, $(\lambda_c, \varphi_c) = (\pi, 0)$

[6-2-0] $\Omega = 0$ s^{-1}, isothermal, $N^2 = g^2/(c_p T_0)$, $u_0 = 40$ m s^{-1}, $(\lambda_c, \varphi_c) = (\pi, 0)$

[6-3-0] $\Omega = \frac{2\pi}{86164}$ s^{-1}, isothermal, $N^2 = g^2/(c_p T_0)$, $u_0 = 0$ m s^{-1}, $(\lambda_c, \varphi_c) = (\pi, \pi/4)$

Test variant [6-3-0] utilizes the Earth angular velocity Ω and triggers inertio-gravity waves. Note that the global mean surface pressure for test variant [6-2-0] is $\bar{p}_s \approx 996.912$ hPa which might be important for models with mass fixers. The global mean surface pressure is $\bar{p}_s = 1000$ hPa for all other test variants.

The propagating wave packets are best displayed via the potential temperature perturbation Θ' that is defined by

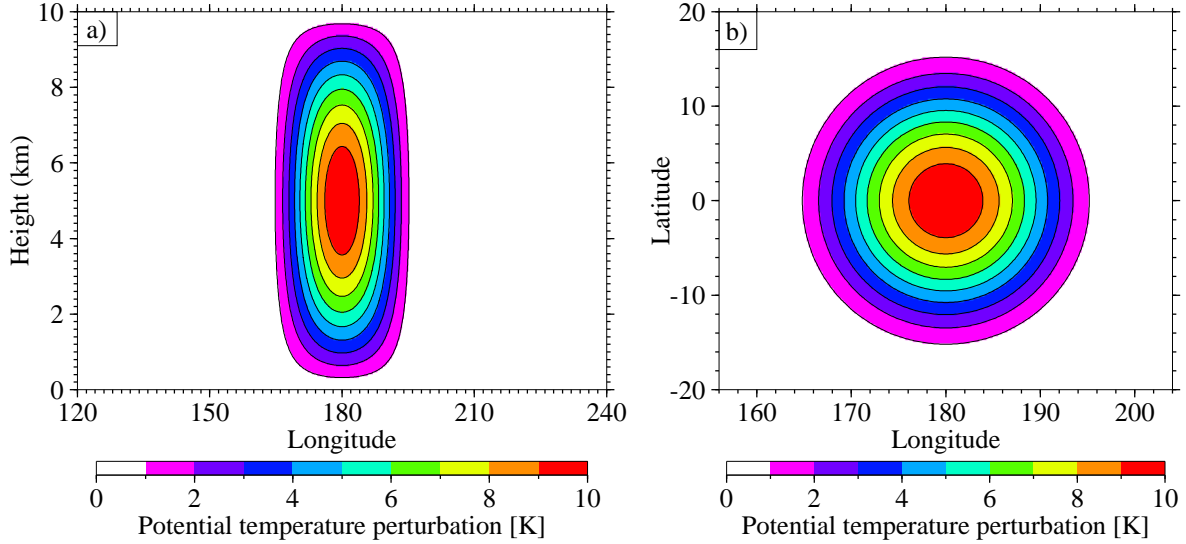$$\Theta' = \Theta - \bar{\Theta}(z). \tag{113}$$

Figure 21: Initial potential temperature perturbation (a) $\lambda - z$ cross-section along the equator, (b) $\lambda - \varphi$ cross section at 5 km. The zero contour is omitted.

$\Theta = T(p_0/p)^\kappa$ represents the instantaneous potential temperature field on the model levels (no vertical interpolations) and $\bar{\Theta}(z)$ is given by Eq. (101). This technique assumes that the height positions z of the model levels remain almost constant. The pressure p can be determined via

$$p(\lambda, \varphi, \sigma, t) = \sigma \left[p_s(\lambda, \varphi, t) - p_{top} \right] + p_{top} \tag{114}$$

$$p(\lambda, \varphi, \eta, t) = A(\eta)\, p_0 + B(\eta)\, p_s(\lambda, \varphi, t) \tag{115}$$

for models with σ- or η-coordinates. $p_s(\lambda, \varphi, t)$ denotes the instantaneous surface pressure of the model at time t.

Figure 21 shows the initial potential temperature perturbation in a $\lambda - z$ cross section along the equator and $\lambda - \varphi$ cross section at 5 km. The perturbation is centered at $(\lambda_c, \varphi_c) = (\pi, 0)$.

1.6.1 Resolution, output data and analysis

We suggest testing two horizontal resolutions. The first resolution is of order $\Delta\lambda = \Delta\varphi \approx 1°$ in longitudinal and latitudinal direction, respectively. The second resolution is halved and of order $\Delta\lambda = \Delta\varphi \approx 2°$. The first resolution corresponds to 181×360 grid points in a latitude-longitude grid when including the pole points in the meridional direction. In the vertical direction, 20 approximately equidistant ($Deltaz \approx 500$ m) levels are prescribed as explained above. The model output variables for the NetCDF files are U, V, OMEGA, T, Z3 and PS on the model levels. In addition, the output variables T850, T300, U850, U200, V850, V200, OMEGA850, OMEGA500 are recommended (if available). The model should be run for 4 days for test case variants [6-0-0], [6-1-0] and [6-2-0] with 6-hourly output intervals. The test variant [6-3-0] should be run for 15 days with a 12-hourly output interval. This reduces the size of the output file.

For test variant [6-0-0], [6-1-0] and [6-2-0] we recommend plotting the Θ' wave packets at $t = 6, 12, 24, 48, 72, 96$ hours as a longitude-height ($\lambda - z$) cross section along the equator. For test variant [6-3-0] we suggest plotting the Θ' wave packets at $t = 0.5, 1, 2, 5, 10, 15$ days along

$\varphi = 45°$. The vertical plotting range is $z \in [0, 10]$ km. The horizontal plotting range spans all longitudes from $\lambda \in [0°, 360°]$. Both horizontal resolutions should be compared. The symmetry of the westward and eastward traveling wave packets can be analyzed if no background flow is chosen.

In addition, we recommend plotting latitude-longitude cross sections of the wind anomalies (u-u(t=0)), v and the temperature anomaly $(T - \bar{T})$ at selected levels (850 hPa, 500 hPa, 300 hPa) as well as the surface pressure anomaly $(p_s - p_s(t = 0))$. The radially outward propagating gravity wave packets can clearly be seen in all fields at hour 6, 12, 24, 48, 72 and 96. Note that the amplitudes of the wave packets are small. The horizontal temperature anomalies lie between 0-1 K, the wind variations are on the order of a few m s^{-1} and the surface pressure anomalies are a few hPa.

Figures 22 and 23 show snapshots of the potential temperature perturbation Θ' and surface pressure anomaly from an NCAR CAM3.5.41 Eulerian simulation for test variant [6-0-0]. The snapshots are taken at times 6, 12, 24, 48, 72 and 96 hours from a run with the spectral resolution T106 (approx. $1° \times 1°$) and 20 vertical levels .

Examples of the potential temperature perturbation from EULT106L20 for test variants [6-1-0] and [6-2-0] are shown in Figs. 24 and 25.

In addition, Figs. 26 and 27 depict the potential temperature perturbation and surface pressure anomaly from an NCAR CAM3.5.41 FV simulation for test variant [6-3-0]. The snapshots are taken at times 0.5, 1, 2, 5, 10, 15 days from a run with the resolution $1° \times 1°$ and 20 vertical levels .

2 Typical resolutions, time steps and diffusion coefficients

All dynamical cores should be run in their operational configurations which includes the typical diffusion mechanisms and coefficients, filters, time steps and other tunable parameters. In addition, the runs should utilizes their standard *a posteriori* fixers like mass or energy fixers if applicable. These standard runs serve as a control simulation. All parameters and fixers need to be documented to foster model comparisons. In addition, the documentation needs to list the prognostic variables, the equation set (e.g. shallow-atmosphere hydrostatic, or shallow-atmosphere nonhydrostatic), the horizontal grid staggering, time stepping approach, vertical coordinate and resolution. As an example, we list typical time steps, resolutions and diffusion coefficients for various dynamical cores with different numerical approaches in the tables below.

The modeling groups are also invited to test their models in non-operational configurations that, for example, use less explicit diffusion. These configurations are often viable for idealized test cases as considered here, but might not be applicable in real weather or climate simulations. Therefore, any conclusions need to be carefully drawn and are not necessarily valid for models with physics parameterizations.

2.1 Gaussian grids for spectral transform methods

Table 4 lists the horizontal resolutions, time steps and ∇^4diffusion coefficients K_4 for the spectral transform Eulerian dynamical core that is part of NCAR's CAM3.5 modeling framework. The abbreviation T symbolizes a triangular truncation which is followed by the maximum resolved wavenumber. The Eulerian dynamical core in vorticity-divergence form is based on

euIT106L20 6-0-0 gw, with del-4 & del-2 diffusion
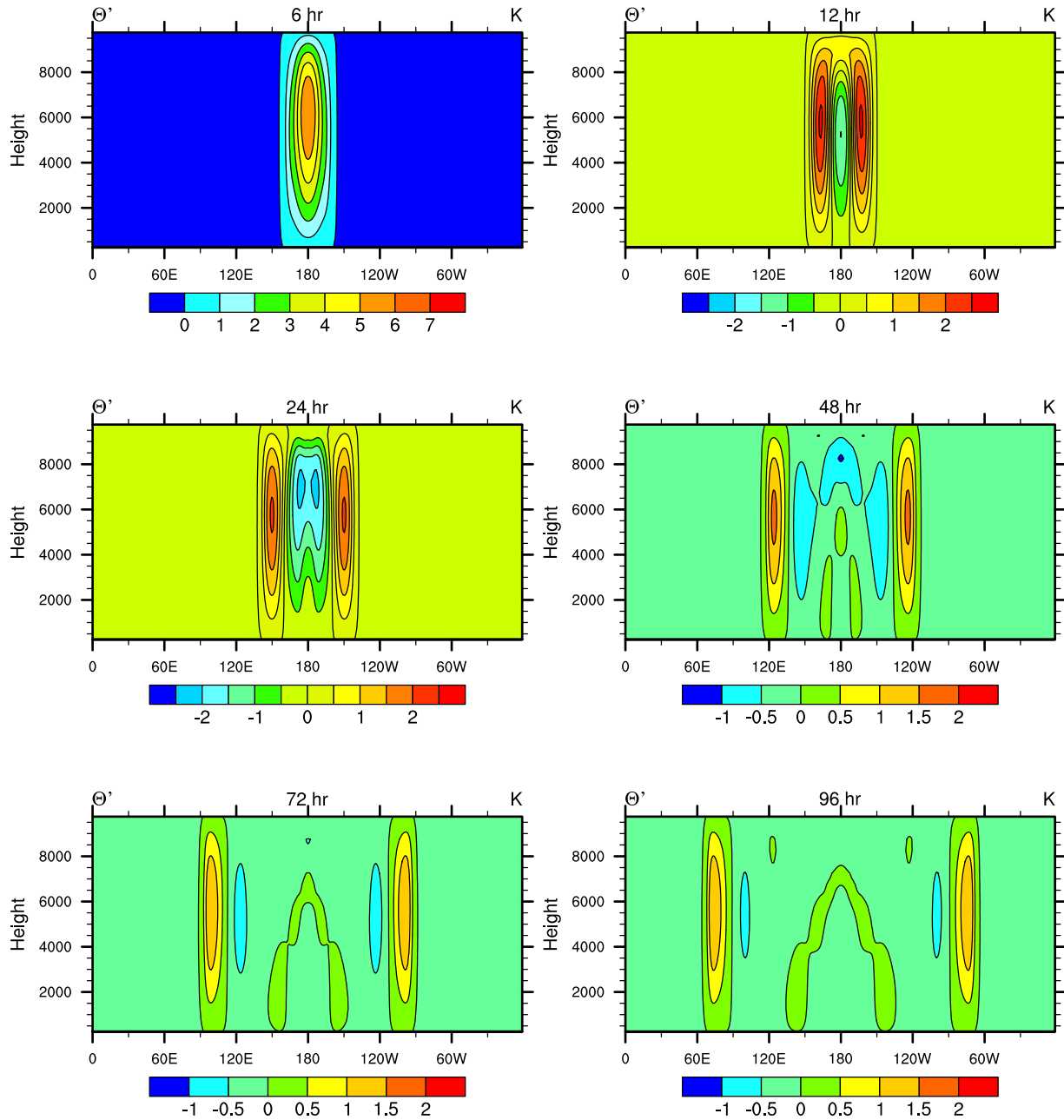
Figure 22: Gravity waves at the equator on a non-rotating planet simulated with EULT106L20: Potential temperature perturbation Θ' at 6, 12, 24, 48, 72 and 96 hours for test scenario 6-0-0.

euIT106L20 6-0-0 gw, with del-4 & del-2 diffusion

Figure 23: Gravity waves on a non-rotating planet simulated with EULT106L20: Surface pressure anomaly at 6, 12, 24, 48, 72 and 96 hours for test scenario 6-0-0.

eulT106L20 6-1-0 gw, with del-4 & del-2 diffusion
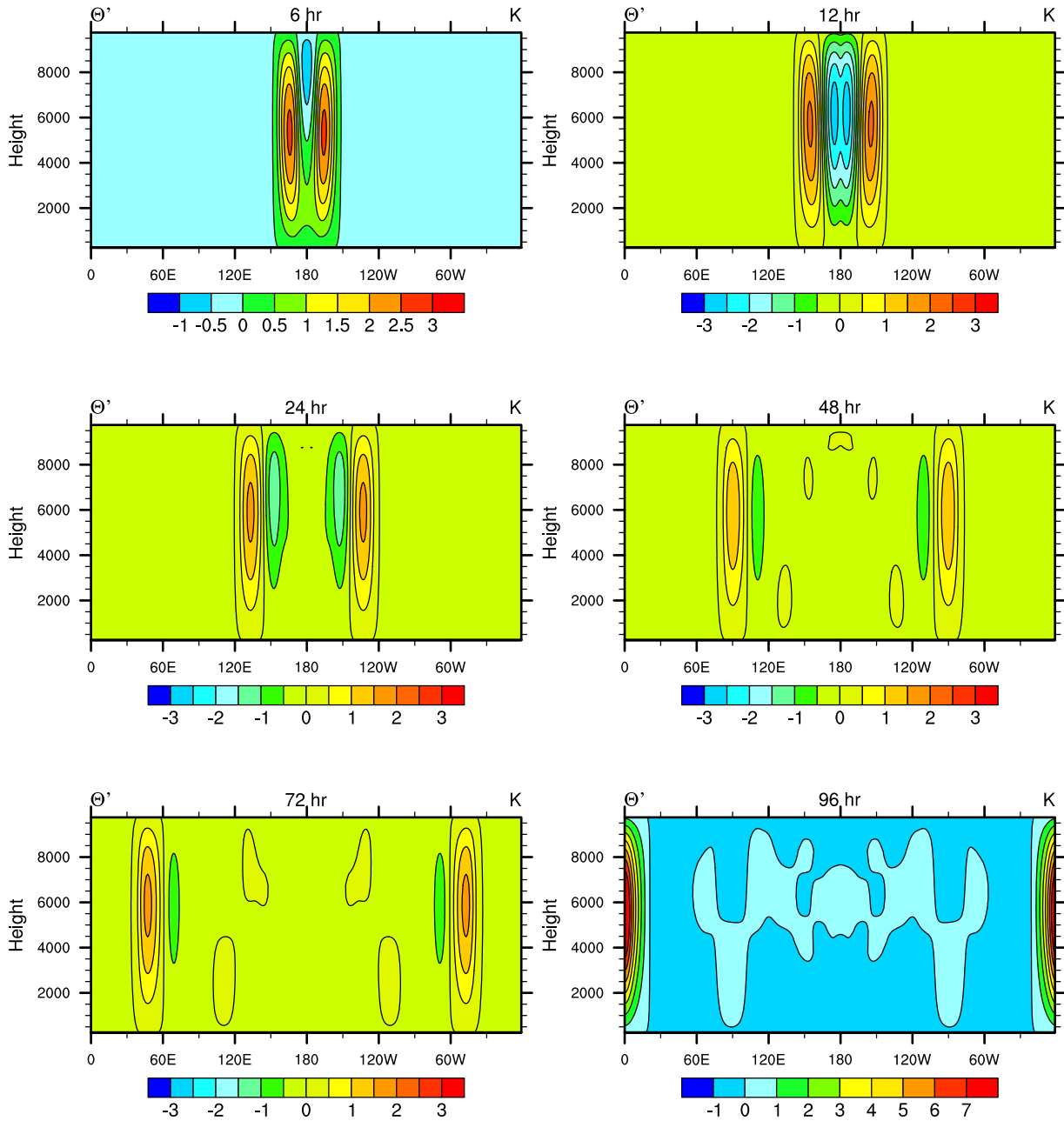
Figure 24: Gravity waves at the equator on a non-rotating planet simulated with EULT106L20: Potential temperature perturbation Θ' at 6, 12, 24, 48, 72 and 96 hours for test scenario 6-1-0.

eulT106L20 6-2-0 gw, with del-4 & del-2 diffusion
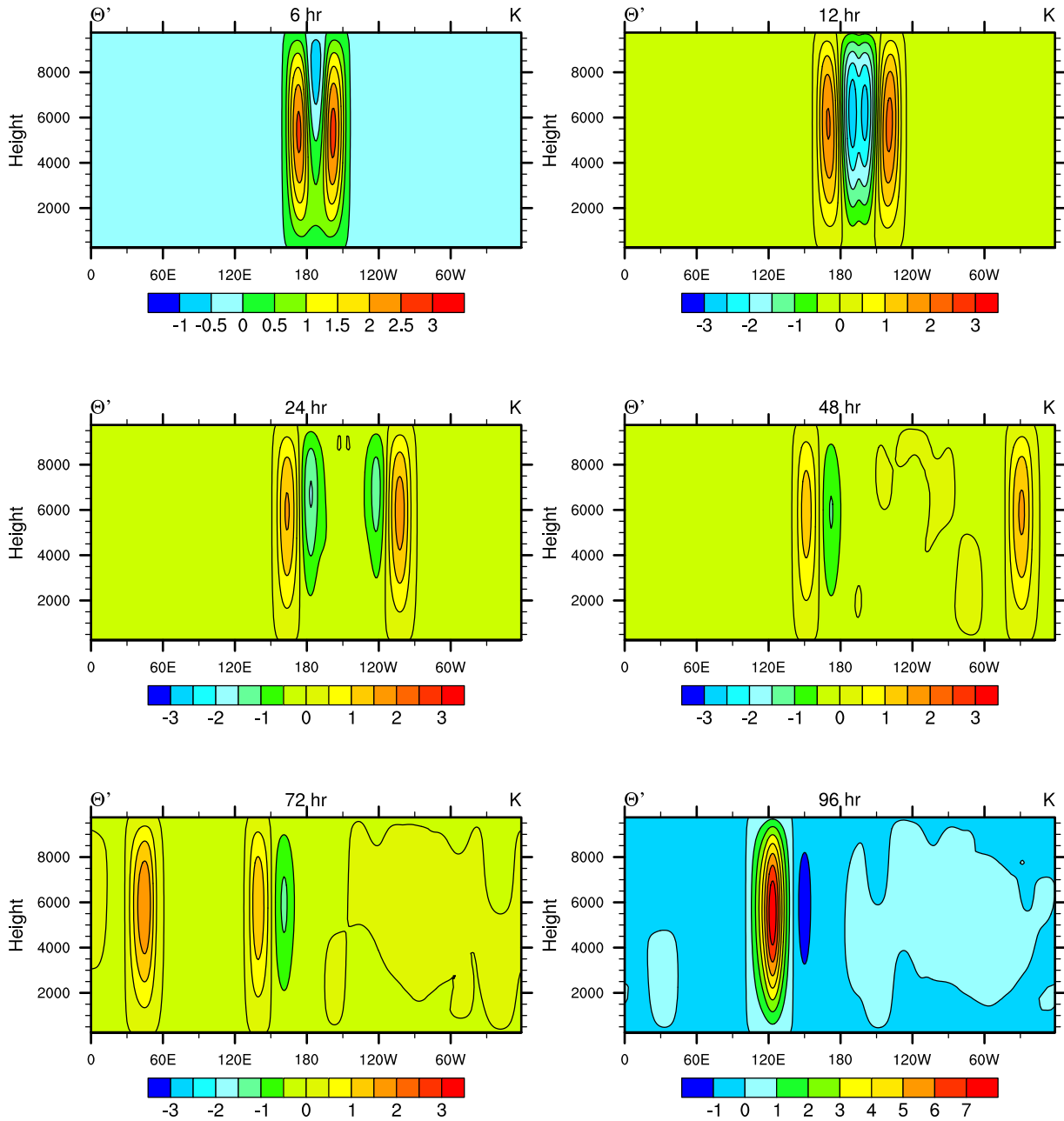
Figure 25: Gravity waves at the equator on a non-rotating planet simulated with EULT106L20: Potential temperature perturbation Θ' at 6, 12, 24, 48, 72 and 96 hours for test scenario 6-2-0.

fv181x360L20 6-3-0 gw

Figure 26: Inertio-gravity waves at $45°$ N on a rotating planet simulated with FV181x360L20: Potential temperature perturbation Θ' at 0.5, 1, 2, 5, 10 and 15 days for test scenario 6-3-0.
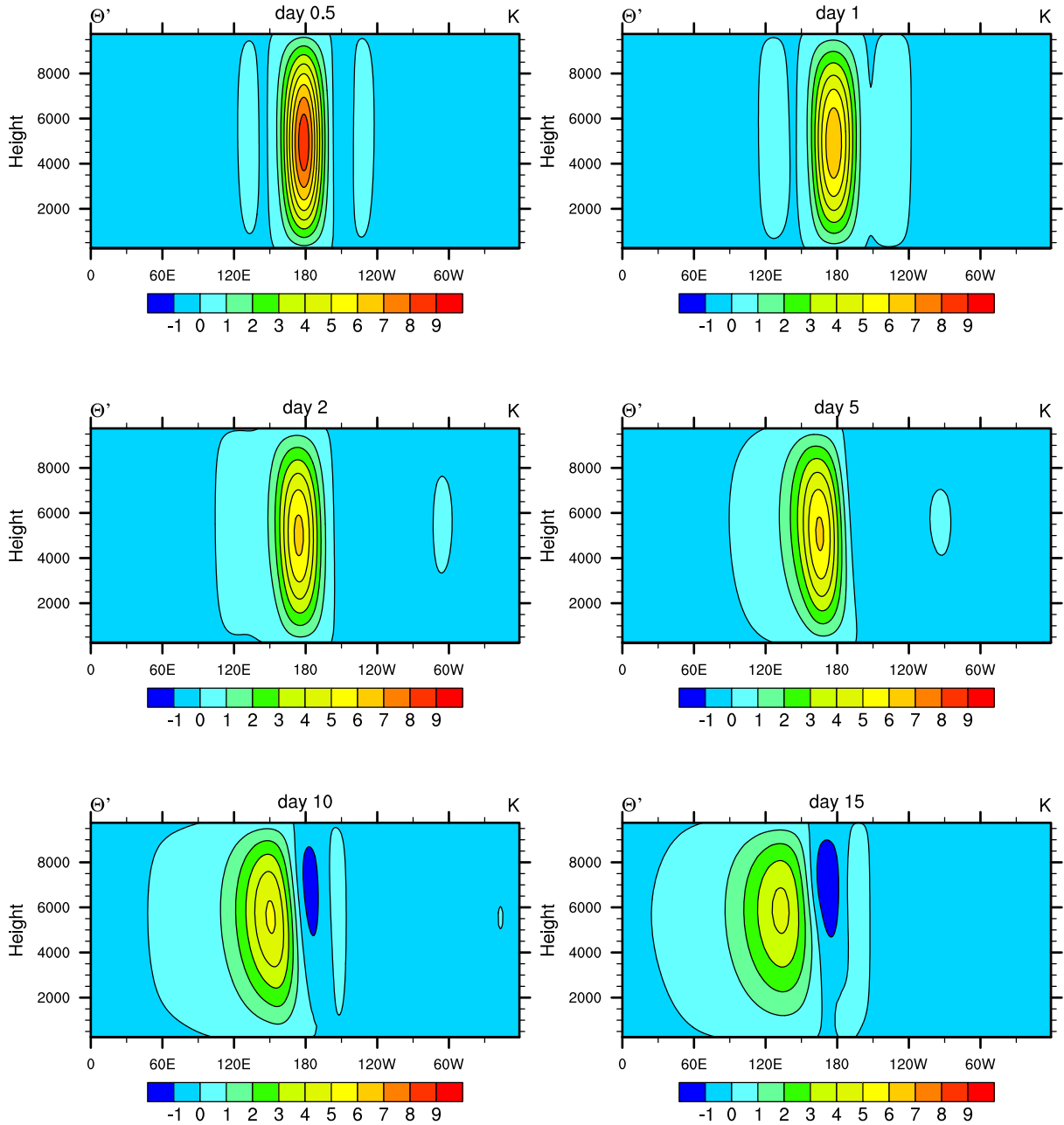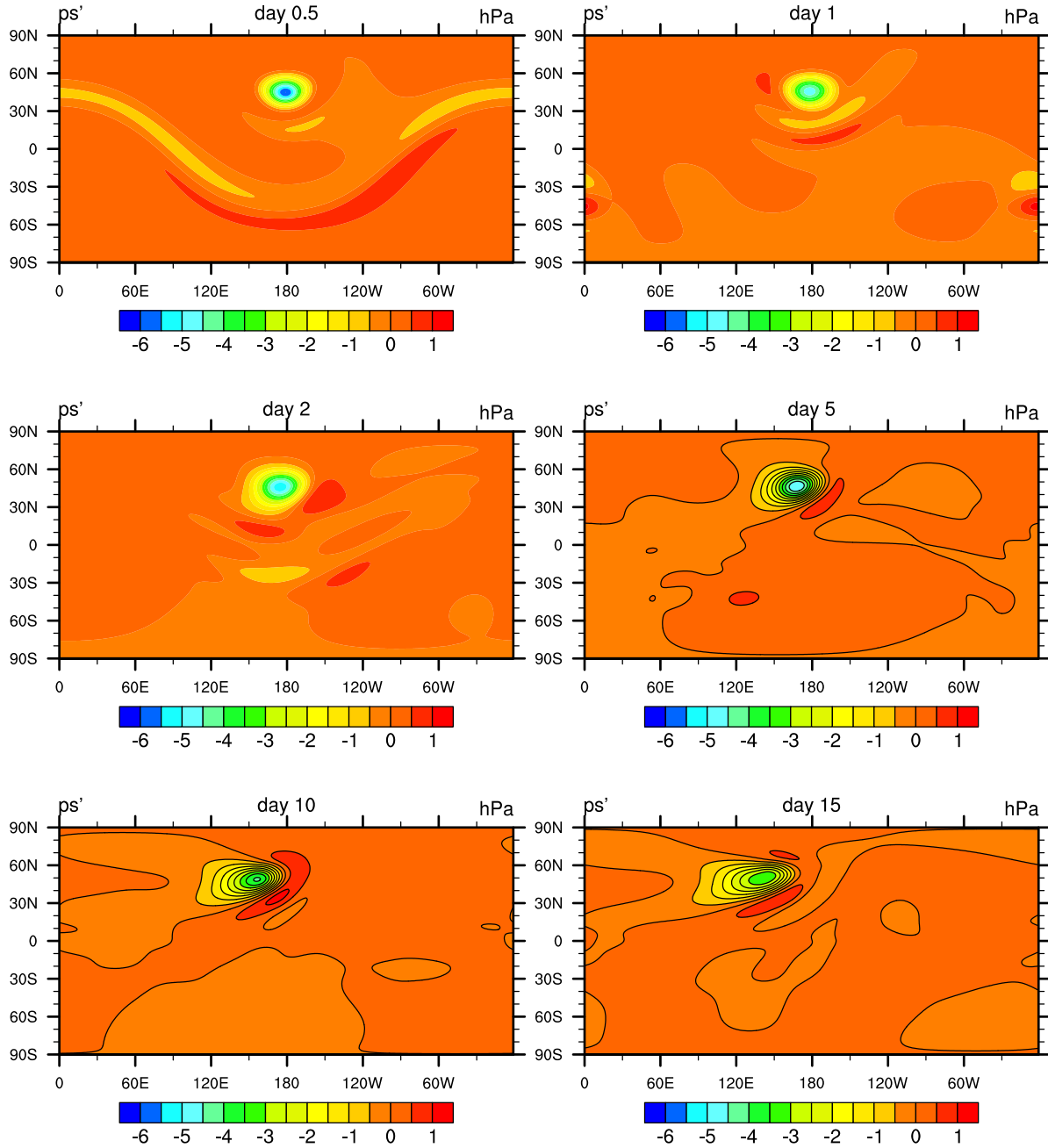
fv181x360L20 6-3-0 gw

Figure 27: Inertio-gravity waves on a rotating planet simulated with FV181x360L20: Surface pressure anomaly at 0.5, 1, 2, 5, 10 and 15 days for test scenario 6-3-0.

Eulerian spectral transform dynamical core(EUL)				
Spectral Resolution	# Grid points lat × lon	Grid distance at the equator	Time step Δt	Diffusion coefficient K_4 (m^4 s^{-1})
T21	32×64	625 km	2400 s	2.0×10^{16}
T42	64×128	313 km	1200 s	1.0×10^{16}
T85	128×256	156 km	600 s	1.0×10^{15}
T106	160×320	125 km	450 s	0.5×10^{15}
T170	256×512	78 km	300 s	1.5×10^{14}
T340	512×1024	39 km	150 s	1.5×10^{13}

Table 4: Horizontal grid resolutions, time steps and diffusion coefficients for the spectral Eulerian (EUL) dynamical core in CAM3.5. The ∇^2 horizontal diffusion coefficient, $K_2 = 2.5 \times 10^5$ m^2 s^{-1}, is independent of horizontal resolution.

the traditional three-time-level, semi-implicit spectral transform approximations applied on a quadratically unaliased transform grid with horizontal triangular truncation (Machenhauer 1979). The three-time-level core includes a time filter to control the $2\Delta t$ time computational modes. The vertical coordinate is terrain following hybrid pressure. The core includes ∇^4 horizontal diffusion on temperature, divergence and vorticity to control the energy at the smallest resolved scales. The coefficient has been chosen for each resolution to yield a reasonably straight tail for the kinetic energy spectra in realistically forced simulations. The model also includes a ∇^2 horizontal diffusion on the top three levels of the model which serves as a top boundary condition to control upward propagating waves. The temperature equation includes a frictional heating term corresponding to the momentum diffusion. The ∇^2 horizontal diffusion coefficient, $K_2 = 2.5 \times 10^5$ m^2 s^{-1}, is independent of horizontal resolution.

The NCAR CAM3.5 model also provides a configuration for a two-time-level semi-Lagrangian semi-implicit spectral transform dynamical core (SLD). Then the time step Δt can be set to three times the corresponding Eulerian value. The diffusion coefficients K_4 and K_2 might possibly be reduced since SLD provides inherent diffusion due to the semi-Lagrangian interpolations. Since the energy loss due to the damping by the interpolants is not explicitly known, a term corresponding to the ∇^4 diffusive heating in the Eulerian core cannot be derived. Thus an *a posteriori* energy fixer is applied every time step in the model which acts as a globally uniform heating term. (see also the discussion in Williamson et al. (2008)). In addition, the *a posteriori* mass fixer is invoked every time step as in the Eulerian core. Note that the semi-Lagrangian dynamical core applies a decentering technique to damp the noise induced by orographic resonance (Collins et al. 2004). Although not needed for stability reasons in idealized studies, the standard CAM3 decentering parameter $\epsilon = 0.2$ is used, here in the spirit of evaluating the core as it would be applied in practice.

Both the EUl and SLD model designs are non-conservative. Therefore, both dynamical cores apply an *a posteriori* mass and energy fixer. They are based on the shallow-atmosphere hydrostatic equation set, and utilize the Arakawa A-grid staggering and hybrid η (hybrid $\sigma - p$) coordinate (Simmons and Burridge 1981). The prognostic variables are $\zeta, \delta, \ln p_s, T$.

Finite Volume dynamical core (FV)			
Resolution $\Delta\varphi \times \Delta\lambda$	# Grid points lat $\times$ lon	Grid distance at the equator $\Delta y, \Delta x$	Time step Δt
$4° \times 4°$	46×90	435 km	720 s
$2° \times 2°$	91×180	220 km	360 s
$1° \times 1°$	181×360	111 km	180 s
$0.5° \times 0.5°$	361×720	55 km	90 s
$0.25° \times 0.25°$	721×1440	28 km	45 s

Table 5: Recommended horizontal grid resolutions and time steps for NCAR's CAM3.5 Finite Volume (FV) dynamical core. The regular latitude-longitude resolutions are also recommended for other models with regular grids or as the target interpolation grids.

2.2 Regular latitude-longitude grids

The NCAR CAM3.5 Finite Volume dynamical core is built upon a regular latitude-longitude grid. For these types of grids we recommend using the horizontal resolutions listed in Table 5. Note that the latitudes should include both pole points if possible. The longitudes start at position $\lambda = 0$. These regular latitude-longitude resolutions are also recommended as the target interpolation grids for models with cubed-sphere or icosahedral meshes. The table also lists the approximate equatorial grid distances in physical space to ease the comparison to the other dynamical cores.

The NCAR FV advection algorithm makes use of the monotonic third-order piecewise parabolic method PPM (Colella and Woodward 1984) with an explicit time-stepping scheme. Lower order approximations are applied near the model top to add extra diffusion at the upper boundary. The FV dynamics package also employs both a weak 3-point digital filter in mid-latitudes as well as a fast Fourier transform (FFT) filter in polar regions. These control the unstable waves in the zonal direction that result from the convergence of the computational grid near the poles. The FV dynamical core does not include explicit horizontal ∇^4 or ∇^2 diffusion terms. The smallest scales are controlled by the monotonicity constraints of the numerical scheme. In addition, a divergence damping mechanism is applied that damps the divergence δ in the form of $\nabla^2(\nu\delta)$ where ν is a spatially varying divergence damping coefficient. As with the NCAR's semi-Lagrangian SLD core, the energy loss due to the numerical damping is not explicitly known. Therefore, an *a posteriori* energy fixer is applied. The algorithms is inherently mass-conservative. The prognostic variable are $u, v, \Delta p, (\Delta p\Theta)$ and held on a staggered Arakawa D grid.

2.3 Icosahedral grids in the dynamical core GME

The dynamical core of the weather prediction system GME at the German Weather Service applies a finite-difference approximation with local spherical basis functions at each grid point. The horizontal grid is based on an icosahedron which is further subdivided into smaller triangles. An Arakawa-A grid staggering is chosen that places the prognostic variables u, v, p_s, T at the vertices of the triangles. In the vertical direction GME utilizes the same terrain following η coordinate as the NCAR CAM3.5 Eulerian dynamics package. The model is based on the shallow-atmosphere hydrostatic equation set.

GME						
Resolution ni	# Grid points	Min. grid distance	Max. grid distance	Time step Δt	Diffusion coefficients	
					K_4 (m^4 s^{-1})	K_2 (m^2 s^{-1})
16	2562	440 km	526 km	1440 s	5.0×10^{16}	2.0×10^6
32	10242	220 km	263 km	720 s	6.0×10^{15}	1.5×10^6
64	40962	110 km	132 km	400 s	1.0×10^{15}	1.0×10^6
128	163842	55 km	66 km	200 s	1.2×10^{14}	2.0×10^5
256	655362	26 km	33 km	100 s	1.2×10^{13}	2.5×10^4

Table 6: Horizontal grid resolutions, time steps and diffusion coefficients for GME with an icosahedral grid.

The semi-implicit numerical scheme is second-order accurate and applies a classical Leapfrog three-time-level approach with an Asselin time filter. Due to the quasi-uniformity of the computational grid no longitudinal FFT-filtering is needed. The smallest scales are controlled by a ∇^4 horizontal diffusion mechanism that is applied to the prognostic wind and temperature variables u, v and T. Near the model top the ∇^4 diffusion is replaced with a stronger ∇^2 diffusion operator that serves as a top boundary condition. Neither a mass fixer nor an energy fixer is applied.

The horizontal grid of GME is based on an icosahedron with 20 equilateral triangles. The sides of these base triangles are further subdivided into ni equal intervals. The corresponding maximum and minimum grid distances, time steps and diffusion coefficients are listed in Table 6. We recommend interpolating the model results in the output file to regular latitude-longitude grids as listed in Table 5.

Appendices

A NetCDF model output conventions

To facilitate the analysis of the results and model intercomparison we ask the modeling group to provide the output data in NetCDF format on a co-located (Arakawa-A type) regular latitude-longitude grid. This does not mean that the model should output directly to NetCDF but the output should be converted to NetCDF format.

   The resolution of the chosen latitude-longitude grid should either reflect the actual grid resolution of the model run or should be comparable to the native grid (e.g. comparable to the resolution of a cubed-sphere or icosahedral mesh). Ideally, the horizontal grid should include the Greenwich ($\lambda = 0$) meridian and both pole points. In the vertical direction the data should be output on the native grid (full model levels). If variables are staggered in the vertical direction we suggest interpolating them to the full model levels before outputting them. Additional vertical interpolations to fixed pressure levels (e.g. 850 hPa or 250 hPa) are considered a post-processing step.

   The following model variables need to be written to the output NetCDF file. We ask the modeling group to select the upper-case variable names shown below and to use the keywords lat, lon, lev and time for the dimensions. This choice eases the use of standard analysis packages.

   The standard output model variables on model levels are:

PHIS (time,lat,lon) Surface geopotential ($\mathrm{m^2\ s^{-2}}$)

PS (time,lat,lon) Surface Pressure (Pa)

U (time,lev,lat,lon) Zonal wind (m/s)

V (time,lev,lat,lon) Meridional wind (m/s)

T (time,lev,lat,lon) Temperature (K)

OMEGA (time,lev,lat,lon) Vertical pressure velocity (Pa/s)

P(time,lev,lat,lon) optional: Pressure at each grid point (Pa), optional if an analytic reconstruction is possible (e.g. for sigma or eta levels)

For selected test cases, the following post-processed variables are also desirable if offered as output quantities by the dynamical core:

Z3 (time,lev,lat,lon) Geopotential height above sea level on model levels (m)

Z700(time,lat,lon) Geopotential height at 700 hPa (m)

Z500(time,lat,lon) Geopotential height at 500 hPa (m)

Z300(time,lat,lon) Geopotential height at 300 hPa (m)

T850(time,lat,lon) Temperature at 850 hPa (K)

T300(time,lat,lon) Temperature at 300 hPa (K)

U850(time,lat,lon) zonal wind at 850 hPa (m s^{-1})

U200(time,lat,lon) zonal wind at 200 hPa (m s^{-1})

V850(time,lat,lon) meridional wind at 850 hPa (m s^{-1})

V200(time,lat,lon) meridional wind at 200 hPa (m s^{-1})

OMEGA850 (time,lat,lon) Vertical pressure velocity at 850 hPa (Pa/s)

OMEGA500 (time,lat,lon) Vertical pressure velocity at 500 hPa (Pa/s)

If the dynamical core does not provide these output quantities they can be computed with the help of NCL (NCAR Command Language) post-processing routines after the model run. The 850 hPa pressure level requires extrapolations for the mountain-induced Rossby wave test (test case 5) and is therefore less accurate and optional. The analysis of test case 5 will concentrate on the 700 hPa level. If height-based vertical coordinates are used, the vertical velocity might also be output as 'W' in m/s. Note that the notation of the variables above uses the NetCDF-specific order of the dimensions (time,lev,lat,lon). This does not imply that the model needs to work with this data structure. We request the model data with single precision (float) accuracy using 4 bytes per datum. In addition, the NetCDF file must contain information about the grid and time dimensions, the positions of the horizontal grid and vertical model levels as well as information on the time stamps (the latter are preferred in double precision accuracy, 8 bytes per datum).

An example of an NCAR CAM3 output file on a regular 91×180 latitude-longitude grid with grid spacing $2° \times 2°$ and 26 hybrid η-levels is shown below. Note that this output data set also lists the approximate pressure positions of the 26 full levels (lev) and 27 model interface levels (ilev) as well as the hybrid coefficients for the full (hyam, hybm) and half levels (hyai, hybi). The latter can be used in combination with the surface pressure to reconstruct the actual pressure at each grid point. The surface geopotential PHIS is provided as a 3D data set despite its time-independency. The time-dependent data sets PS, U, V, T and OMEGA (data not listed) contain 11 instantaneous snapshots in time at day 0, 1, 2, 3, ... 10. In addition, the NetCDF header also lists the post-processed variables. In general, shorter output intervals will also be needed (e.g. 6-hourly) for the gravity wave test (test case 6). The output frequency should be an input parameter for the model run. The NetCDF entry P0 corresponds to the reference pressure used by hybrid η coordinates. It should be set to P0 = 10^5 Pa for all model runs. The meta data of all model variables in netcdf format need to list their physical unit in the 'units' identifier. These units are used by the provided NCL plotting routines.

Example of a NetCDF file (header and selected data sets):

```
netcdf fv180x091L26g_cam1.10_days {
dimensions:
  lat = 91 ;
  lon = 180 ;
  lev = 26 ;
  ilev = 27 ;
```

```
    time = UNLIMITED ; // (11 currently)
variables:
  double P0 ;
    P0:long_name = "reference pressure" ;
    P0:units = "Pa" ;
  double lat(lat) ;
    lat:long_name = "latitude" ;
    lat:units = "degrees_north" ;
  double lon(lon) ;
    lon:long_name = "longitude" ;
    lon:units = "degrees_east" ;
  double lev(lev) ;
    lev:long_name = "hybrid level at midpoints(1000*(A+B))" ;
    lev:units = "level" ;
    lev:positive = "down" ;
    lev:standard_name = "atmosphere_hybrid_sigma_pressure_coordinate" ;
    lev:formula_terms = "a: hyam b: hybm p0: P0 ps: PS" ;
  double ilev(ilev) ;
    ilev:long_name = "hybrid level at interfaces (1000*(A+B))" ;
    ilev:units = "level" ;
    ilev:positive = "down" ;
    ilev:standard_name = "atmosphere_hybrid_sigma_pressure_coordinate" ;
    ilev:formula_terms = "a: hyai b: hybi p0: P0 ps: PS" ;
  double time(time) ;
    time:long_name = "time" ;
    time:units = "days since 0000-01-01 00:00:00" ;
  double hyai(ilev) ;
    hyai:long_name = "hybrid A coefficient at layer interfaces" ;
  double hybi(ilev) ;
    hybi:long_name = "hybrid B coefficient at layer interfaces" ;
  double hyam(lev) ;
    hyam:long_name = "hybrid A coefficient at layer midpoints" ;
  double hybm(lev) ;
    hybm:long_name = "hybrid B coefficient at layer midpoints" ;
  float PHIS(lat, lon) ;
    PHIS:units = m^2/s^2" ;
    PHIS:long_name = "Surface geopotential" ;
  float PS(time, lat, lon) ;
    PS:units = "Pa" ;
    PS:long_name = "Surface pressure" ;
  float T(time, lev, lat, lon) ;
    T:units = "K" ;
    T:long_name = "Temperature" ;
  float U(time, lev, lat, lon) ;
    U:units = "m/s" ;
    U:long_name = "Zonal wind" ;
```

```
  float V(time, lev, lat, lon) ;
    V:units = "m/s" ;
    V:long_name = "Meridional wind" ;
  float OMEGA(time, lev, lat, lon) ;
    OMEGA:units = Pa/s" ;
    OMEGA:long_name = "Vertical pressure velocity" ;
  float OMEGA850(time, lat, lon) ;
    OMEGA850:units = Pa/s" ;
    OMEGA850:long_name = "Vertical pressure velocity at 850 hPa" ;
  float OMEGA500(time, lat, lon) ;
    OMEGA500:units = Pa/s" ;
    OMEGA500:long_name = "Vertical pressure velocity at 500 hPa" ;
  float T850(time, lat, lon) ;
    T850:units = "K" ;
    T850:long_name = "Temperature at 850 hPa" ;
  float T300(time, lat, lon) ;
    T300:units = "K" ;
    T300:long_name = "Temperature at 300 hPa" ;
  float U850(time, lat, lon) ;
    U850:units = "m/s" ;
    U850:long_name = "Zonal wind at 850 hPa" ;
  float U200(time, lat, lon) ;
    U200:units = "m/s" ;
    U200:long_name = "Zonal wind at 200 hPa" ;
  float V850(time, lat, lon) ;
    V850:units = "m/s" ;
    V850:long_name = "Meridional wind at 850 hPa" ;
  float V200(time, lat, lon) ;
    V200:units = "m/s" ;
    V200:long_name = "Meridional wind at 200 hPa" ;
  float Z3(time, lev, lat, lon) ;
    Z3:units = "m" ;
    Z3:long_name = "Geopotential height (above sea level)" ;
  float Z300(time, lat, lon) ;
    Z300:units = "m" ;
    Z300:long_name = "Geopotential height at 300 hPa" ;
  float Z500(time, lat, lon) ;
    Z500:units = "m" ;
    Z500:long_name = "Geopotential height at 500 hPa" ;
  float Z700(time, lat, lon) ;
    Z700:units = "m" ;
    Z700:long_name = "Geopotential height at 700 hPa" ;

data:

 P0 = 100000 ;
```

```
lat = -90, -88, -86, -84, -82, -80, -78, -76, -74, -72, -70,
  -68, -66, -64, -62, -60, -58, -56, -54, -52, -50, -48,
  -46, -44, -42, -40, -38, -36, -34, -32, -30, -28, -26,
  -24, -22, -20, -18, -16, -14, -12, -10, -8, -6, -4, -2, 0,
  2, 4, 6, 8, 10, 12, 14, 16, 18, 20, 22, 24, 26, 28, 30,
  32, 34, 36, 38, 40, 42, 44, 46, 48, 50, 52, 54, 56, 58,
  60, 62, 64, 66, 68, 70, 72, 74, 76, 78, 80, 82, 84,
  86, 88, 90 ;

lon =    0,   2,   4,   6,   8,  10,  12,  14,  16,  18,
    20,  22,  24,  26,  28,  30,  32,  34,  36,  38,
    40,  42,  44,  46,  48,  50,  52,  54,  56,  58,
    60,  62,  64,  66,  68,  70,  72,  74,  76,  78,
    80,  82,  84,  86,  88,  90,  92,  94,  96,  98,
   100, 102, 104, 106, 108, 110, 112, 114, 116, 118,
   120, 122, 124, 126, 128, 130, 132, 134, 136, 138,
   140, 142, 144, 146, 148, 150, 152, 154, 156, 158,
   160, 162, 164, 166, 168, 170, 172, 174, 176, 178,
   180, 182, 184, 186, 188, 190, 192, 194, 196, 198,
   200, 202, 204, 206, 208, 210, 212, 214, 216, 218,
   220, 222, 224, 226, 228, 230, 232, 234, 236, 238,
   240, 242, 244, 246, 248, 250, 252, 254, 256, 258,
   260, 262, 264, 266, 268, 270, 272, 274, 276, 278,
   280, 282, 284, 286, 288, 290, 292, 294, 296, 298,
   300, 302, 304, 306, 308, 310, 312, 314, 316, 318,
   320, 322, 324, 326, 328, 330, 332, 334, 336, 338,
   340, 342, 344, 346, 348, 350, 352, 354, 356, 358 ;

lev = 3.544638, 7.388813, 13.96721, 23.94463,
    37.23029,  53.1146,  70.05914, 85.43912,
  100.51469, 118.25033, 139.11538, 163.66205, 192.53994,
  226.51321, 266.48106, 313.50127, 368.81799, 433.89523,
  510.45525, 600.5241, 696.796239999999, 787.70201,
  867.16071, 929.648975, 970.554785, 992.5561 ;

ilev = 2.194067, 4.895209, 9.882418, 18.05201, 29.83724,
    44.62334, 61.60587, 78.51243, 92.3658,
  108.66359, 127.83708, 150.39371, 176.93043, 208.14944,
  244.87709, 288.08522, 338.91731, 398.71865, 469.0718,
  551.83871, 649.20969, 744.38289, 831.02123,
  903.30029, 955.99746, 985.1122, 1000 ;

time = 0, 1, 2, 3, 4, 5, 6, 7, 8, 9, 10 ;

hyai = 0.002194067, 0.004895209, 0.009882418, 0.01805201,
```

```
    0.02983724, 0.04462334, 0.06160587, 0.07851243,
    0.07731271, 0.07590131, 0.07424086,
    0.07228744, 0.06998933, 0.06728574, 0.06410509,
    0.06036322, 0.05596111, 0.05078225,
    0.04468960, 0.03752191, 0.02908949, 0.02084739,
    0.01334443, 0.00708499, 0.00252136, 0, 0 ;

 hybi = 0, 0, 0, 0, 0, 0, 0, 0, 0.01505309, 0.03276228,
    0.05359622, 0.07810627, 0.1069411, 0.1408637,
    0.180772, 0.227722, 0.2829562, 0.3479364, 0.4243822,
    0.5143168, 0.6201202, 0.7235355, 0.8176768,
    0.8962153, 0.9534761, 0.9851122, 1 ;

 hyam = 0.003544638, 0.007388813, 0.01396721,
    0.02394463, 0.03723029, 0.0531146, 0.07005914,
    0.07791257, 0.07660701, 0.0750710800000003, 0.07326415,
    0.07113839, 0.06863754, 0.06569541, 0.06223416,
    0.05816217, 0.05337169, 0.04773593,
    0.04110575, 0.03330570, 0.02496844,
    0.01709591, 0.01021471, 0.004803175, 0.001260685, 0 ;

 hybm = 0, 0, 0, 0, 0, 0, 0, 0.00752655, 0.02390768,
    0.04317925, 0.06585123, 0.09252366, 0.1239024,
    0.1608178, 0.2042469, 0.2553391, 0.3154463, 0.3861593,
    0.4693495, 0.5672184, 0.6718278,
    0.7706061, 0.856946, 0.9248458, 0.9692941,
    0.9925561 ;
}
```

B   Graphics

We recommend using the NCAR Command Language (NCL) and NCAR graphics to visualize the model results. This graphics system is installed on most NCAR platforms and is also available for download via the Earth System Grid (ESG). NCL/NCAR graphics provide many functions for the manipulation of the data such as interpolations to pressure levels or the computation of the geopotential height. We will provide NCL scripts to the modeling groups to ease the visualization and analysis of the model runs.

C Vertical coordinates

The hybrid orography-following η-coordinate (Simmons and Burridge 1981) comprises a pure pressure coordinate and a σ-component with $\sigma = p/p_s$. The pressure p at a vertical level η is given by

$$p(\lambda, \varphi, \eta, t) = a(\eta)\, p_0 + b(\eta)\, p_s(\lambda, \varphi, t) \tag{116}$$

where the coefficients $a(\eta)$ and $b(\eta)$ are height-dependent and provided in tabular form (see below). Most commonly the reference pressure p_0 is set to 10^5 Pa or 1.01325×10^5 Pa. Here, a setup with $p_0 = 10^5$ Pa is chosen which coincides with the constant initial surface pressure p_s. This leads to the simplified expression

$$p(\lambda, \varphi, \eta, t = 0) = (a(\eta) + b(\eta))\, p_0 = \eta\, p_0\,. \tag{117}$$

In the discrete representation, the vertical direction is subdivided into N_{lev} model levels which are bounded by $N_{lev} + 1$ interface levels (denoted by the half indices $k + \frac{1}{2}$ below). The pressure at the interfaces is then given by

$$p_{k+\frac{1}{2}} = a_{k+\frac{1}{2}}\, p_0 + b_{k+\frac{1}{2}}\, p_s = \eta_{k+\frac{1}{2}}\, p_0 \tag{118}$$

with $\eta_{k+\frac{1}{2}} = a_{k+\frac{1}{2}} + b_{k+\frac{1}{2}}$ and $k = 0, 1, 2, \cdots N_{lev}$. The corresponding η_k values at the centers are determined via the average $\eta_k = \frac{1}{2}\left(\eta_{k+\frac{1}{2}} + \eta_{k-\frac{1}{2}}\right)$. It follows $p_k = \eta_k\, p_0$.

For the baroclinic wave tests described here, three setups with 18, 26 and 49 model levels are chosen. The corresponding coefficients for the model interfaces $a_{k+\frac{1}{2}}$ and $b_{k+\frac{1}{2}}$ are listed in Tables 7 and 8. Here it is important to note that some GCMs (for example Majewski et al. (2002)) employ the alternative notation $p_{k+\frac{1}{2}} = a_{k+\frac{1}{2}} + b_{k+\frac{1}{2}}\, p_s$ where the coefficients $a_{k+\frac{1}{2}}$ are given in Pa. If such a setup is encountered, the $a_{k+\frac{1}{2}}$ coefficients in Tables 7 and 8 need to be multiplied by p_0.

If level spacings are prescribed in z-coordinates as in section 1.6 the z positions can be translated into a pressure-based system for idealized temperature profiles. For isothermal conditions with $T = T_0$ the pressure profile is given by

$$p(z) = p_0 \exp\left(\frac{-gz}{R_d\, T_0}\right) \tag{119}$$

where p_0 is the surface pressure. If the atmosphere is characterized by a linear temperature profile $T = T_0 - \Gamma z$ with constant lapse rate $\Gamma = -\partial T/\partial z$ the pressure profile is given by

$$p(z) = p_0 \left(1 - \frac{\Gamma z}{T_0}\right)^{\frac{g}{R_d \Gamma}}. \tag{120}$$

where T_0 symbolizes the surface temperature. For atmospheres with constant Brunt-Väisälä frequency N the pressure profile is

$$p(z) = p_0 \left[\left(1 - \frac{S}{T_0}\right) + \frac{S}{T_0} \exp\left(-\frac{N^2 z}{g}\right)\right]^{\frac{c_p}{R_d}} \tag{121}$$

with the parameter $S = g^2/(c_p\, N^2)$. Again, T_0 and p_0 symbolize the constant surface temperature and pressure. All three pressure profiles assume a flat surface with surface elevation $z_s = 0$ m. Using Eqs. (119), (120) or (121) the σ-levels are

$$\sigma(z) = \frac{p(z) - p(z_{top})}{p_s - p(z_{top})}. \tag{122}$$

Index	18 Model levels (L18)		26 Model levels (L26)	
k	$a_{k+\frac{1}{2}}$	$b_{k+\frac{1}{2}}$	$a_{k+\frac{1}{2}}$	$b_{k+\frac{1}{2}}$
0	0.00251499	0.	0.002194067	0.
1	0.00710361	0.	0.004895209	0.
2	0.01904260	0.	0.009882418	0.
3	0.04607560	0.	0.01805201	0.
4	0.08181860	0.	0.02983724	0.
5	0.07869805	0.03756984	0.04462334	0.
6	0.07463175	0.08652625	0.06160587	0.
7	0.06955308	0.1476709	0.07851243	0.
8	0.06339061	0.221864	0.07731271	0.01505309
9	0.05621774	0.308222	0.07590131	0.03276228
10	0.04815296	0.4053179	0.07424086	0.05359622
11	0.03949230	0.509588	0.07228744	0.07810627
12	0.03058456	0.6168328	0.06998933	0.1069411
13	0.02193336	0.7209891	0.06728574	0.1408637
14	0.01403670	0.816061	0.06410509	0.1807720
15	0.007458598	0.8952581	0.06036322	0.2277220
16	0.002646866	0.953189	0.05596111	0.2829562
17	0.	0.985056	0.05078225	0.3479364
18	0.	1.	0.04468960	0.4243822
19			0.03752191	0.5143168
20			0.02908949	0.6201202
21			0.02084739	0.7235355
22			0.01334443	0.8176768
23			0.00708499	0.8962153
24			0.00252136	0.9534761
25			0.	0.9851122
26			0.	1.

Table 7: Vertical coefficients for a 18- and 26-level setups. The parameter $a_{k+\frac{1}{2}}$ denotes the pure pressure component, $b_{k+\frac{1}{2}}$ defines the σ part of the hybrid η-system.

For hybrid vertical coordinate systems like

$$p(\eta) = A(\eta)\,p_0 + B(\eta)\,p_s \tag{123}$$

we recommend using the hybrid coefficients A and B

$$A(\eta) = \eta - B(\eta) \tag{124}$$

$$B(\eta) = \left(\frac{\eta - \eta_{top}}{1 - \eta_{top}}\right)^c \tag{125}$$

Index k	49 Model levels (L49) $a_{k+\frac{1}{2}}$	$b_{k+\frac{1}{2}}$	Index k	49 Model levels (L49) $a_{k+\frac{1}{2}}$	$b_{k+\frac{1}{2}}$
0	0.002251865	0.	25	0.07118414	0.1556586
1	0.003983890	0.	26	0.06962863	0.1737837
2	0.006704364	0.	27	0.06795950	0.1932327
3	0.01073231	0.	28	0.06616846	0.2141024
4	0.01634233	0.	29	0.06424658	0.2364965
5	0.02367119	0.	30	0.06218433	0.2605264
6	0.03261456	0.	31	0.05997144	0.2863115
7	0.04274527	0.	32	0.05759690	0.3139801
8	0.05382610	0.	33	0.05504892	0.3436697
9	0.06512175	0.	34	0.05231483	0.3755280
10	0.07569850	0.	35	0.04938102	0.4097133
11	0.08454283	0.	36	0.04623292	0.4463958
12	0.08396310	0.006755112	37	0.04285487	0.4857576
13	0.08334103	0.01400364	38	0.03923006	0.5279946
14	0.08267352	0.02178164	39	0.03534049	0.5733168
15	0.08195725	0.03012778	40	0.03116681	0.6219495
16	0.08118866	0.03908356	41	0.02668825	0.6741346
17	0.08036393	0.04869352	42	0.02188257	0.7301315
18	0.07947895	0.05900542	43	0.01676371	0.7897776
19	0.07852934	0.07007056	44	0.01208171	0.8443334
20	0.07751036	0.08194394	45	0.007959612	0.8923650
21	0.07641695	0.09468459	46	0.004510297	0.9325572
22	0.07524368	0.1083559	47	0.001831215	0.9637744
23	0.07398470	0.1230258	48	0.	0.9851122
24	0.07263375	0.1387673	49	0.	1.

Table 8: Same as Table 7 but for a 49-level setup.

for the interface levels as suggested by Laprise and Girard (1990). For $p_s = p_0$, the definitions are $\eta = p(z)/p_s$ and $\eta_{top} = p(z_{top})/p_s$. The exponent c determines the smoothness of the transition between the σ-coordinate at low levels to the pressure coordinate near the upper boundary. We recommend choosing $c = 1$ which closely resembles the σ-system. Bigger coefficients $c > 1$ would allow for a more gradual transition and could also be tested (e.g. $c = 2$). This hybrid coordinate system is a variant of the one used by Simmons and Burridge (1981). It guarantees the conditions $p(\eta = \eta_{top}) = p_{top}$ and $p(\eta = 1) = p_s$ at the top and bottom boundaries. The hybrid coefficients at the full model levels can then be computed via the linear average

$$A_k = \frac{1}{2}\big(A_{k+1/2} + A_{k-1/2}\big), \tag{126}$$

$$B_k = \frac{1}{2}\big(B_{k+1/2} + B_{k-1/2}\big) \tag{127}$$

where the index k denotes the discrete full model level which is surrounded by the two inter-face levels shown with half indices. The linear average guarantees that vertical differencing operations conserve energy. We again note that some models (Majewski et al. 2002) use the alternative definition of Eq. (123)

$$p(\eta) = A(\eta) + B(\eta) \, p_s. \tag{128}$$

Then Eq. (124) is represented by $A(\eta) = p_0[\eta - B(\eta)]$.

D Iterative Method for Dynamical Cores with z- or Θ-Based Vertical Coordinates

In sections 1.1 and 1.2 the initial conditions are shown in closed form for pressure-based vertical coordinates with $\eta = \sigma = p/p_s$. For dynamical cores with z- or Θ-based vertical coordinates a root-finding technique (Newton's method) is suggested. It determines the corresponding η-level for any given height z or isentropic level Θ with high accuracy. This technique therefore avoids vertical interpolations of the initial data set. The iterative method is given by

$$\eta^{n+1} = \eta^n - \frac{F(\lambda, \varphi, \eta^n)}{\frac{\partial F}{\partial \eta}(\lambda, \varphi, \eta^n)} \tag{129}$$

where the superscript $n = 0, 1, 2, 3, \ldots$ indicates the iteration count.

For a given z-level the functions F and $\partial F/\partial \eta$ are determined by

$$F(\lambda, \varphi, \eta^n) = -g\,z + \Phi(\lambda, \varphi, \eta^n) \tag{130}$$

$$\frac{\partial F}{\partial \eta}(\lambda, \varphi, \eta^n) = -\frac{R_d}{\eta^n}\,T(\lambda, \varphi, \eta^n) \tag{131}$$

where T and Φ are shown in Eqs. (10) and (11), respectively.

If isentropic vertical coordinates with given Θ-levels are utilized the function F is defined by

$$F(\lambda, \varphi, \eta^n) = -\Theta + (\eta^n)^{-\kappa}\,T(\lambda, \varphi, \eta^n) \tag{132}$$

with $\kappa = R_d/c_p$. The specific heat of dry air at constant pressure c_p is set to 1004.64 J (kg K)$^{-1}$. Using $R_d = 287.04$ J (kg K)$^{-1}$, κ is identical to 2/7. For $\partial F/\partial \eta$ it follows

$$\frac{\partial F}{\partial \eta}(\lambda, \varphi, \eta^n) = G(\eta^n) - \frac{3\,\pi\,u_0}{4\,R_d\,(\eta^n)^\kappa}\cos^{\frac{1}{2}}\eta_v^n \left\{ \frac{3\,\pi}{2}u_0\eta^n C \sin^2 \eta_v^n\,\cos^{\frac{1}{2}}\eta_v^n - \right. \tag{133}$$

$$\left. \left(2C\,u_0\cos^{\frac{3}{2}}\eta_v^n + D\,a\,\Omega\right)\left((1-\kappa)\sin\eta_v^n + \frac{\pi\,\eta^n}{4\cos\eta_v^n}(2 - 3\sin^2\eta_v^n)\right)\right\}$$

with

$$C = \left(-2\sin^6\varphi\,(\cos^2\varphi + \frac{1}{3}) + \frac{10}{63}\right) \tag{134}$$

$$D = \left(\frac{8}{5}\cos^3\varphi\,(\sin^2\varphi + \frac{2}{3}) - \frac{\pi}{4}\right) \tag{135}$$

and $\eta_v^n = ((\eta^n - \eta_0)\,\pi/2)$. As before, η_0 is set to 0.252 and $\eta_t = 0.2$ is the tropopause level. G symbolizes the vertical derivative of the horizontal-mean potential temperature $\bar{\Theta}(\eta) = \eta^{-\kappa}\bar{T}(\eta)$. It is given by

$$G(\eta^n) = T_0\left(\frac{R_d\,\Gamma}{g} - \kappa\right)(\eta^n)^{(\frac{R_d\Gamma}{g} - \kappa - 1)} \qquad \text{(for } \eta_s \geq \eta^n \geq \eta_t) \tag{136}$$

$$G(\eta^n) = T_0\left(\frac{R_d\,\Gamma}{g} - \kappa\right)(\eta^n)^{(\frac{R_d\Gamma}{g} - \kappa - 1)} - \frac{\Delta T}{(\eta^n)^{(\kappa+1)}}(\eta_t - \eta^n)^4\left(\kappa\,\eta_t + \eta^n(5 - \kappa)\right)$$

$$\qquad \text{(for } \eta_t > \eta^n)\,. \tag{137}$$

The starting value $\eta^0 = 10^{-7}$ is recommended for all Newton iterations following Eq. (129). Then Newton's method converges for any given height z below $z_{max} = 100$ km or any given potential temperature Θ below $\Theta_{max} = 15000$ K. Note that the convergence is only achieved if η^0 is greater than zero and physically lies above the uppermost model level. If models with higher model tops are used, η^0 needs to be decreased. We have observed that this iterative technique converges within a maximum of 25 iterations. Then the absolute error $|\eta - \eta^n|$ is decreased to machine precision (10^{-14} for double-precision arithmetics). Most often, the convergence is already achieved with fewer iterations. The resulting η-level can now be used for the computation of the analytic initial conditions at the location (λ, φ, η).

E   Transformations for rotated coordinates

The rotation of the coordinates, together with their inverse relations, has been described in Nair and Jablonowski (2008) and Staniforth and White (2007). Here, we partly cite from the reference by Staniforth and White (2007) and add the details for the initial conditions of the steady-state and baroclinic wave test cases. Note that the trigonometric functions as outlined below might suffer from precision problems due to the nesting and the application of inverse trigonometric functions. Therefore, a slightly different but highly precise method has been implemented in the Fortran example code made available to the modeling groups on the NCAR Wiki web page

https://wiki.ucar.edu/display/dycores/Test+cases

The following steps illustrate the basic principle behind the rotations. Let the North pole of a rotated coordinate system be located at the point (λ_p, φ_p) of the unrotated geographical coordinate system. This is schematically shown in Fig. 28 (Nair and Jablonowski 2008). Let us assume $\lambda_p = 0$ for the calculations here. For a flow orientation angle α the North Pole position is given by $(\lambda_p, \pi/2 - \alpha)$. From Ritchie (1987), the following relations hold between the rotated (λ', φ') and unrotated (λ, φ) coordinate systems:

$$\sin \varphi' = \sin \varphi \, \sin \varphi_p + \cos \varphi \, \cos \varphi_p \, \cos(\lambda - \lambda_p), \tag{138}$$

$$\sin \varphi = \sin \varphi' \, \sin \varphi_p - \cos \varphi' \, \cos \varphi_p \, \cos \lambda', \tag{139}$$

$$\cos \varphi \sin(\lambda - \lambda_p) = \cos \varphi' \, \sin \lambda'. \tag{140}$$

For the steady-state conditions of section 1.1, expressed in the unrotated (λ, φ) coordinate system, the horizontal wind components at each vertical level satisfy

$$u(\varphi) = a \, \cos \varphi \frac{D\lambda}{Dt}, \ \ v = a \, \frac{D\varphi}{Dt} = 0, \tag{141}$$

whilst the wind components in the rotated system satisfy

$$u'(\lambda', \varphi') = a \, \cos \varphi' \frac{D\lambda'}{Dt}, \ \ v'(\lambda', \varphi') = a \, \frac{D\varphi'}{Dt}. \tag{142}$$

Differentiating Eq. (138) with respect to time and using Eqs. (141) and (142) gives

$$v'(\lambda', \varphi') \cos \varphi' = -\cos \varphi_p \, \sin(\lambda - \lambda_p) \, u(\varphi). \tag{143}$$

Differentiating Eqs. (139) and (140) with respect to time and manipulating the resulting equations using (140) - (143) then yields

$$u'(\lambda', \varphi') = \left[\cos \lambda' \, \cos(\lambda - \lambda_p) + \sin \varphi_p \sin \lambda' \sin(\lambda - \lambda_p) \right] u(\varphi). \tag{144}$$

Suppose now that the initial conditions in section 1.1 are to be expressed in the (λ', φ') coordinate system, whose North Pole is located at the point (λ_p, φ_p) of the unrotated geographical coordinate system (λ, φ). The steps for obtaining the initial conditions at the meshpoints (λ', φ') of the rotated system are:
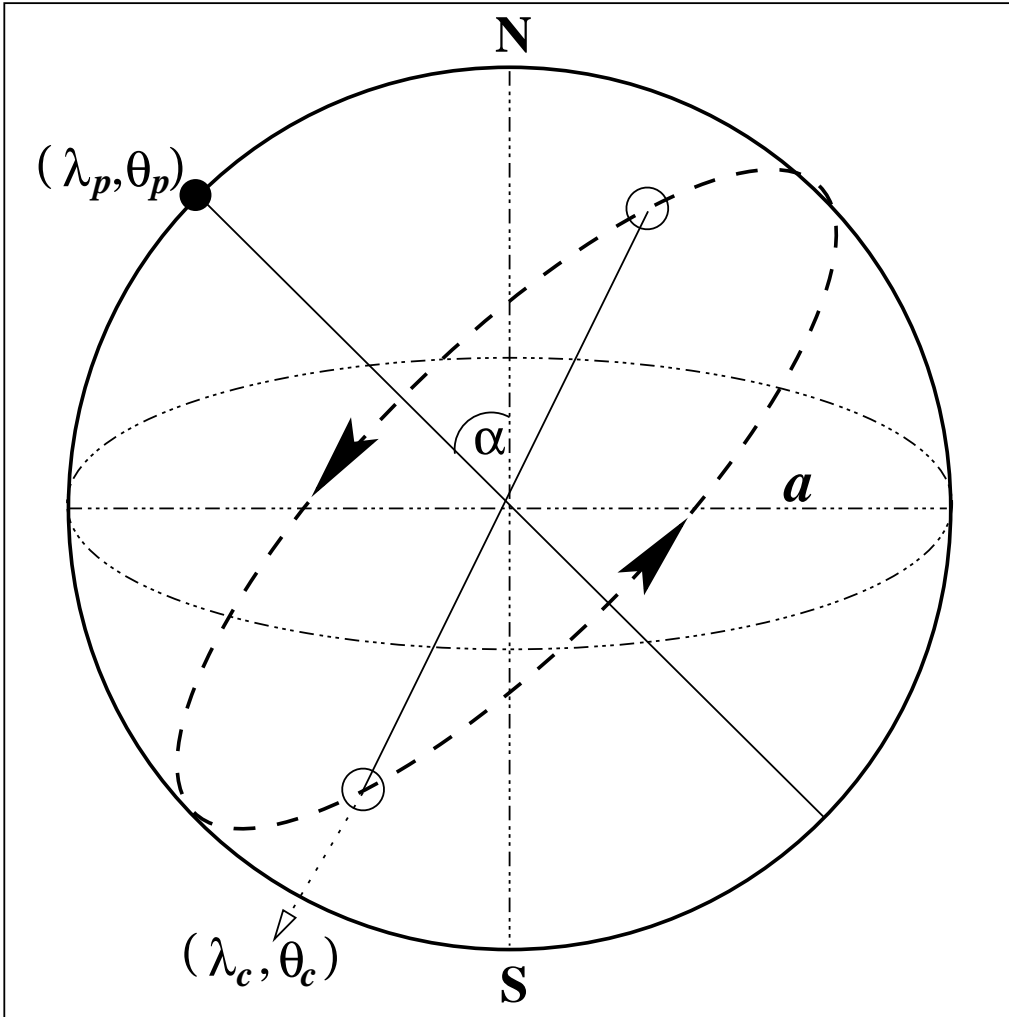
Figure 28: A center position (λ_c, θ_c) at the equator (dashed line) of a rotated coordinate system (λ', θ') whose North pole is at (λ_p, θ_p) with respect to the regular (λ, θ) sphere with radius a. N and S are the poles of the unrotated Earth. The flow orientation parameter α is the angle between the axis of the unrotated Earth and the polar axis of the rotated Earth.

1. Compute φ from Eq. (139) which yields

$$\varphi = \arcsin\left(\sin\varphi'\,\sin\varphi_p - \cos\varphi'\,\cos\varphi_p\,\cos\lambda'\right) \qquad (145)$$

2. Compute the inverse relation λ derived as

$$\lambda = \lambda_p + \arctan\left(\frac{\cos\varphi'\,\sin\lambda'}{\sin\varphi\,\cos\varphi_p + \cos\varphi'\,\cos\lambda'\,\sin\varphi_p}\right) \qquad (146)$$

This step is necessary for the computation of the zonal wind perturbation for the baroclinic wave. It can be omitted for the steady-state test case. Inverting the trigonometric functions, particularly for λ can be problematic due to the non-unique nature of the inverted (arctan) function values. To avoid this problem we recommend using the intrinsic Fortran function `atan2(y,x)` for $\arctan(y/x)$ which provides values in the range $[-\pi, \pi]$. The negative values between $[-\pi, 0)$ then need to be *shifted* by adding 2π. This guarantees the proper branch cut in the longitudinal direction between $[0, 2\pi]$.

3. Compute $\cos(\lambda - \lambda')$ from Eq. (138) and $\sin(\lambda - \lambda')$ from Eq. (140) which yields

$$\cos(\lambda - \lambda_p) = \frac{\sin\varphi' - \sin\varphi\,\sin\varphi_p}{\cos\varphi\,\cos\varphi_p} \qquad (147)$$

$$\sin(\lambda - \lambda_p) = \frac{\cos\varphi'\,\sin\lambda'}{\cos\varphi} \qquad (148)$$

4. Depending on the choice of the test case compute the zonal wind field for either the unperturbed conditions according to section 1.1 Eq. (5)

$$u(\varphi, \eta) = u_0\,\cos^{\frac{3}{2}}\eta_v\,\sin^2(2\,\varphi) \qquad (149)$$

or the perturbed initial conditions for the baroclinic wave test. The latter is given as

$$u(\lambda, \varphi, \eta) = u_0\,\cos^{\frac{3}{2}}\eta_v\,\sin^2(2\,\varphi) + u_p\,\exp\left(-\left(\frac{r}{R}\right)^2\right) \qquad (150)$$

where the parameters u_p and R are explained in section 1.2. The great circle distance r is given by

$$r = a\,\arccos\left(\sin\varphi_c\,\sin\varphi + \cos\varphi_c\,\cos\varphi\,\cos(\lambda - \lambda_c)\right) \quad . \qquad (151)$$

with the original (unrotated) center position (λ_c, φ_c). Use the results from Eqs. (145) and (146) for φ and λ.

5. Use Eqs. (147), (148) and (149)/(150) to compute the $u'(\lambda', \varphi', \eta)$ and $v('\lambda', \varphi', \eta)$ as shown in Eqs. (144) and (143). The (λ', φ') coordinates are the meshpoints of the computational grid.

6. Compute the scalar fields $T'(\lambda', \varphi', \eta)$ and $\Phi'_s(\lambda', \varphi', \eta)$ in the rotated system by using the result of Eq. (145) in the temperature equation (Eq. (10)) and the expression for the surface geopotential (Eq. (14)) from section 1.1.

F Conservation of total energy

In the continuous primitive equations with hybrid vertical coordinates total energy is conserved if the rate of change

$$\frac{\partial}{\partial t} \int_A \int_{\eta_{top}}^{\eta_s} \left(\frac{\mathbf{v}^2}{2} + c_p T\right) \frac{\partial p}{\partial \eta} \, d\eta \, dA = -\int_A \left(\Phi_s \frac{\partial p_s}{\partial t} - \Phi_{top} \frac{\partial p_{top}}{\partial t}\right) dA \qquad (152)$$

is obtained (Laprise and Girard 1990). This equation is valid in the absence of diabatic and frictional effects. Φ_s, p_s and Φ_{top}, p_{top} are the geopotential and pressure at the surface and the model top, c_p is the specific heat of dry air at constant pressure and $\mathbf{v} = (u, v)^T$ stands for the horizontal velocity vector with the zonal and meridional wind components u and v. Furthermore, T symbolizes the temperature, p is the pressure, and t denotes the time. The integrals span the 3D and 2D domains where A symbolizes the horizontal area of the sphere and η stands for the hybrid vertical coordinate. The vertical integral is bounded by the value η_s at the surface and η_{top} at the model top. Here, η_s is identical to unity and η_{top} is set p_{top}/p_0 with $p_0 = 1000$ hPa. Note that η_{top} is non-zero for constant $p_{top} > 0$ hPa. A constant pressure at the model top ensures the global conservation of total energy in the continuous equations and simplifies the 2D integral. Eq. (152) then becomes

$$\frac{\partial}{\partial t} \left\{ \int_A \frac{1}{g} \left[\left(\int_{\eta_{top}}^{\eta_s} \left(\frac{\mathbf{v}^2}{2} + c_p T\right) \frac{\partial p}{\partial \eta} \, d\eta \right) + \Phi_s p_s \right] dA \right\} = 0. \qquad (153)$$

Here we divided Eq. (152) by the gravitational constant g to recover energy units (Kasahara 1974). This expression is equivalent to

$$\frac{\partial}{\partial t} E = 0$$

where E symbolizes the global integral of the total energy as shown by the term in the curly bracket in Eq. (153). In the semi-discrete system with $\partial p/\partial \eta \approx \Delta p/\Delta \eta$ and $d\eta \approx \Delta \eta$, the domain-integrated total energy E is given by

$$E = \int_A \frac{1}{g} \left[\left(\sum_{k=1}^{K_{max}} \left(\frac{u_k^2 + v_k^2}{2} + c_p T_k\right) \Delta p_k \right) + \Phi_s p_s \right] dA. \qquad (154)$$

The summation index k indicates the vertical index of a full model level with the maximum level number K_{max} near the surface. The pressure difference Δp_k is defined as

$$\Delta p_k = p_{k+1/2} - p_{k-1/2} = p_0 \, \Delta A_k + p_s \, \Delta B_k \qquad (155)$$

with $\Delta A_k = A_{k+1/2} - A_{k-1/2}$ and $\Delta B_k = B_{k+1/2} - B_{k-1/2}$. The discrete positions of the hybrid coefficients $A_{k+1/2}$ and $B_{k+1/2}$ at the model interface levels are listed in Appendix C. $\Delta \eta_k$ is given by $\Delta \eta_k = \eta_{k+1/2} - \eta_{k-1/2} = \Delta A_k + \Delta B_k$.

If hydrostatic models with σ coordinates like

$$\sigma = \frac{p - p_{top}}{p_s - p_{top}} \qquad (156)$$

are considered the global integral of the total energy becomes

$$E = \frac{1}{g} \int_A \int_{\sigma_{top}}^{\sigma_s} \left(\frac{\mathbf{v}^2}{2} + c_p T + \Phi_s \right) \frac{\partial p}{\partial \sigma} \, d\sigma \, dA \tag{157}$$

$$\approx \frac{1}{g} \int_A \left[\sum_{k=1}^{K_{max}} \left(\frac{u_k^2 + v_k^2}{2} + c_p T_k + \Phi_s \right) \Delta p_k \right] dA. \tag{158}$$

The pressure differences Δp_k are determined with the help of Eq. (114) which leads to

$$\Delta p_k = p_{k+1/2} - p_{k-1/2} = (\sigma_{k+1/2} - \sigma_{k-1/2}) (p_s - p_{top}). \tag{159}$$

Note that the conservation of energy requires $\sigma_{top} = 0$ which is guaranteed in Eq. (156). The lower boundary at the surface is $\sigma_s = 1$.

As noted in Kasahara (1974) the global integral of the total energy for hydrostatic models with a pure height coordinate z in the vertical direction is represented by

$$E = \int_A \int_{z_{top}}^{z_s} \left(\frac{\mathbf{v}^2}{2} + c_v T + gz \right) \rho \, dz \, dA \tag{160}$$

$$\approx \int_A \left[\sum_{k=1}^{K_{max}} \left(\frac{u_k^2 + v_k^2}{2} + c_v T_k + gz_k \right) \rho_k \, \Delta z_k \right] dA. \tag{161}$$

The quantities $\rho \, \mathbf{v}^2/2$, $\rho \, c_v T$ and $\rho g z$ are the kinetic, internal and potential energy per unit volume, respectively. c_v is the specific heat at constant volume and defined by $c_v = R_d - c_p = 717.6 \, \text{J kg}^{-1} \, \text{K}^{-1}$. ρ denotes the density which is defined by the ideal gas law $\rho = p/(R_d T)$. z_s is the height of the orography. If height-based orography-following coordinates like

$$\xi = \frac{z_{top} - z}{z_{top} - z_s} \tag{162}$$

are used the domain integral of the total energy transforms to

$$E = \int_A \int_{\xi_{top}}^{\xi_s} \left(\frac{\mathbf{v}^2}{2} + c_v T + gz \right) \rho \, d\xi \, dA \tag{163}$$

$$\approx \int_A \left[\sum_{k=1}^{K_{max}} \left(\frac{u_k^2 + v_k^2}{2} + c_v T_k + gz_k \right) \rho_k \, \Delta \xi_k \right] dA \tag{164}$$

with the lower and upper integration limits ξ_s and ξ_{top}.

Note that the full 3D velocity vector $\mathbf{v}_{3D} = (u, v, w)^T$ need to be used for the computation of the kinetic energy in nonhydrostatic dynamical cores.

G Constants and symbols

Physical constants and model coordinates

a	mean radius of the Earth	$a = 6.371229 \times 10^6$ m
g	gravitational acceleration	$g = 9.80616$ m s^{-2}
Ω	Earth's angular velocity $\Omega = 2\pi/$sidereal day	$\Omega = 7.29211 * 10^{-5}$ s^{-1}
	length of a sidereal day	86164 s
f	Coriolis parameter	$f = 2\Omega \sin\varphi$
R_d	ideal gas constant for dry air	$R = 287.04$ J kg^{-1} K^{-1}
c_p	specific heat at constant pressure	$c_p = 1004.64$ J kg^{-1} K^{-1}
c_v	specific heat at constant volume $c_v = R_d - c_p$	$c_v = 717.6$ J kg^{-1} K^{-1}
κ		$\kappa = R_d/c_p = 2/7$
π		$\pi = 3.141592654$
λ	longitude	$\lambda \in [0, 2\pi]$
φ	latitude	$\varphi \in [-\pi/2, \pi/2]$
η	hybrid level	$\eta \in [0, 1]$
σ	sigma level	$\sigma \in [0, 1]$
t	time	
$A(\eta)$	hybrid coefficients for η coordinate, also A_k	
$B(\eta)$	hybrid coefficients for η coordinate, also B_k	

Symbols and parameters

u	zonal wind (unrotated)	
v	meridional wind (unrotated)	
$u_{perturb}$	perturbation of the zonal wind	
u'	rotated zonal wind	
v'	rotated meridional wind	
ω	vertical pressure velocity	$\omega = \dot{p} = dp/dt$
$\dot{\eta}$	vertical velocity in η coordinates	$\dot{\eta} = d\eta/dt$
$\dot{\sigma}$	vertical velocity in σ coordinates	$\dot{\sigma} = d\sigma/dt$
$q1 - q6$	tracer distributions	
p	pressure	
ρ	density	$\rho = p/(R_d T)$
p_s	surface pressure	
T	temperature	
$\bar{T}$	horizontal mean temperature	
Θ	potential temperature	$\Theta = T \left(\frac{1000\,hPa}{p}\right)^\kappa$
Θ'	potential temperature perturbation	
$\bar{\Theta}$	horizontal mean potential temperature	
$\Delta\Theta$	potential temperature perturbation amplitude	$\Delta\Theta = 10$ K
Φ	geopotential	
Φ'	geopotential perturbation	
$\bar{\Phi}$	horizontal mean geopotential	
Φ_s	surface geopotential $\Phi_s = gz_s$	
ζ	relative vorticity	

δ	horizontal divergence	
ζ'	perturbation of the relative vorticity	
δ'	perturbation of the horizontal divergence	
α	flow orientation angle	$\alpha \in [0, \pi/2]$
N	Brunt-Väisälä frequency	
S	parameter	$S = g^2/(c_p\,N^2)$
T_0	horizontal mean surface temperature	
H	scale height	$H = (R_d\,T)/g$
τ	time period (waves)	
u_0	horizontal wind amplitude or constant background velocity	
u_p	maximum wind amplitude of the perturbation	$u_p = 1 \text{ m s}^{-1}$
ω_0	maximum vertical pressure velocity	
ΔT	empirical temperature difference	$\Delta T = 4.8 \times 10^5 \text{ K}$
Γ	temperature lapse rate in K m^{-1}	$\Gamma = -\partial T/\partial z$
p_0	reference pressure at the surface	$p_0 = 1000 \text{ hPa}$
p_{top}	pressure at the model top	
η_v	auxiliary variable	$\eta_v = (\eta - \eta_0)\pi/2$
η_0	center of the zonal jet	$\eta_0 = 0.252$
η_t	tropopause level in η coordinates	$\eta_t = 0.2$
η_{top}	top level in η coordinates	
η_s	surface level in η coordinates	$\eta_s = 1$
η_{hw}	half width of the tracer distribution	$\eta_{hw} = 0.1$
σ_{top}	top level in σ coordinates	$\sigma_{top} = 0$
σ_s	surface level in σ coordinates	$\sigma_s = 1$
z_{top}	height at the model top	
z_s	surface height	
z_0	center of the tracer distribution, also interpolation level	
h_0	height of the mountain	$h_0 = 2000 \text{ m}$
d	half width of the mountain	$d = 1250 \text{ km}$
ξ	height-based orography following coordinate system	$\xi = (z_{top} - z)/(z_{top} - z_s)$
E	domain integrated total energy	
K_{max}	maximum vertical level number	
r	great circle distance	
R	distance or half width in the horizontal direction	
Z	half width in the vertical direction	$Z = 1 \text{ km}$
λ_p	longitudinal position of the rotated North pole	set to $\lambda_p = 0$
φ_p	latitudinal position of the rotated North pole	$\varphi_p = \pi/2 - \alpha$
λ_c	center point in longitudinal direction	
φ_c	center point in latitudinal direction	
η_c	center point in the vertical direction	
τ	wave period in s	
ν	wave frequency or angular velocity	
n	generic wave number	
K	frequency parameter for Rossby-Haurwitz wave	$K = u_0/(n\,a)$
M	frequency parameter for Rossby-Haurwitz wave	$M = K = u_0/(n\,a)$
k	wave number in the zonal direction	$k = 2\pi/L_x$

l	wave number in the meridional direction	$l = 2\pi/L_y$
m	wave number in the vertical direction	$m = 2\pi/L_z$
c_x	gravity wave phase speed in the zonal direction	
L_x	wave length in zonal direction	
L_y	wave length in meridional direction	
L_z	wave length in the vertical direction	

Key symbols for output quantities

U	zonal wind, unstaggered
V	meridional wind, unstaggered
OMEGA	vertical pressure velocity
T	temperature
PS	surface pressure
PHIS	surface geopotential
Z3	geopotential height
Z700	geopotential height at 700 hPa
Z500	geopotential height at 500 hPa
Z300	geopotential height at 300 hPa
T850	temperature at 850 hPa
T300	temperature at 300 hPa
U850	zonal wind at 850 hPa
U200	zonal wind at 200 hPa
V850	zonal wind at 850 hPa
V200	zonal wind at 200 hPa
OMEGA850	vertical pressure velocity at 850 hPa
OMEGA500	vertical pressure velocity at 500 hPa

References

Colella, P. and P. R. Woodward, 1984: The Piecewise Parabolic Method (PPM) for gas-dynamical simulations. *J. Comput. Phys.*, **54**, 174–201.

Collins, W. D., P. J. Rasch, B. A. Boville, J. J. Hack, J. R. McCaa, D. L. Williamson, B. P. Briegleb, C. M. Bitz, S.-J. Lin, M. Zhang, and Y. Dai, 2006: The formulation and atmospheric simulation of the Community Atmosphere Model: CAM3. *J. Climate*, **19**, 2144–2161.

Collins, W. D., P. J. Rasch, B. A. Boville, J. J. Hack, J. R. McCaa, D. L. Williamson, J. T. Kiehl, B. Briegleb, C. Bitz, S.-J. Lin, M. Zhang, and Y. Dai, 2004: Description of the NCAR Community Atmosphere Model (CAM3.0). NCAR Tech. Note NCAR/TN-464+STR, National Center for Atmospheric Research, Boulder, Colorado, 226 pp.

Giraldo, F. X. and T. E. Rosmond, 2004: A scalable Spectral Element Eulerian Atmospheric Model (SEE-AM) for NWP: Dynamical core tests. *Mon. Wea. Rev.*, **132**, 133–153.

Haurwitz, B., 1940: The motion of atmospheric disturbances on the spherical earth. *J. Mar. Res.*, **3**, 254–267.

Jablonowski, C., 2004: *Adaptive Grids in Weather and Climate Modeling*. Ph.D. dissertation, University of Michigan, Ann Arbor, MI, Department of Atmospheric, Oceanic and Space Sciences, 292 pp.

Jablonowski, C. and D. L. Williamson, 2006a: A baroclinic instability test case for atmospheric model dynamical cores. *Quart. J. Roy. Meteor. Soc.*, **132**, 2943–2975.

— 2006b: A baroclinic wave test case for dynamical cores of General Circulation Models: Model intercomparisons. NCAR Tech. Note NCAR/TN-469+STR, National Center for Atmospheric Research, Boulder, Colorado, 89 pp.

Kasahara, A., 1974: Various vertical coordinate systems used for numerical weather prediction. *Mon. Wea. Rev.*, **102**, 509–522.

Laprise, R. and C. Girard, 1990: A spectral General Circulation Model using the piecewise-constant finite-element representation on a hybrid vertical coordinate system. *J. Climate*, **3**, 32–52.

Lin, S.-J., 2004: A "vertically Lagrangian" finite-volume dynamical core for global models. *Mon. Wea. Rev.*, **132**, 2293–2307.

Machenhauer, B., 1979: The spectral method. *Numerical Methods Used in Atmospheric Models*, A. Kasahara, ed., GARP Publications Series No 17, WMO and ICSU, Geneva, volume 2, 121–275.

Majewski, D., D. Liermann, P. Prohl, B. Ritter, M. Buchhold, T. Hanisch, G. Paul, W. Wergen, and J. Baumgardner, 2002: The operational global icosahedral-hexagonal gridpoint model GME: Description and high-resolution tests. *Mon. Wea. Rev.*, **130**, 319–338.

Monaco, A. V. and R. T. Williams, 1975: An atmospheric global prediction model using a modified Arakawa differencing scheme. Technical report, Dept. of Meteorology, Naval Postgraduate School, Monterey, CA, NPS-51WU75041, 86pp.

Nair, R. D. and C. Jablonowski, 2008: Moving vortices on the sphere: A test case for horizontal advection problems. *Mon. Wea. Rev.*, **136**, 699–711.

Phillips, N. A., 1957: A coordinate system having some special advantages for numerical forecasting. *J. Meteor.*, **14**, 184–185.

— 1959: Numerical integration of the primitive equations on the hemisphere. *Mon. Wea. Rev.*, **87**, 333–345.

Ritchie, H., 1987: Semi-Lagrangian advection on a Gaussian grid. *Mon. Wea. Rev.*, **115**, 608–619.

Simmons, A. J. and D. M. Burridge, 1981: An energy and angular-momentum conserving vertical finite-difference scheme and hybrid vertical coordinates. *Mon. Wea. Rev.*, **109**, 758–766.

Simmons, A. J. and B. J. Hoskins, 1977: Baroclinic instability on the sphere: Solutions with a more realistic tropopause. *J. Atmos. Sci.*, **34**, 581–588.

— 1979: The downstream and upstream development of unstable baroclinic waves. *J. Atmos. Sci.*, **36**, 1239–1254.

Staniforth, A. and A. A. White, 2007: Some exact solutions of geophysical fluid dynamics equations for testing models in spherical and plane geometry. *Quart. J. Roy. Meteor. Soc.*, **133**, 1605–1614.

Tomita, H. and M. Sato, 2004: A new dynamical framework of nonhydrostatic global model using the icosahedral grid. *Fluid Dyn. Res.*, **34**, 357–400.

U.S. Standard Atmosphere, 1976: U.S. Government Printing Office, Washington D.C.

Wan, H., 2008: University of Hamburg and Max-Planck Institute for Meteorology, Hamburg. Ph.D. thesis, to be submitted.

Williamson, D. L., J. B. Drake, J. J. Hack, R. Jakob, and P. N. Swarztrauber, 1992: A standard test set for numerical approximations to the shallow water equations in spherical geometry. *J. Comput. Phys.*, **102**, 211–224.

Williamson, D. L., J. Olson, and C. Jablonowski, 2008: Two dynamical core formulation flaws exposed by a baroclinic instability test case. Mon. Wea. Rev., in review, available at http://www-personal.umich.edu/c̃jablono/MWR_Williamson_et_al_2008.pdf.